AD-A032 076 ROCKWELL INTERNATIONAL CANOGA PARK CALIF ROCKETDYNE DIV F/G 10/2
60-WATT POWER SOURCE.(U)
APR 76 J A SPEEDS, R SPIES F33615-73-C-4071
UNCLASSIFIED R-9651 AFAPL-TR-76-44 NL

1 OF 2
ADA032076

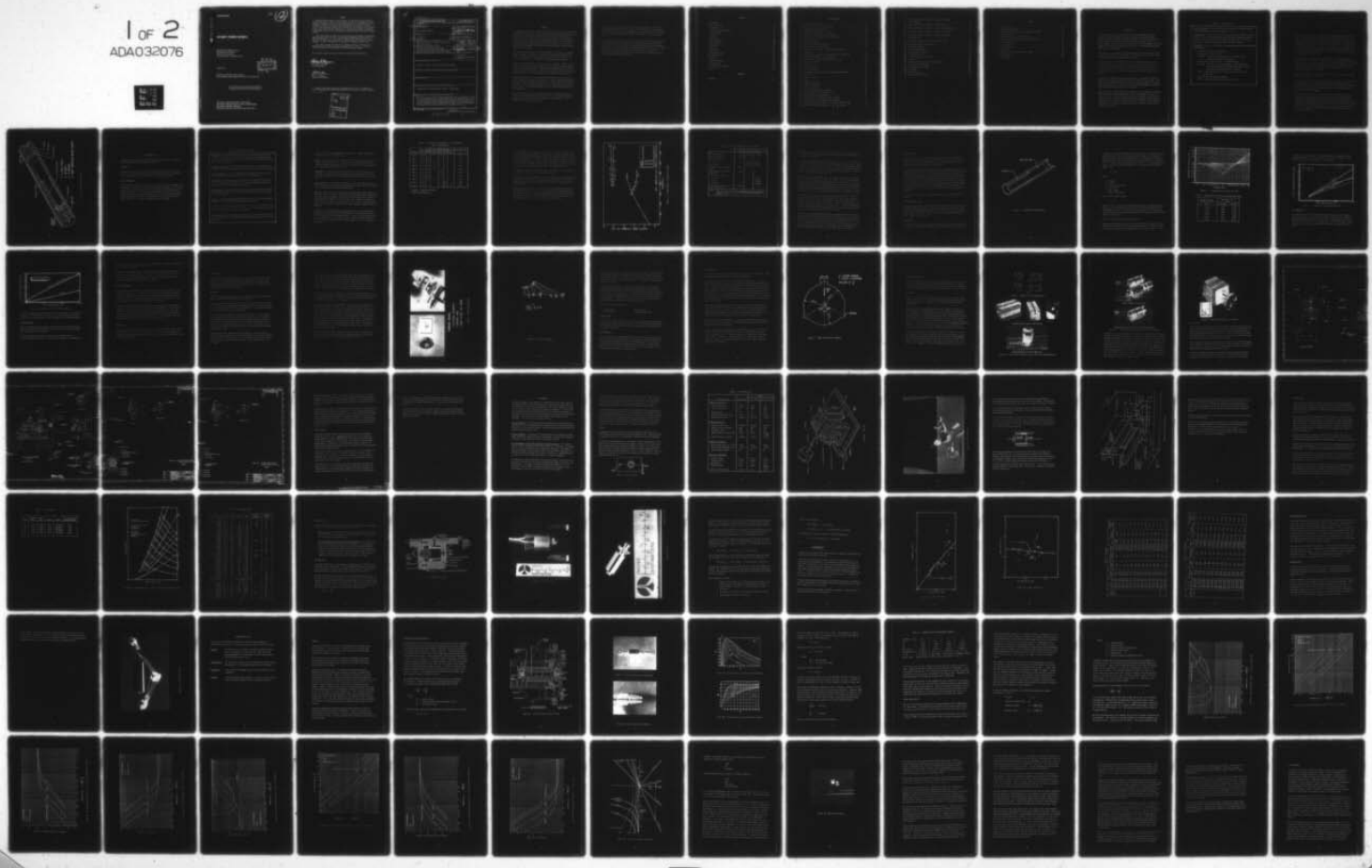

AFAPL-TR-76-44

FG (12)

60-WATT POWER SOURCE

ROCKWELL INTERNATIONAL
ROCKETDYNE DIVISION
6633 CANOGA AVENUE
CANOGA PARK, CALIFORNIA 91304

APRIL 1976

TECHNICAL REPORT AFAPL-TR-76-44
FINAL REPORT FOR PERIOD APRIL 1973 - JANUARY 1976

AIR FORCE AERO-PROPULSION LABORATORY
AIR FORCE WRIGHT AERONAUTICAL LABORATORIES
AIR FORCE SYSTEMS COMMAND
WRIGHT-PATTERSON AIR FORCE BASE, OHIO 45433

NOTICE

When Government drawings, specifications, or other data are used for any purpose other than in connection with a definitely related Government procurement operation, the United States Government thereby incurs no responsibility nor any obligation whatsoever; and the fact that the government may have formulated, furnished, or in any way supplied the said drawings, specifications, or other data, is not to be regarded by implication or otherwise as in any manner licensing the holder or any other person or corporation, or conveying any rights or permission to manufacture, use, or sell any patented invention that may in any way be related thereto.

This final report was submitted by Rocketdyne Division/Rockwell International, under Contract F33615-73-C-4071. The effort was sponsored by the Air Force Aero Propulsion Laboratory, Air Force Systems Command, Wright-Patterson AFB, Ohio, under Project 691X, Task 03 and Work Unit 08, with Phillip G. Colegrove as Project Engineer. R. Spies of Rocketdyne was technically responsible for the work.

This report has been reviewed by the Information Office, (ASD/OIP) and is releasable to the National Technical Information Service (NTIS). At NTIS, it will be available to the general public, including foreign nations.

This technical report has been reviewed and is approved for publication.

Phillip G. Colegrove
Project Engineer

Buryl L. McFadden
Technical Area Manager

PE G37 15F

Copies of this report should not be returned unless return is required by security considerations, contractual obligations, or notice on a specific document.

AIR FORCE - 20 OCTOBER 76 - 100

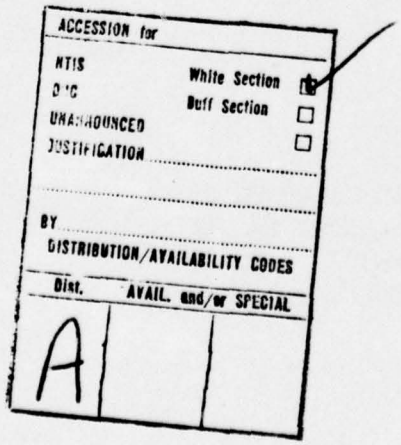

Unclassified

SECURITY CLASSIFICATION OF THIS PAGE (When Data Entered)

REPORT DOCUMENTATION PAGE

READ INSTRUCTIONS BEFORE COMPLETING FORM

1. REPORT NUMBER: AFAPL-TR-76-44	2. GOVT ACCESSION NO.
3. RECIPIENT'S CATALOG NUMBER	
4. TITLE (and Subtitle): 60-WATT POWER SOURCE,	5. TYPE OF REPORT & PERIOD COVERED: Final rept. April 1973-January 1976,
6. PERFORMING ORG. REPORT NUMBER: R-9651	
7. AUTHOR(s): J. A. Speeds, R. Spies	8. CONTRACT OR GRANT NUMBER(s): F33615-73-C-4071 NEW
9. PERFORMING ORGANIZATION NAME AND ADDRESS: Rocketdyne Division of Rockwell International, 6633 Canoga Avenue, Canoga Park, California 91304	10. PROGRAM ELEMENT, PROJECT, TASK AREA & WORK UNIT NUMBERS: Project 691X, Task 03, Work Unit 08
11. CONTROLLING OFFICE NAME AND ADDRESS: Air Force Aero-Propulsion Laboratory, Air Force Wright Aeronautical Laboratories, ASC, Wright-Patterson Air Force Base, Ohio 45433	12. REPORT DATE: April 1976 13. NUMBER OF PAGES: 116
14. MONITORING AGENCY NAME & ADDRESS (if different from Controlling Office)	15. SECURITY CLASS. (of this report): Unclassified 15a. DECLASSIFICATION/DOWNGRADING SCHEDULE

16. DISTRIBUTION STATEMENT (of this Report)

Approved for public release; distribution unlimited

17. DISTRIBUTION STATEMENT (of the abstract entered in Block 20, if different from Report)

18. SUPPLEMENTARY NOTES

19. KEY WORDS (Continue on reverse side if necessary and identify by block number)

turbogenerators, hydrazine, power supply, electric power

20. ABSTRACT (Continue on reverse side if necessary and identify by block number)

The feasibility of a 60-watt output dynamic power system contained in 6 cubic inches were demonstrated. A high-speed (300,000 rpm) turboalternator driven by the decomposition products from a hydrazine gas generator was developed for this application. Overall and component performance were determined experimentally with GN_2, and the program culminated with a series of demonstration tests with hydrazine and the delivery of a brassboard system.

DD FORM 1 JAN 73 1473 EDITION OF 1 NOV 65 IS OBSOLETE

Unclassified

SECURITY CLASSIFICATION OF THIS PAGE (When Data Entered)

390199

SUMMARY

An experimental program was completed to demonstrate the feasibility of generating 60-watts of electricity with a dynamic power system having a volume of no more than 6 cubic inches. Although the feasibility of this concept was demonstrated, it became evident that a more realistic application would be in the 200-watt and greater power level application. By increasing the power level, the fixed parasitic losses become a smaller percentage of the total power, thus easing the bearing friction requirements which do not change significantly within the power range of 60 to 400 watts.

The basic components selected for this system were a terry turbine, a permanent-magnet alternator, a hydrazine gas generator, and hydrodynamic bearings. Each of these components were evaluated individually by a series of cold-gas (GN_2) tests, and performance of the components was established experimentally.

A number of different component configurations were evaluated. Single-entry and re-entry terry turbines were tested with a number of different bearings ranging from plain hydrodynamic bearings to three-lobe hydrodynamic bearings, including as well, instrument ball bearings, conical spiral-groove bearings, pivot bearings, and hybrid bearings. The selected bearing was a three-lobe gas film bearing.

Several permanent-magnet rotor configurations were developed. Each of these operated successfully at speeds of 300,000 rpm. Initially, samarium/cobalt magnets were used for their extremely high magnetic flux. However, due to the low tensile properties of samarium/cobalt, the magnets had to be encapsulated for operation at 300,000 rpm. A platimum/cobalt magnet was used in the final application without encapsulation.

A short development program was conducted to optimize a microgas generator for this unit. Tests with MH5-A as fuel resulted in very slow initiation; therefore hydrazine was selected with a Shell 405 packed microgas generator. A high-reliability gas generator was developed.

Several variations of the alternator stator were investigated. The variations were primarily concerned with the type and size of the back-iron. Elimination of excess eddy current losses (very difficult at very high frequencies) was achieved, and only minor adjustments in the windings were required to achieve the design goal.

All components were assembled into a brassboard system and tested in the hydrazine facility during a series of system tests. The brassboard 60-watt power system was then delivered to the Air Force Aero Propulsion Laboratory at Wright-Patterson Air Force Base. The brass-board system demonstrated the feasibility of the concept, but required additional development to reduce bearing drag. Although it is feasible that a suitable bearing can be developed for this application, considerable development work would be required.

CONTENTS

ILLUSTRATIONS

TABLES

INTRODUCTION

Power systems for low power levels (< 500 watts) have traditionally been considered to be static conversion (as opposed to dynamic conversion) devices--typically batteries. However, conventional batteries cannot meet long-term storage requirements unless steps are taken to maintain the battery passive, i.e., that the battery is not activated until ready to use. This necessitates a "dynamic" sequence to initiate battery operation as the fluid is transferred to the battery compartment for power release.

Power density is also a problem. The best batteries available today yield volume densities of between 1.0 and 2.0 watt-hours per cubic inch. This results in some severe space limitations on volume-sensitive systems.

On the other hand, recent advances in miniature turbomachinery make it possible to consider dynamic power sources for low power output. Among these advances is the work being done on dental drills, surgical saws, miniature alternators for various applications, and cryogenic devices. By developing this technology for low-power-output systems, a battery replacement which has smaller volume will be feasible.

The task set for analysis and demonstration was for a unit capable of producing 60 watts for 12 minutes and having a volume of no more than 6 cubic inches. This results in an energy density of 2.0 watt-hours per pound equivalent to the upper limit of battery goals. In addition, low system cost was identified as a design goal, with a cost set at $50 per unit in large lots.

Specifically, the program objective was to demonstrate the feasibility of building a 60-watt dynamic auxiliary power source which can be produced in quantity at a low cost per unit. While the precise application was undefined, the initial application for this device was a power source for an expendable electronic countermeasure package. The technical feasibility of this concept was to be determined by measuring the performance of all key components of the power system with the design goals in Table 1.

TABLE 1. DESIGN GOALS

Electrical Output: 28 vdc, ±3 volts, 2.14 amperes, 12 minutes duration, and no load transients other than startup.

Cost Per Unit: The power unit shall be conceived and designed in such a way that it can be manufactured in mass quantities (thousands) and sold to the Air Force for less than 50 dollars ($50) per unit. All design decisions and tradeoff studies must take this into account.

Environment: The power unit shall be designed to operate under the following conditions:

Altitude: Sea level to 100,000 feet

Temperature: -65 F to +130 F

Attitude: The unit shall operate at all attitudes within ±30 degrees from the horizontal

Maximum Rate of Yaw or Pitch: 1.0 radian/second

"g" Load: 0.5 to 5 g's in all directions. In addition, the unit shall be capable of withstanding up to 10 g's shock load immediately prior to starting

Life: 5 years shelf life; 40 minutes at full power is the design goal

Startup Time: Less than 10 seconds

Start: At -65 F after 4 hours cold soak at -65 F

With the precise application undefined, the packaging scheme was open to determination. The contractual goal was that the volume of the entire unit was to be 6 cubic inches or less. This included the fuel, tankage, starting device, power conditioning, and everything else needed to make a complete, self-contained system. The diameter of the unit was to be made as small as feasible, consistent with optimization of the efficiency. The goal was to make the overall diameter of the unit less than 1 inch, but the diameter could be larger if it was necessary for successful demonstration of feasibility. However, the diameter could not exceed 1.5 inches under *any* circumstances.

Based on this goal, an envelope 1 inch in diameter and 7.66 inches long was selected to size all components of the system. It was recognized that the configuration resulting in this way could not be optimum, but the emphasis of the program was to be placed on measurement of the efficiency of key components and not on design optimization. It was intended that once component efficiency levels were defined, optimization could be pursued.

Figure 1 is an isometric representation of the unit. It was designed in accordance with the design goals in Table 1.

The key component in the system is the prime mover. Efficiency must be maintained at reasonable levels to ensure meeting the volume requirements. Therefore, the majority of attention was placed on the power module: the turbine, gas generator, alternator, and bearings. Testing was accomplished for these components and performance parameters were measured.

In this report the results and history of the work performed are presented. All components of the power module were successfully operated and demonstrated. A system test at less than full speed was performed with adequate power output. Sufficient data were obtained to ensure that a dynamic device is feasible although the parasitic losses (bearings and windage) were shown to be larger than expected and, therefore, realistic system efficiencies would require higher design power levels. For example, at a 400-watt power level, parasitic losses of about 60 watts could be tolerated.

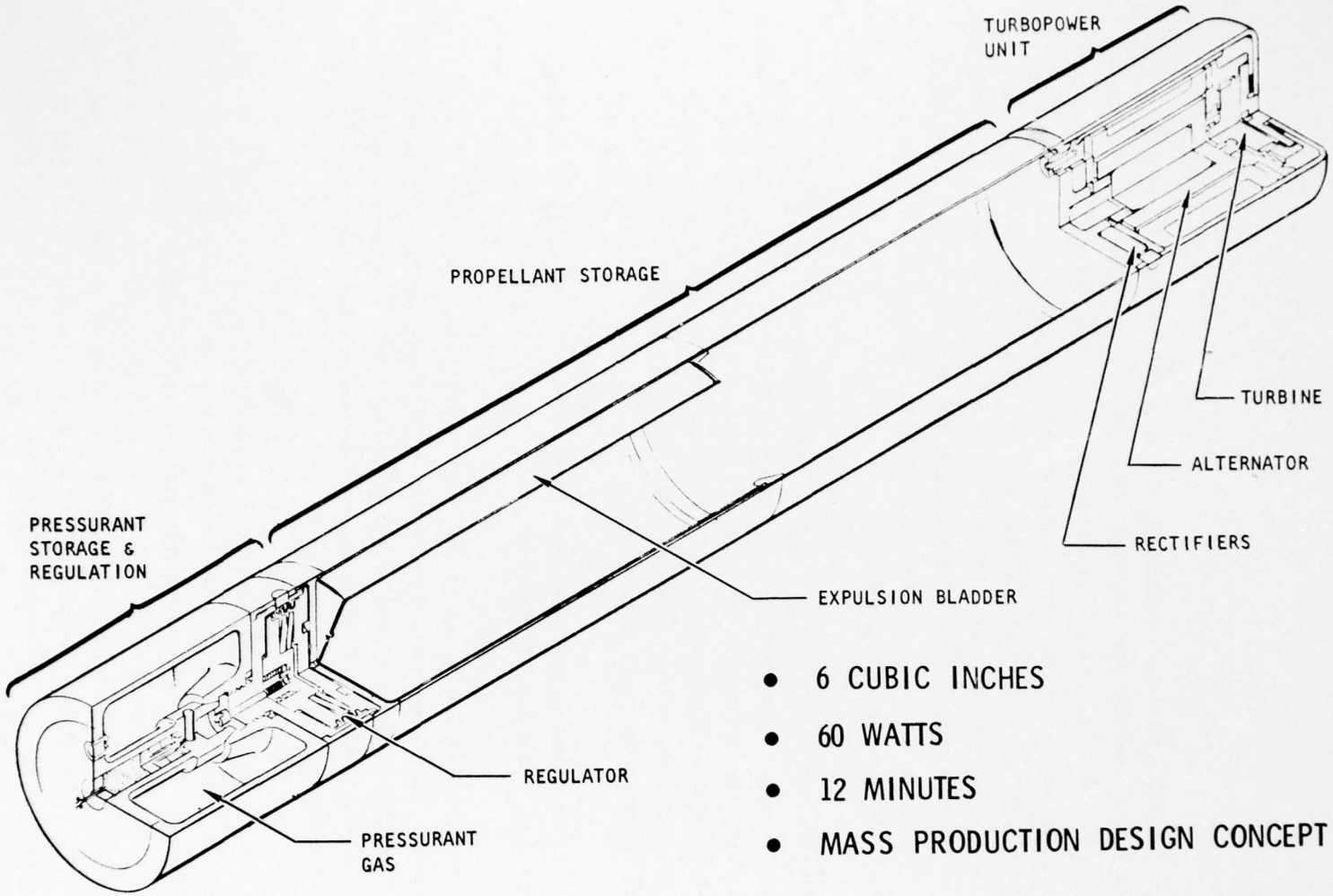

Figure 1. 60-Watt Power Source

PRELIMINARY DESIGN

A preliminary design analysis was made of the system components. Table 2 lists the design goals which were addressed in this task.

PROPELLANTS

The choice of MHF-5A as the most logical propellant was completed early in the program. Its selection was based on factors discussed in Ref. 1. This discussion is repeated here in slightly edited form to bring it up to date.

Liquid Propellants

Liquid propellant systems may be either of the monopropellant or bipropellant types. Bipropellants use two fluids, one a fuel and the other an oxidizer. Monopropellants involve only one component, usually a fuel which decomposes exothermically in contact with a catalyst. For some types of monopropellants, notably the hydrazine types, the exothermic hydrazine dissociation is followed by an endothermic ammonia dissociation (ammonia being one of the products of the hydrazine dissociation) which yields a gas in the required temperature range for turbines.

TABLE 2. COMPONENT DESIGN GOALS

Propellant(s): The propellant shall be chosen to provide the simplest system consistent with the other design goals. For this reason, propellants such as hydrazine and hydrazine derivatives, ethylene oxide, Otto fuel, and solid propellants should be considered.

Propellant Supply System: The propellant shall be stored in a tankage system capable of generating and maintaining the required hot gas generator inlet pressure.

Hot Gas Generator: The hot gas generator shall be capable of start-up at -65 F and stable operation at the required power level and temperature.

Prime Mover: The contractor shall investigate various prime mover designs and select a configuration which offers the best overall performance potential but which uses as much proven technology as possible.

Exhaust System: The exhaust products must be passed through reaction vanes which will provide sufficient reactive torque to prevent spinning of the entire power unit during free fall.

Controls: To minimize and hopefully eliminate the control system, the speed and output voltage of the power unit shall be inherently stable.

Generator: The contractor shall investigate several generator configurations and select a configuration which offers the best overall efficiency while maintaining the intent of the power conditioning requirement.

Power Conditioning: The contractor shall design the power conditioning required to convert the output of the generator to the required electrical output specified in Table I.

A survey of available monopropellants was undertaken. A number of restrictive requirements limit the available choices:

Volume. Based on the preliminary design, 3.624 cubic inches are available for propellant with a requirement of 12 watt-hours, and a probable system efficiency (turbine/alternator/gas generator) of 40 percent results in a minimum energy density requirement of about 8.5 wt-hr/in.^{3}.

Temperature. For the turbine to operate successfully for the ultimate goal of 40 minutes, gas temperatures must be maintained at reasonable levels. For the gas temperature upper limit, 2000 F has been selected with 1700 F as the design value.

Freezing Point. A design objective is startup at -65F. This greatly limits the available propellants because most have freezing points above this limit. Table 3 lists the freezing points of some candidate blends.

Clean Gas. Because of the very low power level, small passages and components are required. There is, therefore, some need for combustion gases free of contaminants that could clog these passages. Some compositions, especially those containing a large proportion of MMH (e.g., MHF-3 or M-86), have a tendency to produce free solid carbon in the exhaust. This carbon is very fine in size (submicron) but may deposit and cause buildup. Propellants with lesser tendency to produce carbon are desirable.

In addition to the hydrazine blends, monopropellants such as hydrogen peroxide, ethylene oxide, and Otto fuel have been considered. Hydrogen peroxide is one of the earliest and most developed monopropellants. However, its high freezing point (+31 F) precludes its use. Otto fuel also has a relatively high freezing point (-18 F). Ethylene oxide, while able to remain liquid at -65 F, has a tendency to form carbon.

TABLE 3. COMPOSITION AND FREEZING OF LOW-HYDRAZINE BLEND MONOPROPELLANTS

Designation	Composition, weight percent						Freezing Point, F
	N_2H_4	MMH	$N_2H_5NO_3$*	H_2O	NH_3	N_5H_5**	
MGGP-1	63		10	27			<-65
MHF-3	14	86					-65
MHF-5	26	55	19				~-43
MHF-5A	13	68	19				~-77
MHF-5B	23	58	19				~-48
MHF-6	18	72		10			<-67
MHF-7	14	81		5			~-65
MIXT-1	16	70	14				-65
MIXT-2	38				62		~-58
MIXT-3	28				63	9	~-58

*$N_2H_5NO_3$: hydrazine nitrate

**N_5H_5: hydrazine azide

The hydrazine blends which appear to come closest to meeting the general requirements, and which were evaluated, are shown in Table 3. Some do not quite meet the -65 F freezing point requirement. Others, such as MGGP-1, MIXT-1, -2, and -3 have low energy density. Figure 2 shows the energy density for MGGP-1 to be well below 8 W-hr/in.^{3}; MIXT-1, -2, and -3 fall in the range of 2 W-hr/in.^{3}. Experience with MHF-3 (also known as M-86) indicated that copious quantities of carbon are formed and it was decided not to use MHF-3 for the baseline system.

The addition of water as in MHF-6 and 7 reduces the tendency to form carbon, but also reduces the performance below acceptable standards.

MHF-5A appeared to be an acceptable selection. The freezing point is sufficiently low and detailed calculations have shown adequate performance. The tendency toward carbon formation is greatly reduced by the presence of oxygen from the hydrazine nitrate.

Three variations of MHF-5 were evaluated. While the freezing point of MHF-5 itself has been reported as -71 F, tests at Rocketdyne have shown approximately -43 F to be correct. The lower values appear to be due to supercooling. MHF-5A and 5B were investigated. The data confirmed the usefulness of MHF-5A for program application. Property data available are listed in Table 4.

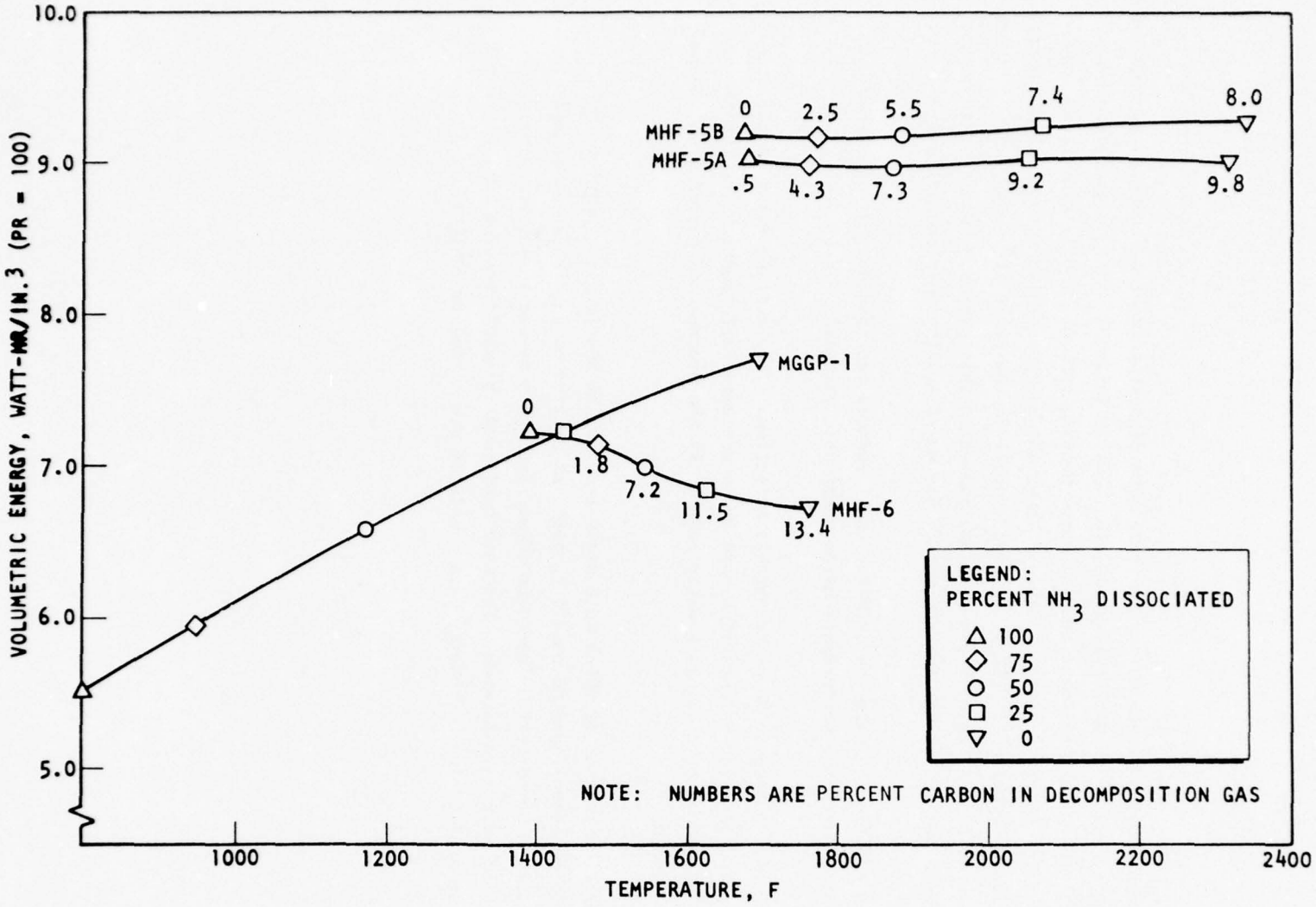

Figure 2. Energy Density of Hydrazine Blends

TABLE 4. PHYSICAL PROPERTIES OF MHF-5 MIXES

	MHF-5	MHF-5A	MHF-5B
Freezing Point, F	~-43	~77	~48
Boiling Point, F	207	-	-
Density, lb/ft^3			
at 77 F	-	62.2(E)	62.64
at 130 F		60.4(E)	60.83
Vapor Pressure, at 130 F, psia	3.8		
Heat Capacity, at 77 F, Btu/lb-F	0.677		
Viscosity, lb/ft-sec			
at -40 F	-	-	0.026
at 77 F	-	-	0.00133
at 130 F	-	-	0.00074
Thermal Conductivity, at 77 F, Btu/hr-ft-F	0.1819		

NOTE: These data were taken from Prepackaged Liquid Propellants Handbook, R-7556, Rocketdyne, Canoga Park, California, November 1970.

Performance figures for the MHF-5 blends are shown in Fig. 2. They are above 9 W-hr/in.^{3} and could provide sufficient energy density to make the 60-watt dynamic power source feasible.

To initiate propellant decomposition, either heat or a catalyst is required. For a one-shot expendable system such as the 60-watt power source, a catalytic initiation appeared to be the most reliable method. The most advanced hydrazine catalyst in use today is Shell 405 which is extremely expensive. However, the amount required is so miniscule that less than $1.00's worth would be needed. It would, of course, be desirable to eliminate this cost.

Tests have shown that while Shell 405 is excellent to initiate hydrazine decomposition, it is not as good when a blend such as MHF-5 is used. Tests conducted during Rocketdyne's Condor development showed that iodine pentonide (I_2O_5) is excellent for MHF-5, and is also considerably cheaper. Tests done on this program (reported later in this report) indicated proper initiation, but the reaction in the bed was poorly sustained because of the configuration of the bed. As will be discussed, this is merely a configurational problem and is susceptible to solution.

The Condor program also yielded data on long-term storage of MHF-5. Storage in aluminum and in 321 CRES vessels was undertaken. Very small ullage volumes (2 percent at 160 F) were used. In CRES, pressure rise was significant--185 psi in 8 months. However, in aluminum (type 2219), 24 months of storage showed a rise of only 5 psi at ambient temperature, and 125 psi at 130 F. It must be remembered that these figures relate to very small ullage values. These data indicated that storage will be possible with proper material selection.

In addition to the monopropellants, bipropellant combinations also were reviewed. While the Rocketdyne-developed chemical APU for the Army utilized a bipropellant combination very successfully, it is doubtful if the volume and ultimate cost objective of the current program could be met with a bipropellant system. Two sets of valves, regulators, and tanks would be required. Also, bipropellants are inherently more energetic, operating at higher temperatures than monopropellant systems. (The chemical APU operated at a gas temperature of about 2700 F.)

Solid Propellants

Rocketdyne's McGregor Division was consulted for possible solid propellants that could be useful, and a survey was made of available formulation that could be applicable. The major restraint was that most solid propellants burn at high temperature, temperatures below 2000 F being unusual.

However, even these low-temperature propellants have acceptable energy densities, values ranging between 10 and 12 W-hr/in.^{3}. As discussed above, this was slightly higher than the energy density for candidate liquid propellants, but here the problem was configurational. At a chamber pressure to 500 psia, the linear burning rate for the applicable solid propellants ranged between 0.055 to 0.18 inch per second. Assuming an end-burning configuration to provide maximum utilization of the propellant volume, the grain shape resulting ranged from a 0.39-inch-diameter by 40-inch-long cylinder to a 0.21-inch diameter by 130 inches long. Some form of helical or sequential burning stackup would be needed to accommodate this requirement.

It was not evident that the configuration problem could lend itself to ready solution.

PROPELLANT SUPPLY SYSTEM

For simplicity and volume conservation, a system employing gas pressurization and diaphragm expulsion was selected. High-pressure helium was stored and expanded through a pressure regulator to 650 psi. At this pressure it acts on an elastomeric diaphragm which folds back on itself to expel the hydrazine blend from the tank. Figure 3 shows the concept.

Pressurant Gas

Pressurization is usually accomplished with either helium or nitrogen, both being inert gases. Nitrogen has the advantage of storing better over long periods, but

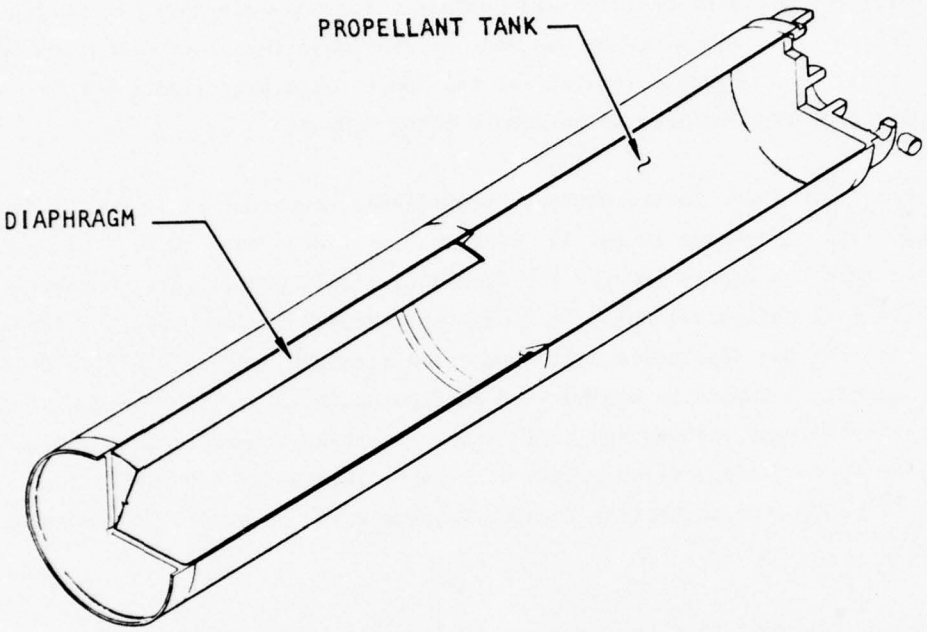

Figure 3. Propellant Tankage Module

it suffers from nonideal compressibility at high pressure. The design of the pressurant tankage must take into account temperature extremes to be encountered. If the tank is filled with a fixed quantity of gas, its pressure will rise as the temperature rises. Therefore, the tank must be stressed when the gas temperature is 130 F. On the other hand, when the tank is chilled to -65 F, the pressure must remain sufficient to expel all of the fuel, i.e., to incur the same volumetric change. Since

$$pV = ZMRT$$

where

p = pressure
V = volume
Z = compressibility factor
M = mass of gas
R = gas constant
T = absolute temperature

and V, M, and R remain constant,

$$p \propto ZT$$

As seen in Fig. 4, values for the compressibility factor for nitrogen are high because $T_r = 2.60$ at 130 F and 1.74 at -65 F, and critical pressure ratios are in the range of 6 to 30. For helium, on the other hand, $T_r > 20$ and p_r varies from 20 to 100 as storage pressure changes from 3000 to 15,000 psi, making Z nearly constant at about 1.1.

Table 5 lists typical results for the two gases.

Expulsion of the liquid is very slow. Data available from tests made show that, for typical rates involved here, the polytropic exponent (n) is between 1.01 and 1.02. Liquid volume which can be expelled at -65 F is shown in Fig. 5 for the

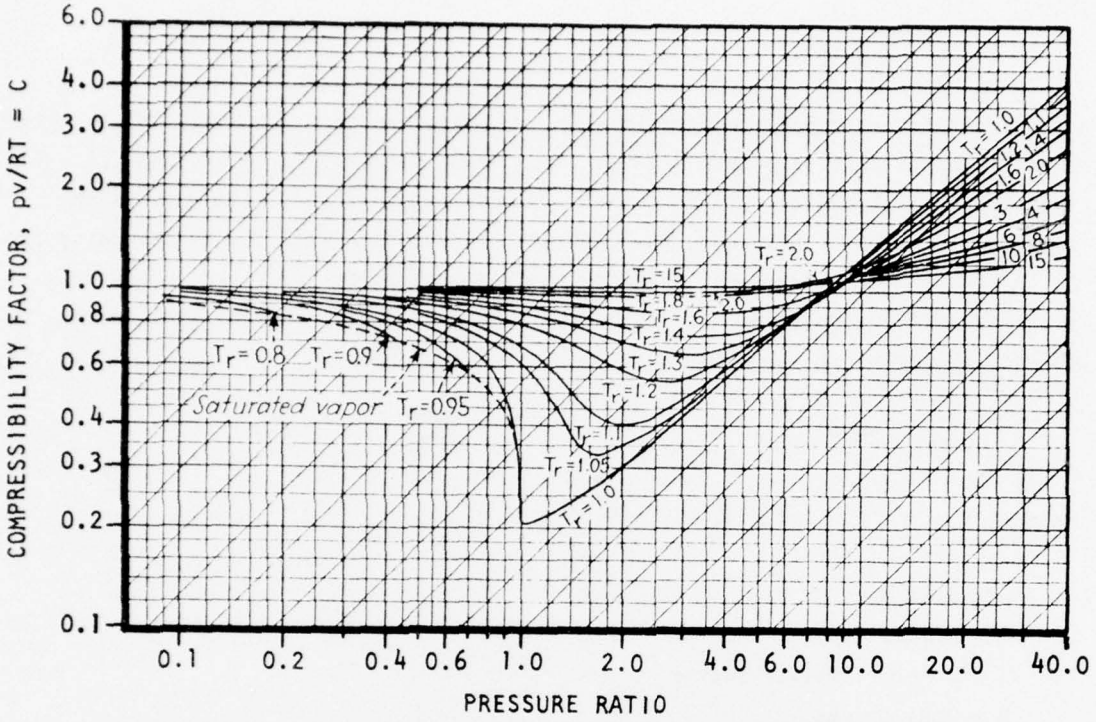

Figure 4. Compressibility Factors for Gases

TABLE 5. PRESSURANT SUPPLY MODULE PRESSURE VARIATIONS

Storage Pressure Maximum at 130 F, psia	Pressure at -65 F, psia	
	Nitrogen	Helium
3,000	1870	2,010
5,000	2940	3,350
8,000	4400	5,356
10,000	5430	6,695
12,000	5965	8,035
15,000	7210	10,050

two gases for two fuel pressures. Helium appears superior, especially at high storage pressure where nitrogen compressibility becomes a major factor. The influence on pressure level regulated to is also apparent.

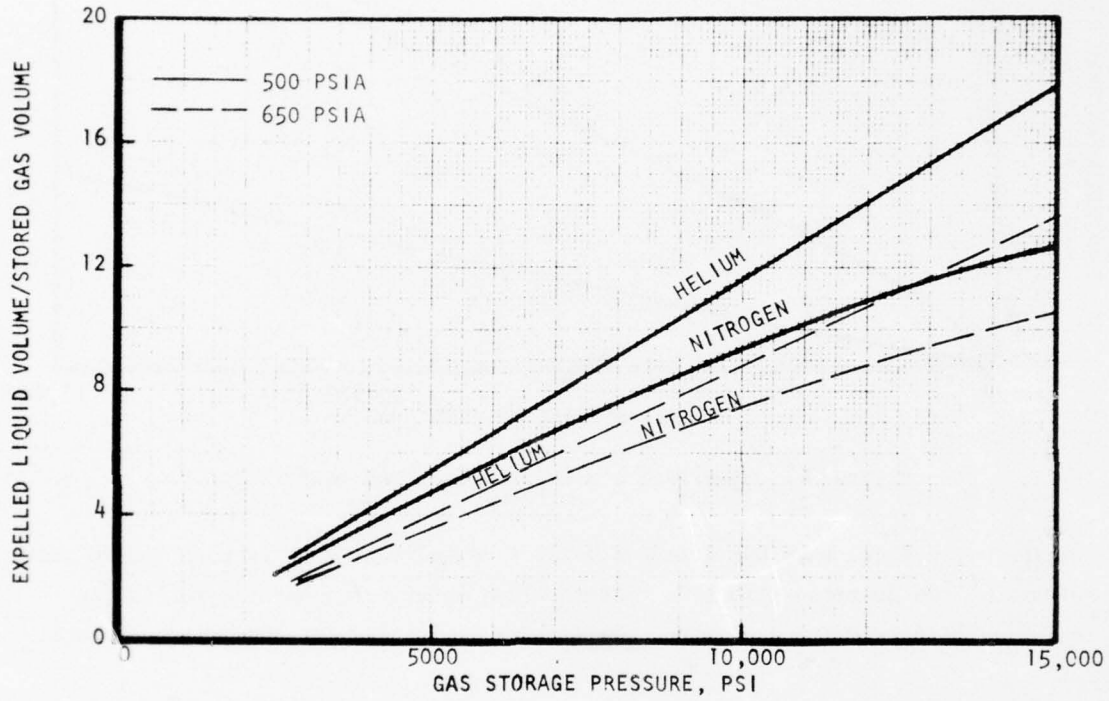

Figure 5. Comparison of Liquid Volume Expulsion

Gas Storage Tank

For volume conservation, a tradeoff is required between minimum wall thickness and internal pressure at the stress level selected. Naturally this is highly dependent on the available space for installation. Normally, spheres yield the minimum volume as far as the tank is concerned (Fig. 6), but if the sphere is then installed in a cylindrical or cubical space, the corner volumes may well go to waste.

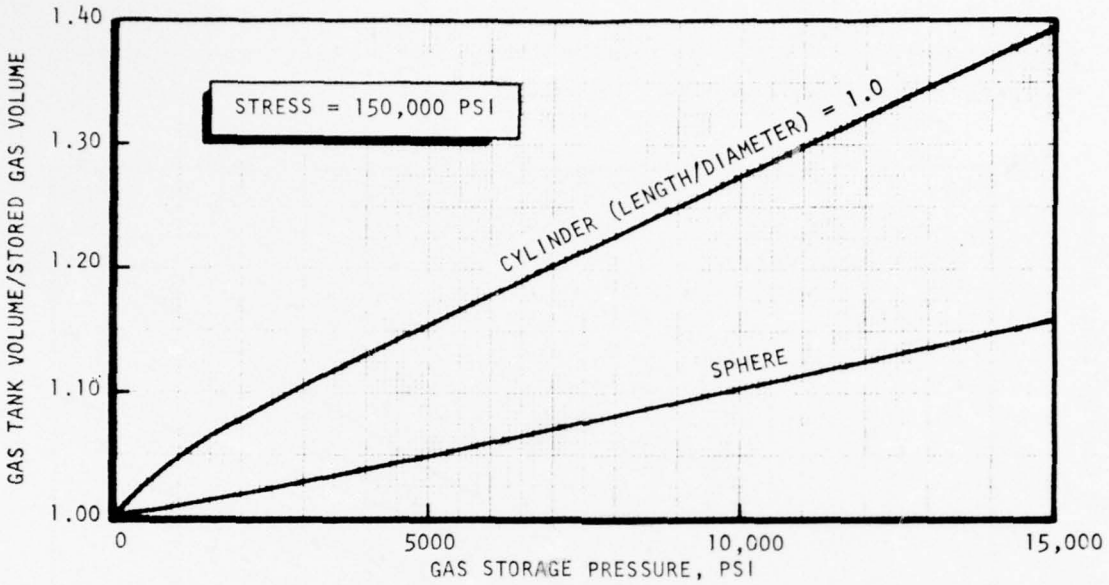

Figure 6. Spherical and Cylindrical Tank Comparison

For the cylindrical envelope selected here, a cylindrical tank is most volume conservative. To decrease stress, a center column is utilized and the initiating squib is built into the structure. Walls have been sized for 8000-psia pressure.

Pressure Regulator

The pressure regulator must control a variable inlet pressure as the gas bleeds down to a constant 650 psia ±5 percent. Because no active controls are desired, the regulator must be self contained.

Rocketdyne conducted a preliminary feasibility study reported in Ref. 2 which is attached in the Appendix. The conclusion was that such a regulator was

feasible but that a company specializing in such devices was to be contacted for a more detailed appraisal.

Contact was established with Mr. Hans Eckardt, who at that time was President of Pyronetics of Santa Fe Springs, California. Their chief designer, Mr. Richard Martin, confirmed the feasibility of the concept, based on similar regulators designed by him for breathing systems.

Propellant Tankage

The consumption of propellant is dependent on power level, run duration, and prime mover efficiency. The volume of the tankage containing the propellant depends, in addition, on the shape of the tank and the effectiveness of the expulsion system. If expulsion is inefficient, that is, if propellant remains at the end of the run, excess propellant must be stored.

Expulsion from the propellant tank depends on the collapse of an elastomeric diaphragm. For the configuration selected, the diaphragm is a sleeve which is expected to fold back on itself under the action of the helium. Long-term storage of various promising elastomers has been under way at the Rockwell International Space Division for a number of years. Long exposure times have indicated that acceptable materials are available (Ref. 3).

Initiator

The initiation is the result of an electrical signal triggering a small squib located in the post of the gas storage tank. This drives a pin through two diaphragms and permits gas flow to the regulator. Simplicity and compact design are thereby maintained.

GAS GENERATOR

Gas generator design was based on the use of a catalytic bed consisting of Shell 405 catalyst. The design considerations are shown in Ref. 4, presented in the Appendix. Basically this design concept was followed in the program, although testing showed some changes were required to get more positive initiation. Test results are discussed later in this report.

PRIME MOVER

Prime mover design represents the most crucial aspect of the 60-watt power source design. Small volume and high efficiency are requisites.

The prime-mover output must be capable of rotating a high-speed electrical generator. Utilizing a reciprocating device appeared to be out of the question because of the poor speed match with the electrical generator. A rotary expander appeared to be more naturally suited to this application.

Of course, the rotary expander can be other than a turbine. Positive expansion can be obtained with a Roots type of machine or a Wankel rotor. The problem to be surmounted here is one of maintaining clearances small enough to prevent excessive leakage. Wankel-type engines have had this problem historically on the face of the rotor and across the tip of the rotor lobe. At the small size required here, this problem would have been greatly magnified because the clearance ratios were very large.

Clearance and geometric problems also cause problems in a turbine prime mover. For the extremely small flows involved, blade heights are very small and clearances are large relative to blade height. Also blade thickness, especially at leading and trailing edges, will be prohibitively high. Precise positioning will also be required.

One type of turbine appeared to be relatively free from these defects, the Terry-type turbine. Figure 7 shows the wheel constructed for this application. The high-speed jet is directed into the side of the semicircular, nearly tangential bucket and is turned 180 degrees. If a proper return channel is cut into the housing, the jet can be turned again to take a second pass, thereby increasing momentum exchange with the wheel. No close clearances are required to position the jet, and no extreme stress problem requiring contoured wheels is encountered.

Research work on Terry-type turbine design is quite limited. Reference 5 is one of the few reports which present test data. However there were strong indications that 40-percent efficiency is achievable. While this may sound low, simple analysis shows why not much more can be expected.

The gas to be expanded is very energetic. Only in this way can flow be kept minimal and fuel storage be kept small enough. When this high energy level is converted to kinetic energy in the nozzle, a high-speed jet results (6600 ft/sec). Stress, life, and design considerations dictated that turbine tip speed should be kept below 1500 ft/sec; a conservative 1200 ft/sec has been chosen for this design. The critical jet-speed ratio (u/c_o) is therefore 0.18. This means that under the most ideal conditions possible (no friction losses in the passages) the velocity leaving the turbine (c_3) will be 64 percent of the spouting velocity, or the leaving energy will be 41 percent of the available energy. The maximum possible efficienty, therefore, will be 59 percent. When losses are added in, 40 percent is not unreasonable.

Efficiency can be increased if the flow is allowed to repass through the blades to permit extration of additional energy from the second momentum interchange. Figure 8 shows that the leaving energy is thereby decreased.

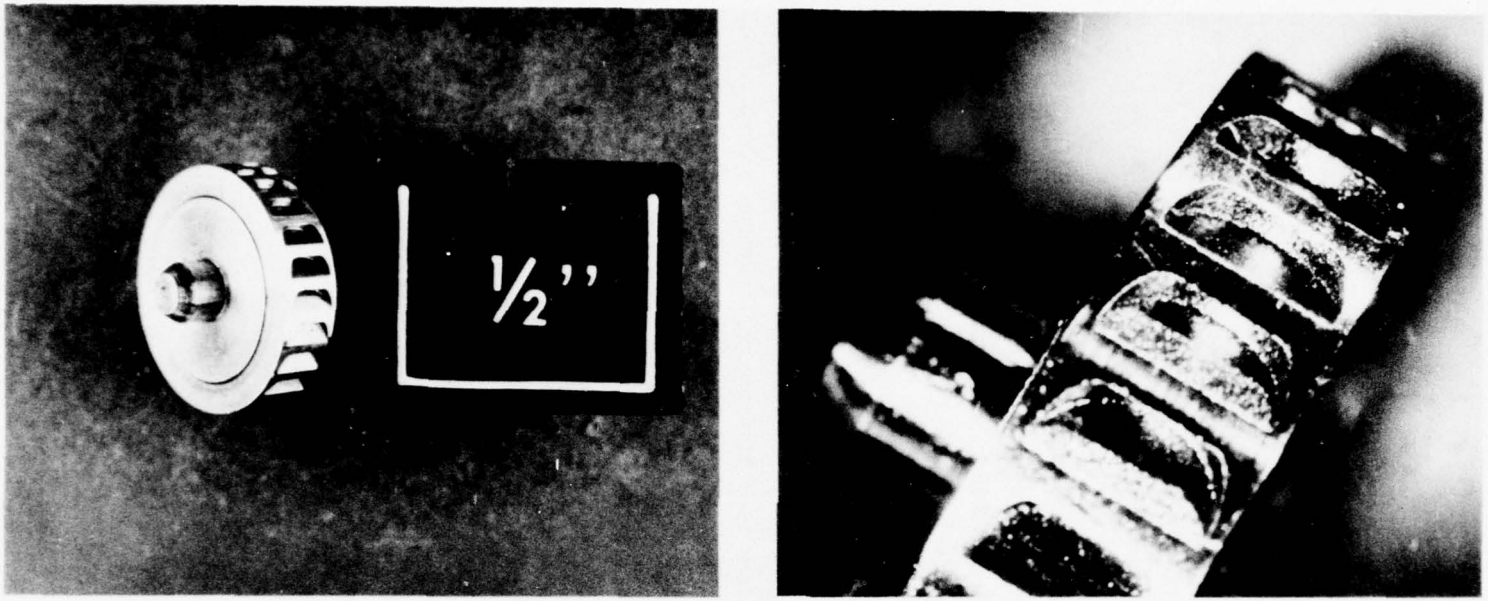

TURBINE WHEEL

- 0.50-INCH DIAMETER
- 550,000 RPM
- 1200 FT/SEC TIP SPEED

Figure 7. 60-Watt Power Source

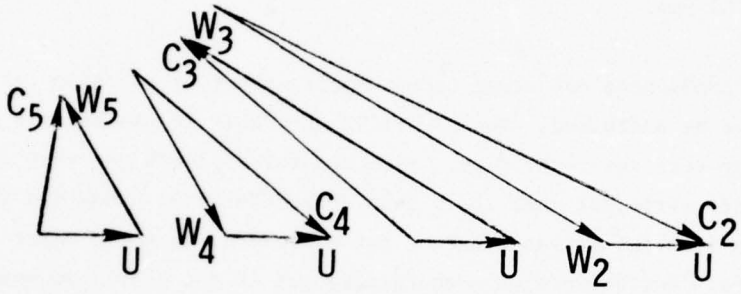

$$\left(\frac{C_5}{C_3}\right)^2 < 0.25$$

Figure 8. Velocity Triangles

A tip speed of 1200 ft/sec requires very high rotative speeds. Here again packaging considerations play an important role. With the 1-inch-diameter envelope, the turbine is limited to approximately 0.5-inch diameter, resulting in a rotative speed of 550,000 rpm. If the package permited a 1-inch diameter, speed would be reduced to 275,000 rpm.

Basically such speeds need not cause undue concern but they do raise certain issues which must be addressed. Dental drills currently in use operate above 250,000 rpm under very severe service. Side and thrust loads are very large, and safety aspects are stringent when it is considered that this hand-held tool operates only inches from the patients brain; but efficiency is not a major factor in these machines. Furthermore, the energizing jet is not nearly so energetic, meaning that the turbine operates at higher values of u/c_o.

The issues of primary concern are:

Critical speed	Bearing design
Rotor balancing	Windage and drag power

Critical Speed

It was logical to expect that the unit would pass through at least the first and second critical speed in reaching 550,000 rpm. The exact location of these critical speeds depends on the bearing stiffness and configuration. Each design must be evaluated individually.

Rotor Balancing

One of the questions was whether sufficient precision existed in the rotor fabrication to avoid the need for balancing. If balancing was required it would have to be done with the bearings to be used in the installation. The smallness of the rotor and the high speed would make balancing difficult and costly, and it should be avoided if possible. Dental drills usually are not balanced. Here it was anticipated that balancing would be required.

Bearing Design

During the preliminary design, various types of bearings were considered. Eventually many of these were tested, as will be detailed below.

Basically, ball bearings and fluid-film bearings are applicable. Very small-diameter ball bearings are used in instruments and also in the high-speed dental drills. However, these bearings were expected to have excessive power absorption. Fluid-film bearings, especially those using a gaseous film, would be less power consumptive. Therefore, the preliminary design was based on gaseous fluid film bearings. At first, plain hydrodynamic bearings were proposed. For these, the load-carrying film is formed by displacing the shaft radially in the journal. They dissipate the least power because only viscous shear and very small pumping losses are involved.

The problem which developed with these bearings was a lack of stability due to misalignment. Because of the very small diameter involved (approximately 0.10 inch) clearances had to be kept very small. It was, of course, impossible to align both bearings perfectly, so that some misalignment was inevitable. This induced excessive forces resulting in loss of stability at high speed.

The second design considered used the alternator as the bearing for the rotor. Because of its larger diameter, misalignment problems were reduced, but power dissipation was greatly increased.

The third bearing type evaluated during the preliminary design was a three-lobe bearing. This bearing provides three circle arcs, offset from the journal center, as shown in Fig. 9. A natural film wedge is formed even as the shaft stays centered. Stability is greatly improved at a slight cost in power dissipation. Eventually this bearing proved to be the best solution. Reference 6 was used for the designs.

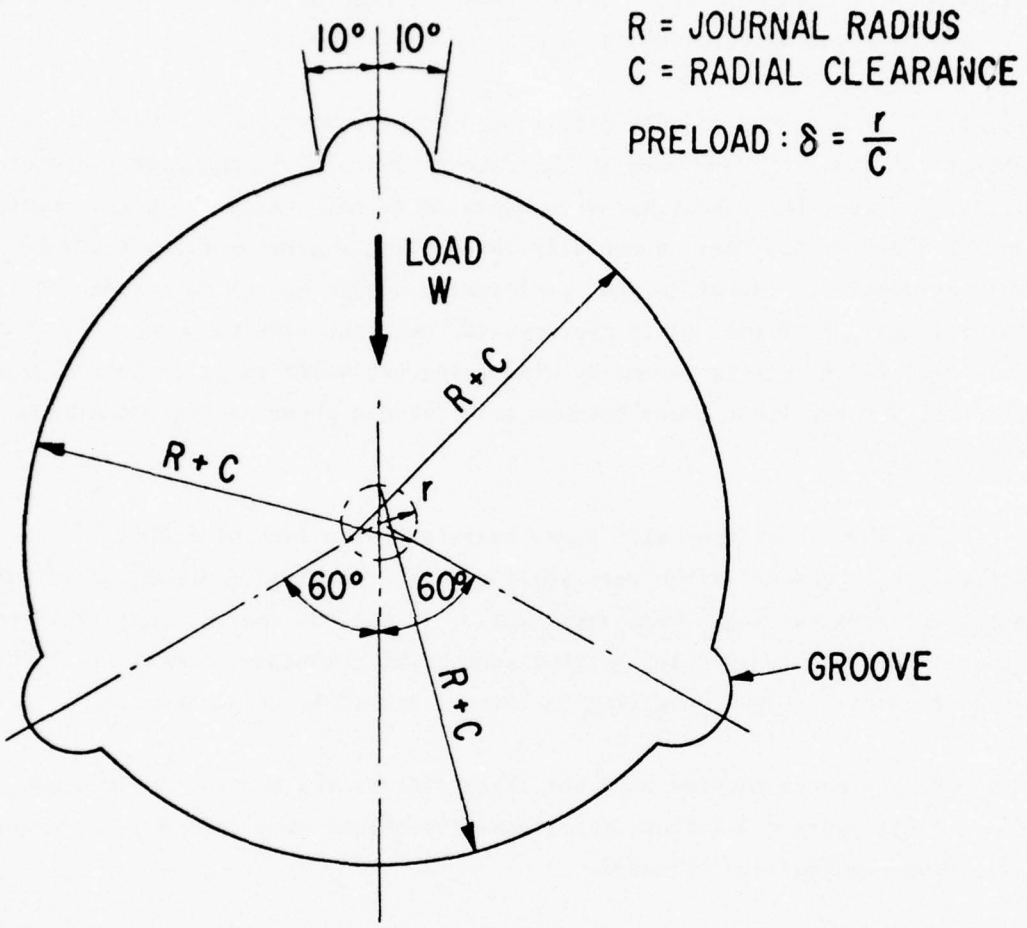

Figure 9. Three-Lobe Bearing, Schematic

Windage and Drag Power

The power dissipation in the bearings and from windage was felt to be the major losses to be accounted for in the aerodynamics design of the unit. Windage losses were expected in the turbine and the alternator rotor. By proportioning the clearances to optimum values, these losses were reduced as far as possible.

ALTERNATOR

Because of the small size and the high-speed requirements, a permanent-magnet alternator was selected. To obtain sufficient power, rare-earth magnets were selected for the design. Reference 7 in the Appendix discusses the design considerations.

Basically, the rare-earth magnets have low tensile strength. At high rpm, centrifugal forces would be sufficient to cause the samarium cobalt magnets to fail. Therefore, a design concept in which the magnet is encapsulated into a metal sleeve was used. The sleeve was expanded with a mandrel before the magnet was introduced so that the magnet was precompressed, allowing larger tensile forces to be applied. In this configuration the magnet was a 0.3-inch-diameter cylinder in a 0.5-inch-diameter sleeve. The sleeve being nonmagnetic caused little interference. However, because this introduced a very wide gap between the magnet poles and the stator winding, power output proved to be very marginal.

A new design concept using a sleeve made of magnetic and nonmagnetic materials was developed. The new rotor consisted of six pieces welded together so as to provide magnetic pole pieces of 4130 SAE steel over the poles and nonmagnetic Rene' 41 pieces between them and over the ends. The poles were thereby transformed to the rotor outer diameter, increasing the flux density in the stator coils (Fig. 10 through 12). With this arrangement, successful tests were made.

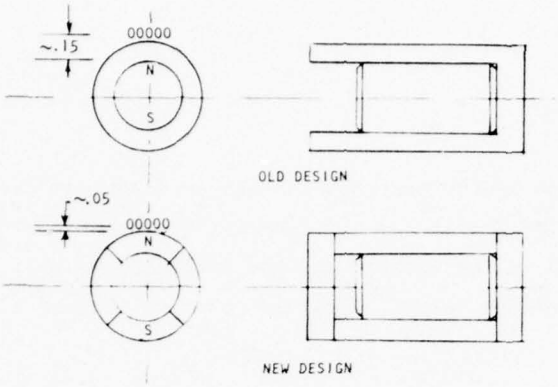

Figure 10. Magnetic Rotor Configurations

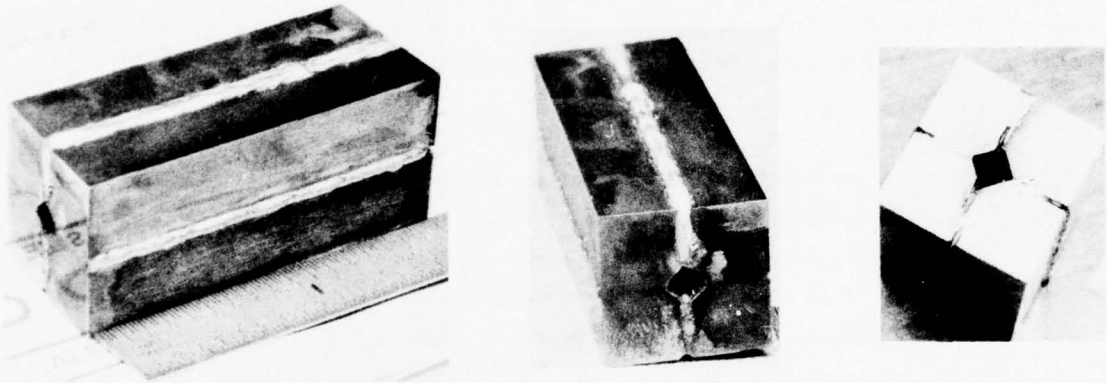

ORIGINAL WELD OF RENE 41 AND 4130 SAE

SECOND MACHINING STEP AFTER ANNEALING

Figure 11. 6-Piece Rotor Assembly, Original Weld and Second Machining

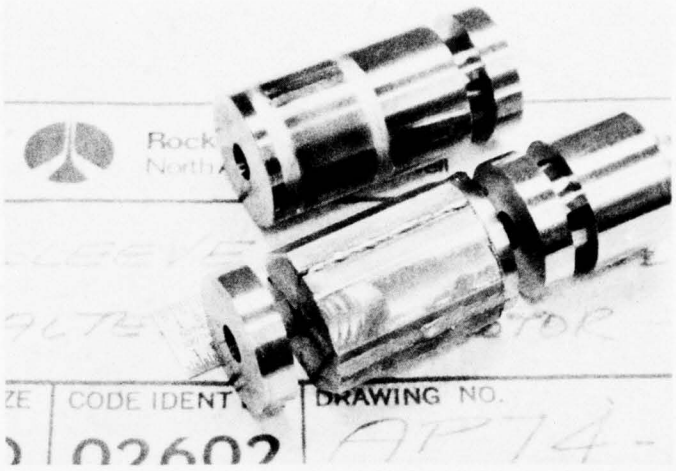

ROTOR COMPONENTS FOR FINAL WELD

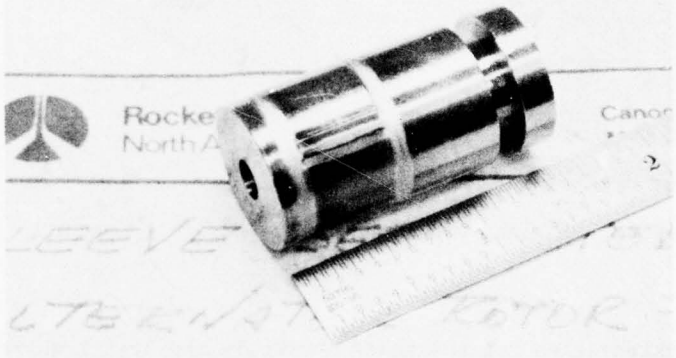

ROTOR ASSEMBLY AFTER HEAT TREAT BEFORE FINAL MACHINING

Figure 12. 6-Piece Rotor Assembly, Final Weld and Final Machining

Subsequent to the initial testing of the alternator, a commercial product designed and built by Hamilton Technology Inc., a subsidiary of HMW Industries (formerly Hamilton Watch Company) was brought to Rocketdyne's attention. Figure 13 and Ref. 8 through 11 describe a unit supplied to Rocketdyne using a 60-watt turbine. This unit provided to require very high starting torque because of its internal configuration. However, the working relationship established led to Hamilton Technology supplying platimum-cobalt magnets for later testing. These magnets are very strong, both magnetically and in tensile properties. Therefore, the magnet can be used without any sleeve for support. The unit operated successfully at the end of the program. The magnet was 0.4-inch diameter with a 0.125-inch-diameter hole through the center for a supporting shaft.

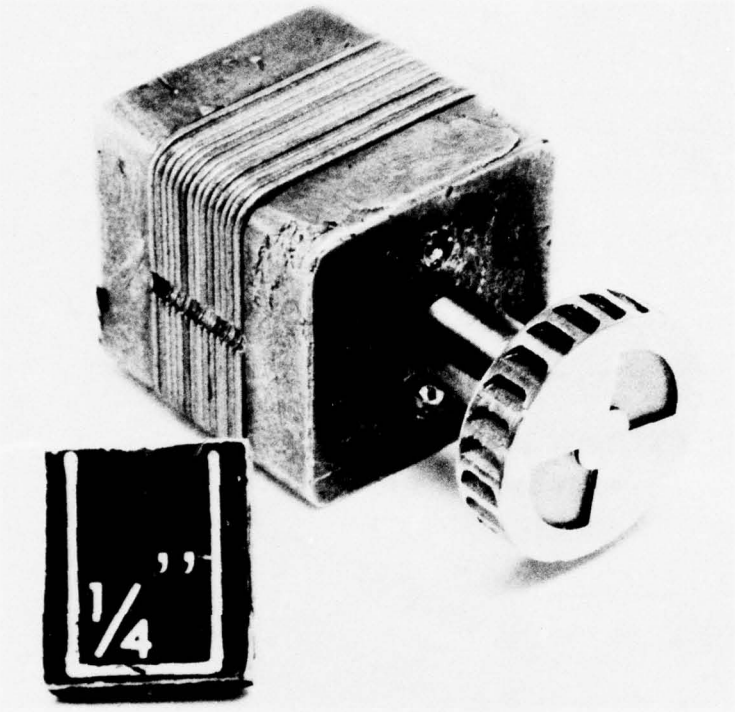

Figure 13. Hamilton Technology, Inc., Alternator

HEAT TRANSFER

A major design consideration for the power source is the heat transfer within the unit and from the unit. Reference 12 in the Appendix shows some calculations performed to determine how much insulation might be required to maintain low heat transfer to equipment around the power source. It may well be necessary to place considerable amounts of insulation around the unit unless it can be installed away from heat-sensitive gear such as electronic components.

The hot gases impinging on the turbine also would serve to heat the turbine disk. It was, therefore, necessary to minimize heat flow down the shaft to the alternator. This was especially important for the permanent-magnet rotor because of loss of magnetization at elevated temperature (Curie point).

A number of different techniques were attempted during this program. The preliminary design utilized a special heat barrier joint between the turbine and the rotor, Fig. 14, Section D-D. This joint has a stub shaft on the turbine

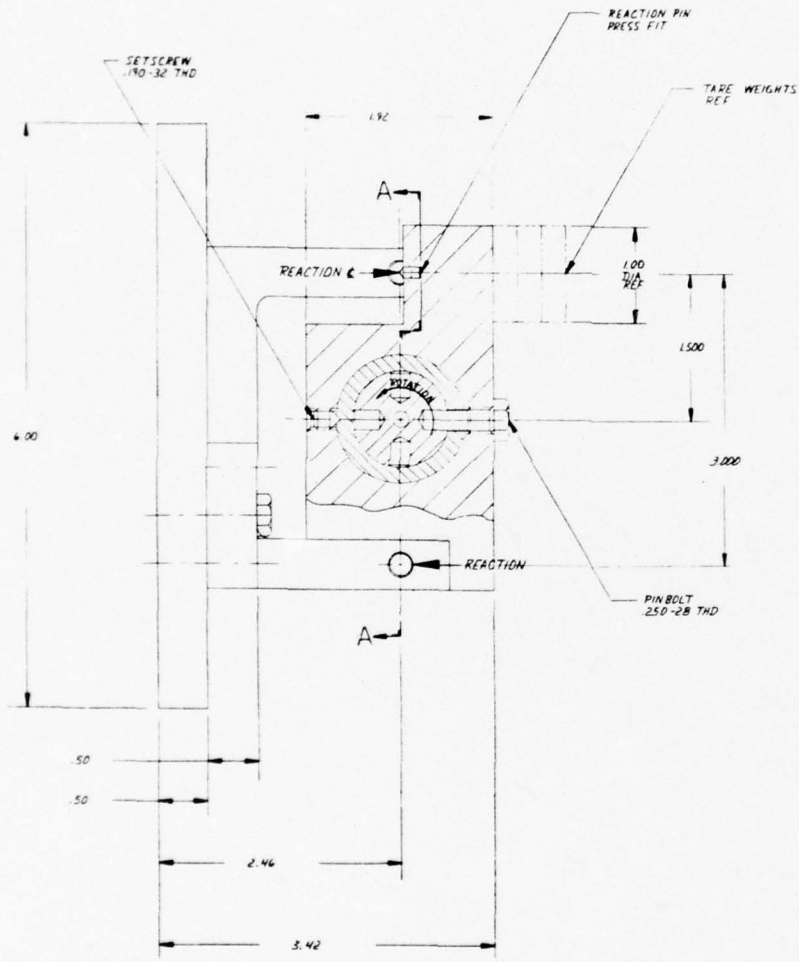

PARTIAL SECTION B-B

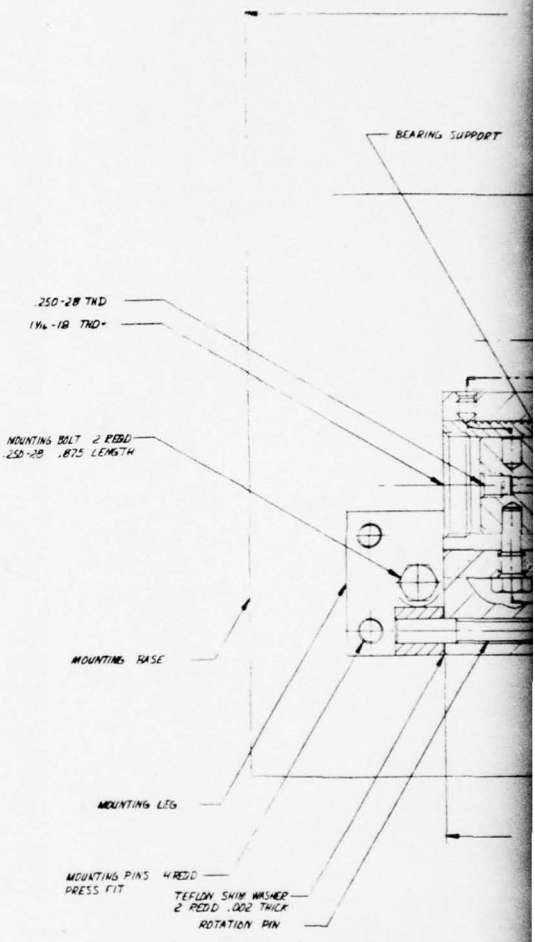

TURBINE

SECTI

(PORTIONS RE

TURBINE OUTPUT PERFORMANCE TEST RIG

SECTION A-A

(PORTIONS ROTATED INTO VIEW)

WINDAGE & FRICTION MEASURING TEST SETUP

ALTERNATOR LOSS MEASURING TEST SETUP

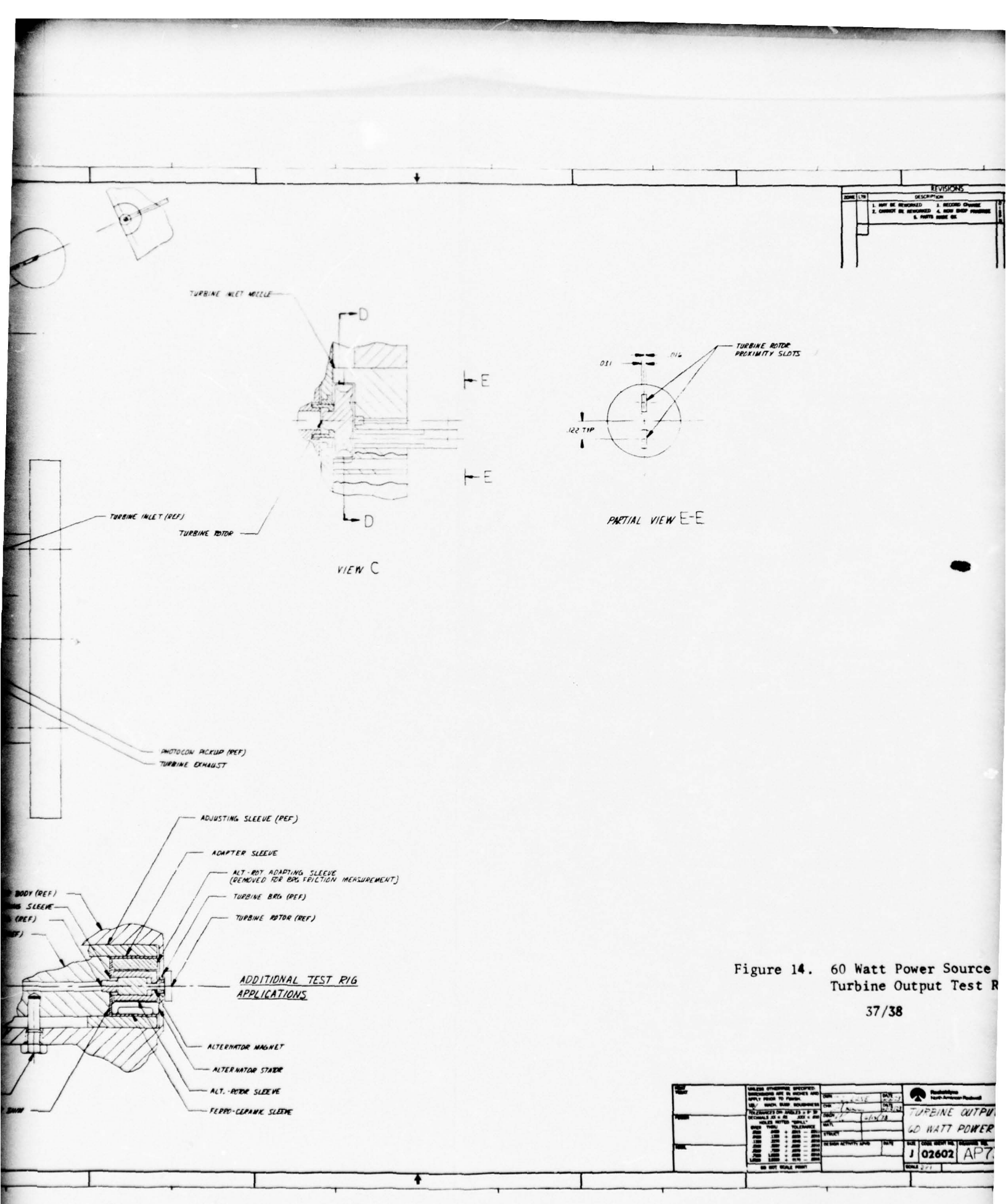

Figure 14. 60 Watt Power Source
Turbine Output Test R

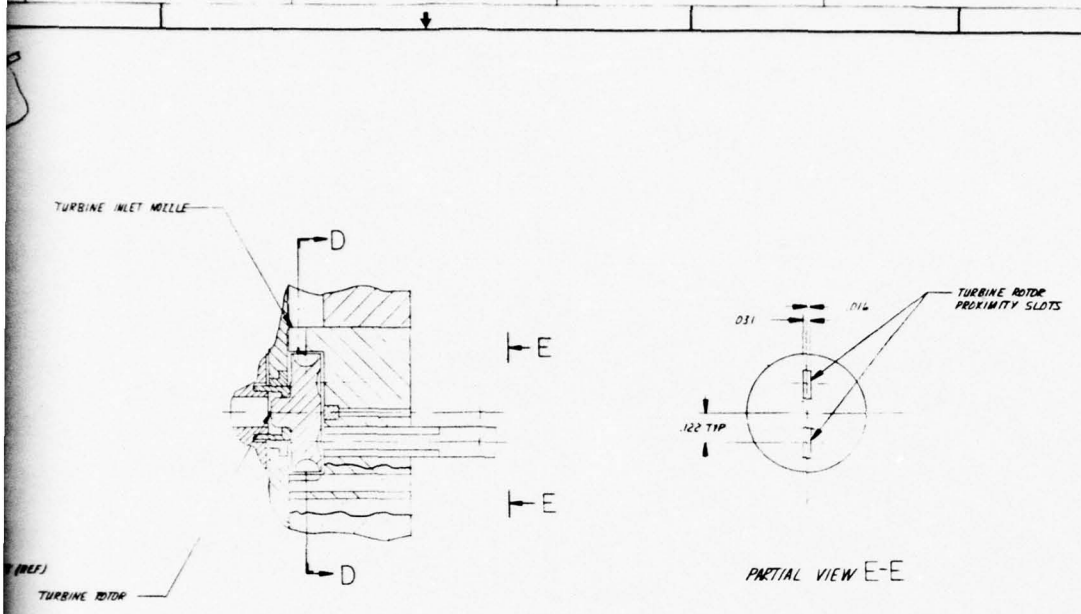

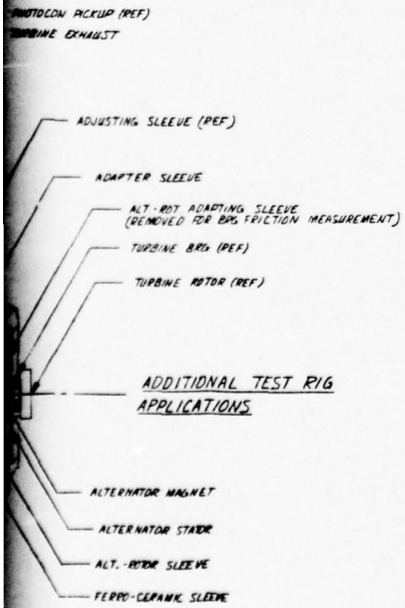

Figure 14. 60 Watt Power Source Turbine Output Test Rig

which is pressed into a sleeve on the rotor. Contact between the two is kept to a minimum. It was found that this joint was too complex to maintain accurate alignment. Later designs utilized flexibile shafting to provide sufficient impedance. Tests showed that a temperature gradient of over 1000 degrees per inch resulted.

The flexibile shaft, while an excellent heat barrier, proved to influence stability adversely and was replaced by a threaded shaft. In this configuration both the turbine and magnetic rotor had through-holes just slightly smaller than the thread O.D. When mounted, the thread tips were slightly deformed but resulted in very minimal contact between the turbine or magnet and the shaft. A large impedance to heat flow was thus formed, preventing heat from flowing from turbine to shaft or from shaft to magnet. Results with this configuration were even better than expected in test.

SYSTEM DYNAMICS

A high-speed rotating assembly will pass through various critical speeds on acceleration. If the unit is perfectly balanced; that is, if the geometric and mass center are exactly identical, then no adverse effects would be noted. In real life, such perfection is impossible; there always is some discrepancy between the two. Therefore, the unit cannot operate without vibration. By minimizing the distance between these centers, vibration and the forces generated can be kept to acceptable limits.

For the 60-Watt Power Source rotor, a balancing goal of 5 to 10 microinches was established. This, of course, is difficult to achieve and requires expert balancing work. It required that the rotor be balanced in its own bearings at relatively high speeds, and machines which have the required sensitivity and capabilities are in limited supply.

The capability to do the balancing is available to Rocketdyne and steps were taken to utilize it. One of the problems which became evident early was that the presence of the very strong magnet influenced the readout equipment, and particles generated by material removal stuck to the rotor and influenced the

balance. This problem was solved by having Hamilton Technology deliver the rotor material, sized but unmagnetized. The rotors were assembled and balanced, after which they were returned for magnetization. In this way, adequate balance was achieved.

As mentioned elsewhere, initial attempts were made to operate without balancing in the hope that very small, inherently symmetrical parts could operate without problems. This failed to be the case. Dynamic balancing was essential for proper operation of the units.

TEST PROGRAM

The original purpose of this phase was to demonstrate the best overall specific propellant consumption readily achievable by a machine of this power level. The test program was to result in the measurement of the specific propellant consumption of the prime mover at design power, speed, and temperature. All tests were to be run under prevailing ambient conditions at the contractor's facility and test hardware of the actual size and configuration was to be used for these component tests. Specifically, the following component test program was to be completed, and is quoted from the Statement of Work.

Hot Gas Generator: A hot gas generator of the required size and design shall be fabricated and tested to demonstrate stable operation with the selected propellant. Measurement of the propellant flowrate, inlet and exhaust pressure, and inlet and exhaust temperature shall be made.

Electric Generator: The efficiency of the generator shall be measured at design speed. Bearing and windage losses shall be measured. This test shall determine the generator input shaft power versus output electrical power.

Hot Gas Generator, Prime Mover and Electric Generator Assembly: This assembly shall be tested to determine the efficiency of the unit. The goal of this testing will be to achieve the minimum specific propellant consumption. Measurements of propellant flowrate, electrical power output, inlet and exhaust temperature, inlet and exhaust pressure, and speed shall be made. In addition, a demonstration and start-up at -65 F after 4 hours cold soak at -65 F shall be performed.

The measurement of turbine efficiency, friction, and windage is best done by testing the unit with warm gas, which makes instrumentation simpler, and permits long-term operation. Of course, the tests must be made under dynamically similar conditions. For the turbine, similarity considerations are discussed in Ref. 13 in the Appendix as part of the original test plan for this program.

As far as the warm gas similarity tests are concerned, analysis showed that the closest modeling would be achieved if CO_2 were used as the test fluid, primarily because the ratio of specific heats would be matched better. Most importantly, the test speed for matching of the velocity transfers would be 170,600 rpm. Details are found in Table 1 of the Test Plan, reproduced here as Table 6.

The test plan discusses in detail the tests contemplated for this program phase. An all-purpose test rig for these tests was fabricated. Unfortunately, it proved to be too comprehensive and complex, and data sufficient for the complete analysis were not obtained. The program therefore had to be redirected to reduce some of the scope of testing to conform with a less ambitious schedule and less sophisticated test hardware. Results indicating that turbine performance requirements can be met and that hot-gas operation is feasible were obtained in this way.

TEST RIG

A comprehensive test rig, which was to have been capable of completing all the tests listed in the Test Plan (Ref. 13), was designed and built. Relatively simple in concept, it proved to be too cumbersome in operation and had to be abandoned.

The concept involved absorbing all of the turbine output by shearing the air film around a drum to which the turbine was attached. In effect this is like a prony brake which substitutes fluid shear for mechanical friction. The test rig housing, pivoted along one edge, would react under this shearing torque and would attempt to deflect, thereby registering a force on a strain transducer. Figure 15 shows this schematically and Fig. 16 is an isometric of the test rig, with the hardware shown in Fig. 17

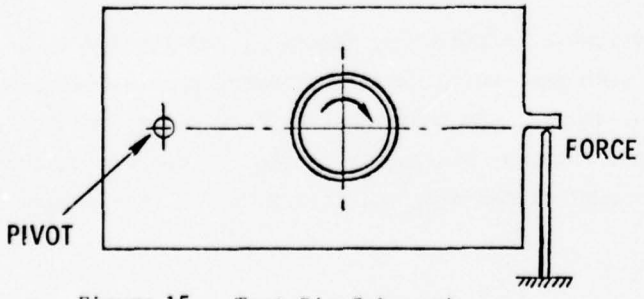

Figure 15. Test Rig Schematic

TABLE 6. TEST COMPARISONS

Test Conditions	Prototype	Model	
		N_2 at 1000 R	CO_2 at 640 R
Operating Quantities			
Inlet Temperature, R	2225.4	1000	640
Inlet Pressure, psi	500	2000	400 (54.3)
Pressure Ratio	100	140	100
Gas Ratio of Specific Heat	1.284	1.41	1.285
Rotative Speed, rpm	550,000	261,100	170,600
Derived Quantities			
Adiabatic Head, feet	684,095	154,200	65,850
Spouting Velocity, ft/sec	6637	3151	2059
Tip Speed, ft/sec	1200	570	372
Weight Flowrate, lb/sec x 10^4	1.919	16.49	4.920 (0.668)
Volume Flowrate, cu ft/sec	0.05659	0.03064	0.01472
Geometric Quantities			
Nozzle Throat Area, $in.^2$ x 10^5	4.927	4.927	4.927
Nozzle Throat Diameter, inch	0.00792	0.00792	0.00792
Nozzle Expansion Ratio	10	10	10
Similarity Parameters			
Specific Speed	5.5	5.87	5.03
Jet-Speed Ratio	0.1808	0.1808	0.1808
Mach Number	3.53	3.95	3.53
Reynolds Number	7650	83,700	56,300 (7650)
Ratio of Specific Heat	1.284	1.41	1.285

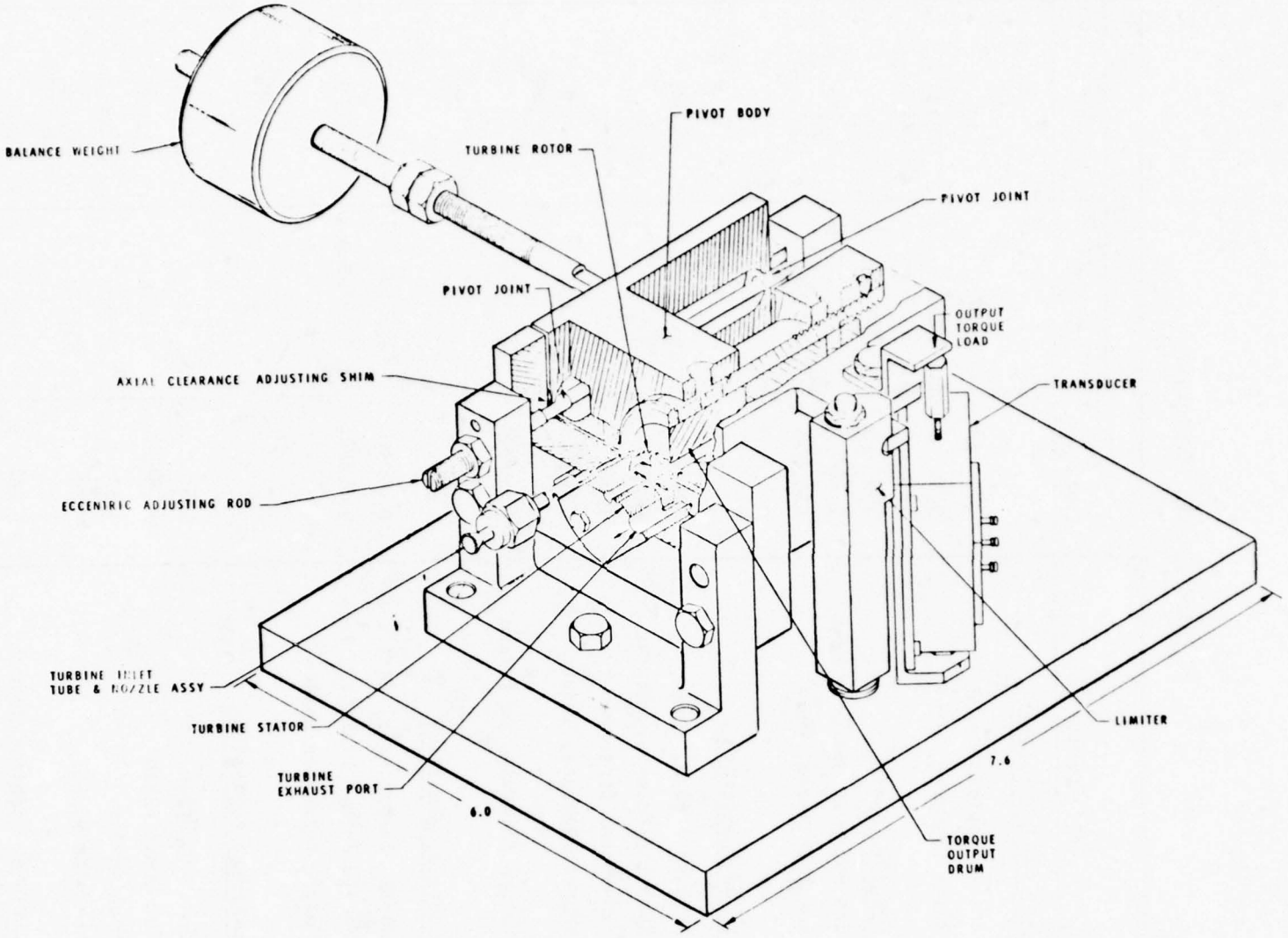

Figure 16. Test Rig

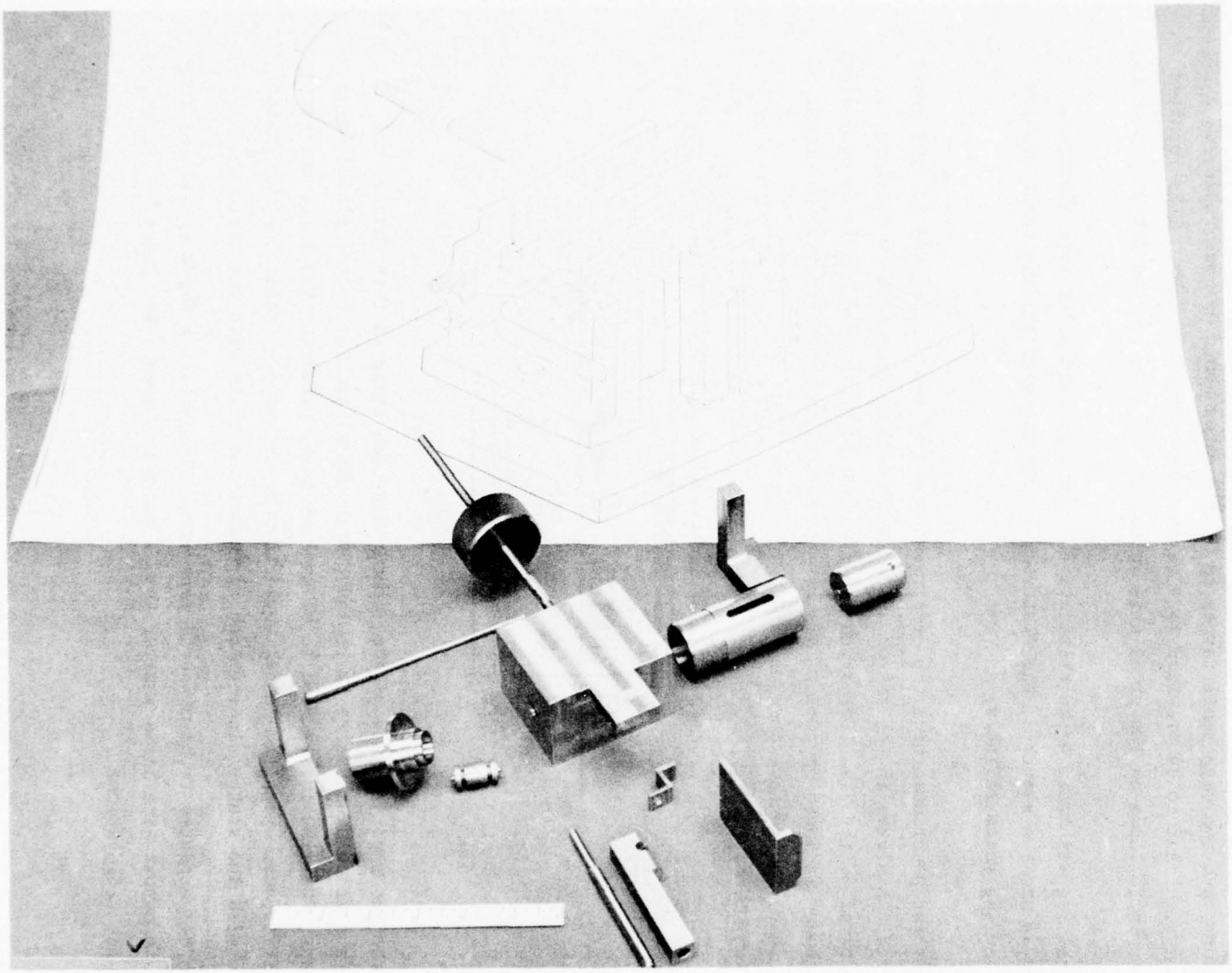

SAJ33-10/22/73-C1A*

Figure 17. Test Rig Hardware

To ensure that the very small forces to be generated would be measurable, a counterweight had to be provided to tare out the test-rig weight. This resulted in very large loads on the pivot axis which, in the long run, resulted in sticking.

The test rig was modified to eliminate the pivot pin and substitute flexures. Figure 18 shows a sketch of the flexures. Their use overcame the basic problem of measuring force reliably.

To vary the power absorbed, the effective length of the bearing was to have been measured. A sleeve in the stator and a stator end plate permitted varying, by a factor of 3, the area over which the fluid would be sheared. This is equivalent to a change in speed of 10:1. This was the method by which gross power output of the turbine was to have been measured.

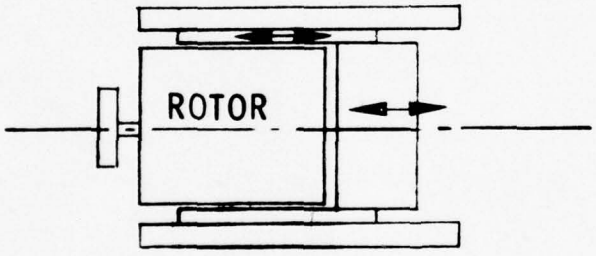

Once the gross performance of the turbine had been found in this manner, the power absorbing drum was to be replaced with the alternator rotor, placed in bearings. Bearing losses were to be determined by repeating the tests and noting the difference. Magnetic losses would then be measured by replacing the stator sleeve with the stator windings and rerunning the tests with the field on.

The forces expected to be measured were extremely small. A force transducer with adequate output with loads smaller than 1 ounce was used. Reference 14 (Appendix) shows the calibration.

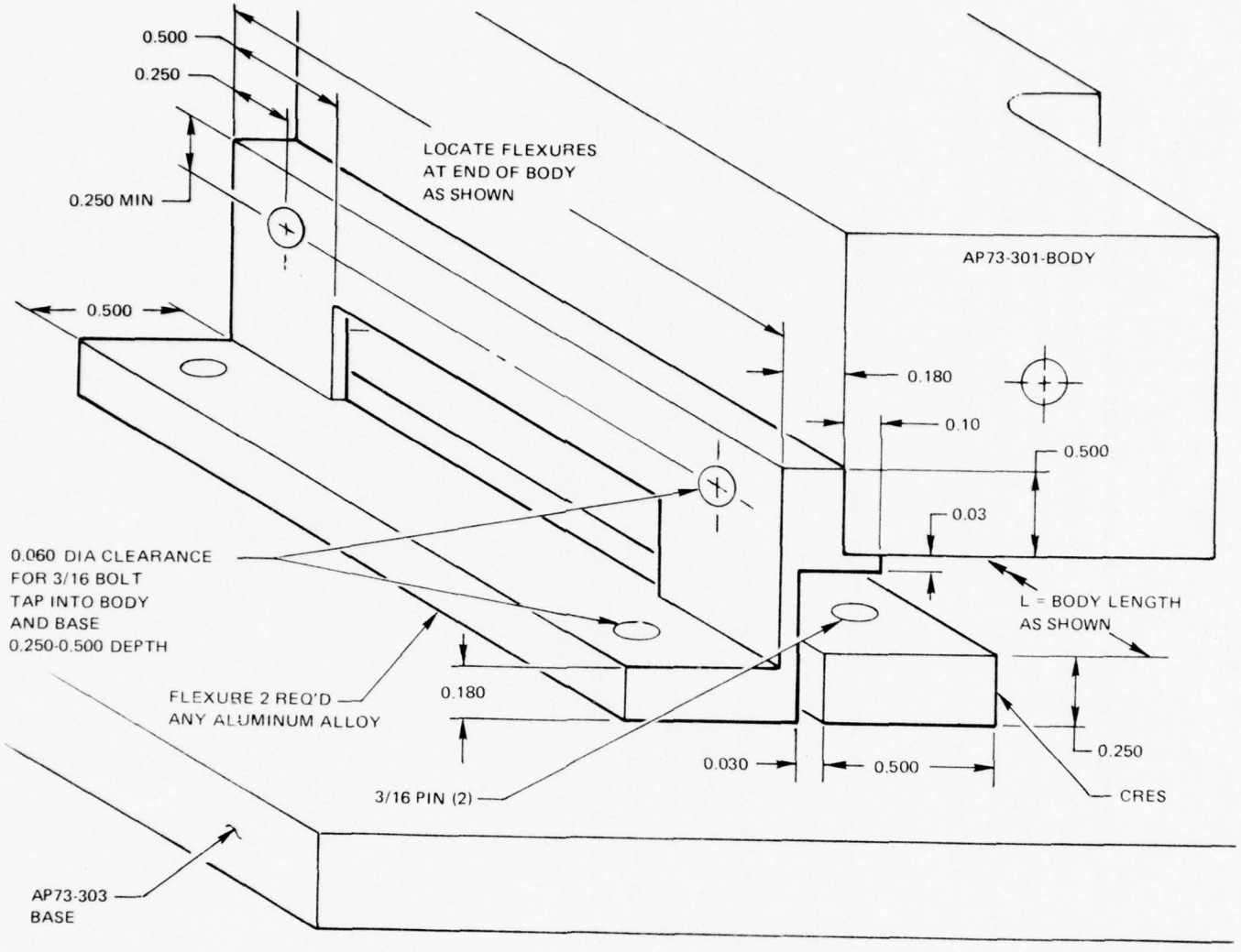

Figure 18. Test Rig Flexures

Moreover, even with this problem solved, other design defects plagued the test rig. As was later forcefully demonstrated, the position of the nozzle relative to the turbine is very critical. A movement of 0.010 inch can influence performance significantly, and movements of 0.001 inch are sufficient to prevent reproducible data. With this test setup it was not possible to position the rotor accurately enough.

Some tests were made, however. The rotor was spun to speeds in excess of 75,000 rpm to demonstrate operation.

The test rig's death knell sounded, however, when it was realized that the alternator could not operate effectively with the massive amount of metal around the stator coil. The metal induces stray electrical fields and results in "cogging" of the rotor which requires very large starting torques. One of the valuable lessons learned from this portion of the program is that simplicity in hardware results in a more reliable test program.

INTERIM TESTS

It was evident from the tests with the large metal test rig that the alternator would have to be surrounded by nonconductive material to ensure reproducible and proper test results; therefore, a wooden test rig was constructed. Very primitive in design, its main purpose was to demonstrate that adequate power could be generated at high speeds.

To eliminate bearings and alignment problems, the alternator stator and rotor were used as the bearing. The stator coil was coated with epoxy and then accurately machined on its internal diameter to accept the rotor with a radial clearance of 0.0003 inch. To eliminate exhaust problems, the turbine was overhung in free air and driven by a jet of compressed nitrogen. Obviously, the only test data to be garnered would be a demonstration that the generator was capable of producing adequate power.

Tests were successfully completed at speeds up to over 200,000 rpm (Table 7). Although an equivalent power output of 53 watts was achieved, it was felt that considerable improvement in performance was possible with a change in rotor design.

The rotor used consisted of a sleeve made of Rene 41, a nonmagnetic material. For stress reasons, this sleeve was 0.10 in. thick, putting the magnetic poles 0.15 inch from the coil. It is evident that this weakens the flux density past the coil.

A new rotor, consisting of six pieces welded together so as to provide two magnetic pole pieces of 4130 steel, two nonmagnetic Rene 41 pieces, and two nonmagnetic Rene 41 end caps, was made. This, in effect, brought the poles closer to the coil and increased flux density (Fig. 10).

With this setup, vastly improved performance resulted. Figure 19 shows the performance map and Table 8 lists data. Maximum power measured was 42.4 watts at 181,000 rpm; maximum speed reached was 335,000 rpm. Extrapolating to 550,000 rpm, a power output of 129 watts would be available. Therefore, alternator size could be reduced in later applications which would result in better volumetric efficiency.

TABLE 7. TEST RESULTS

Run	Voltage AC	Amps AC	Watts	Speed	Watt Equivalent @ 550,000 rpm
C	1.6	3.82	10.6	130,000	44.8
D	2.9	3.98	14.9	205,000	40.0
E	2.35	3.10	12.6	167,5000	41.4
F	1.9	4.16	13.7	141,500	53.2

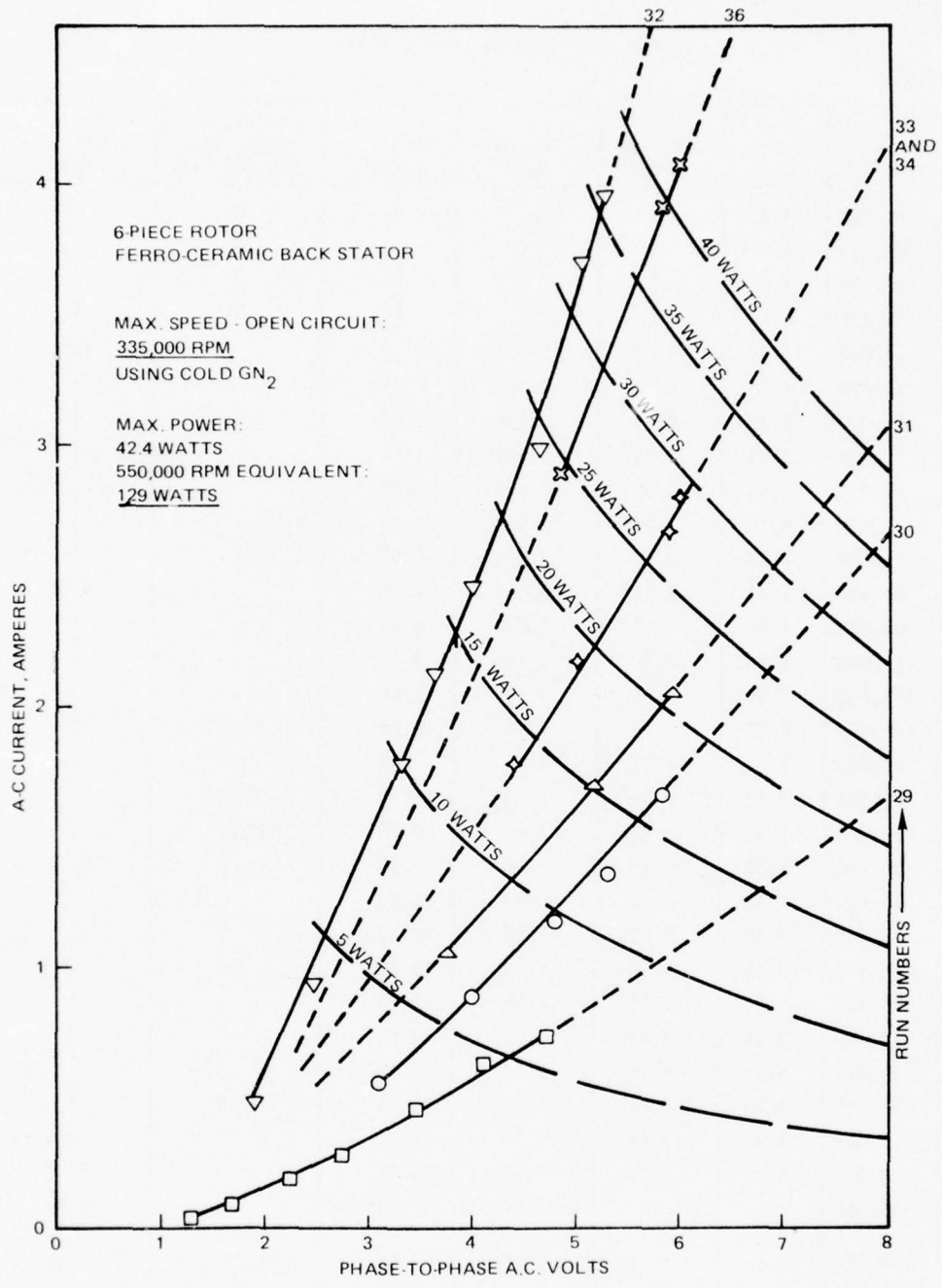

Figure 19. Performance Map, 60-Watt Power System Alternator Test

TABLE 8. PERFORMANCE DATA

Run	Speed, rpm	Volts (ac)	Amperes (dc)	Amperes (ac)	Power, watts	Equivalent Power at 650,000 rpm	Preset Resistance, ohms
A	70,000	3.0	0	0	0	0	∞
28	102,000	4.0	↓	↓	↓	↓	↓
	126,000	5.0					
	164,000	6.0	↓	↓	↓	0	↓
B	30,000	1.25	0.03	0.026	0.06		3.0
	40,400	1.65	0.10	0.085	0.24		↓
	56,000	2.19	0.21	0.178	0.68		
29	71,200	2.69	0.32	0.272	1.27		
	98,000	3.45	0.55	0.468	2.80		
	111,000	4.10	0.71	0.604	4.29		
	126,000	4.70	0.87	0.740	6.02	26.3	↓
C	81,600	3.10	0.65	0.552	2.96		2.0
	108,000	4.00	1.05	0.892	6.18		↓
30	132,800	4.80	1.40	1.19	9.89		
	148,800	5.30	1.60	1.36	12.48		
	170,000	5.80	1.95	1.66	16.68	54.0	↓
D	100,800	3.75	1.25	1.06	6.88		1.5
31	140,000	5.15	2.00	1.70	15.16	59.5	
	164,000	5.90	2.40	2.04	20.85	69.9	
E	51,600	1.90	0.56	0.48	1.58		0.75
	68,000	2.45	1.10	0.94	3.99		↓
	96,000	3.30	2.10	1.78	10.17		
32	105,600	3.65	2.50	2.12	13.40		
	116,800	4.00	2.90	2.46	17.04		
	140,000	4.65	3.48	2.96	23.84		
	154,000	5.05	4.35	3.70	32.36		
	164,000	5.25	4.65	3.95	35.94	120.5	↓
33	121,800	4.40	2.10	1.78	13.56		1.10
	>300,000	5.65	3.00	2.55	24.95		1.10
34	335,000	?	?	Chart speed not turned to high			0.90
35	148,000	5.0	2.55	2.17	18.79		0.90
	170,000	5.9	3.15	2.68	27.39		↓
	175,000	6.0	3.30	2.80	29.10	91.4	
36	134,000	4.8	3.40	2.89	24.03		0.8
	172,000	5.8	4.60	3.91	39.28		↓
	181,000	6.0	4.80	4.08	42.4	128.8	
37	178,000	7.2	0				∞
	200,000	8.0	0				∞

PERFORMANCE TESTS

Following the demonstration of alternator operation, the contract work statement was revised as follows to reflect changes in the test task:

> Warm Gas Tests. Using heated gas, the windage and bearing friction of the rotor unit shall be determined using spin-down techniques. This will permit loss analysis for the power unit.
>
> Hot-Gas Generator, Prime Mover, and Electric Generator. This assembly shall be tested to determine the capability of producing 60 watts of electrical energy using decomposition products gas. Sufficient testing and modification shall be performed to achieve a determination of design requirements. Provisions shall be made to modify the setup to ensure proper testing. Measurements of propellant flowrate, exhaust power output, inlet and exhaust temperature, inlet and exhaust pressure, and speed shall be made.

Warm Gas Tests

To accomplish this task, a new test rig was designed and built. Plastic was used to prevent magnetic interference. To obviate problems with bearings, instrument-type ball bearings of the type used in dental drills were used. Figure 20 is a sketch of the test rig and Fig. 21 shows the rotor (Fig. 22) installed.

A series of tests was made with this test rig to evaluate turbine efficiency. It had been intended to use "spin-down tests" to evaluate windage and from that, performance, but another method was found to be more applicable. For spin-down tests the unit is held steady at one set of conditions. Speed is then increased slightly and pressure suddenly cut off. As the rotor spins down, the dissipative torque can be equated to the product of moment of inertia and deceleration:

$$T_{dis} = I \frac{d\omega}{dt}$$

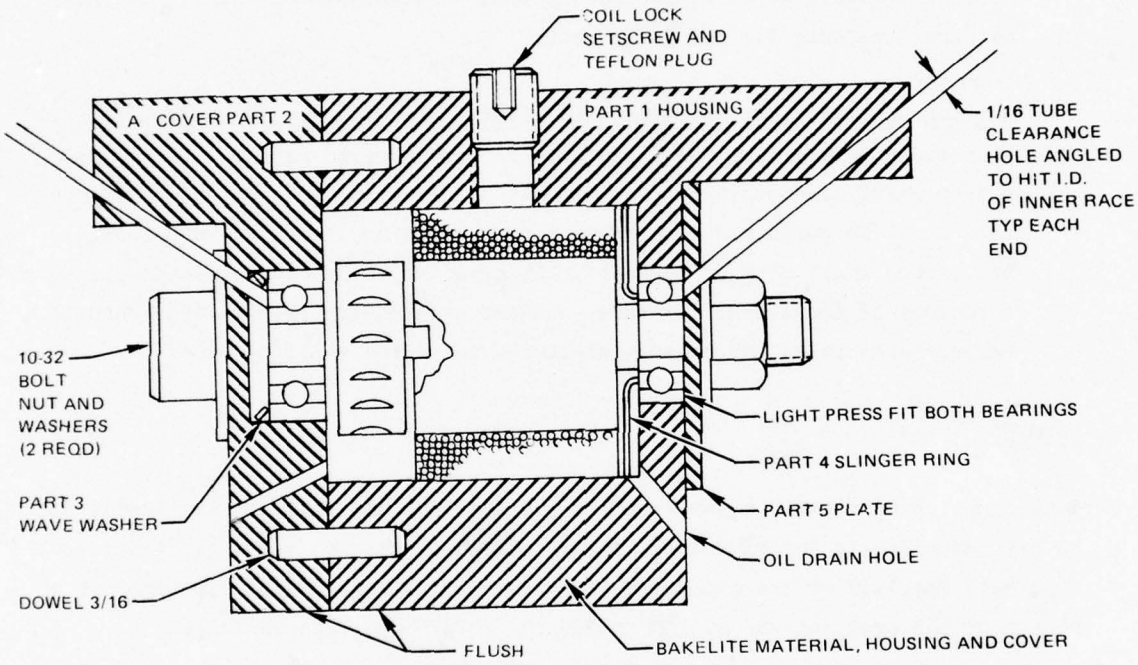

Figure 20. Test Rig

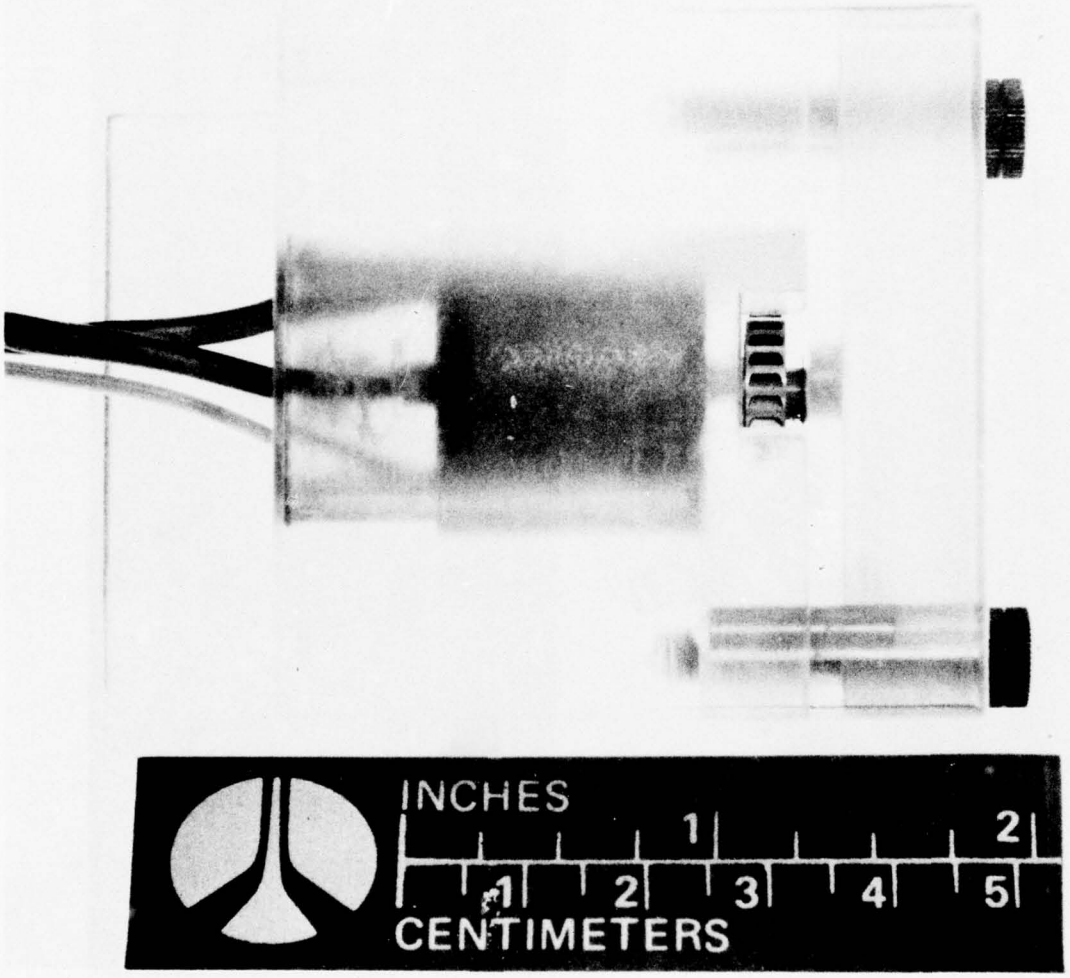

5AJ23--11/13/74-C1C

Figure 21. Plastic Test Rig

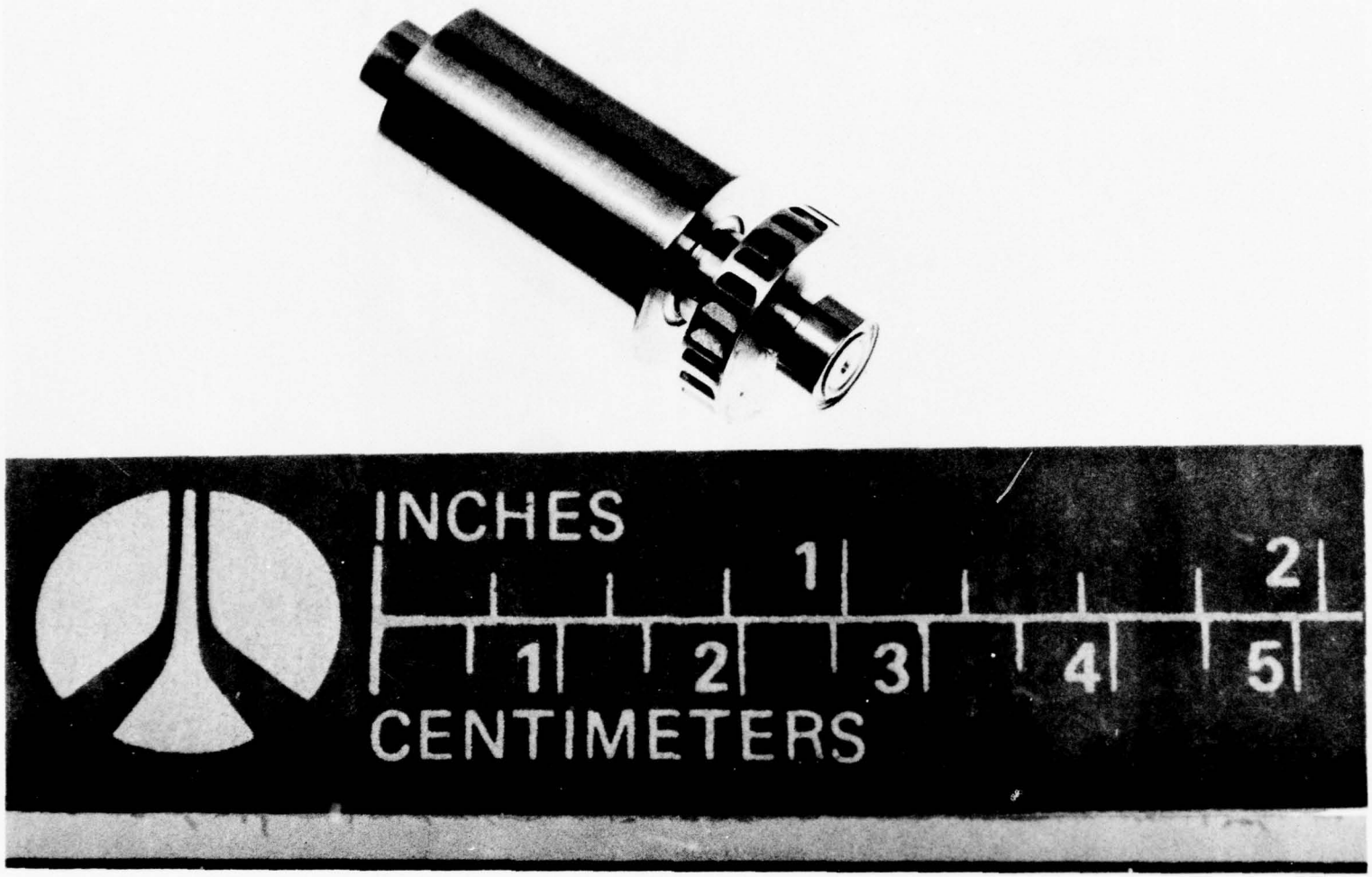

5AJ23-11/13/74-C1A

Figure 22. Rotor

The rate of change of speed is determined from the test data yielding dissipative torque. If this torque is multiplied by speed, the dissipative power is found. Comparing this to the power supplied at the prior steady state yields efficiency.

This method requires the assumption that conditions will be the same when the turbine gas (load) is off as when it is on. It also requires a sudden shutoff of gas flow to ensure that deceleration is due only to dissipative forces.

The method used was easier to apply and turbine loads will not alter as radically because flow is essentially steady. The turboalternator is operated at a set speed without any electrical power being produced. All turbine work goes to overcome losses. Therefore,

$$(\text{Gas Power})_{In} - (\text{Gas Power})_{Out} = \text{Dissipated Power}$$

The dissipated power includes all speed-related values--e.g., friction, windage. When the output circuit is closed, power is produced. The equation then is

$$(\text{Gas Power})_{In} - (\text{Gas Power})_{Out} = \text{Dissipated Power} + \text{Gross Power}$$

Note that the dissipated power now includes windage, friction, and alternator efficiency loss. The natural result of the application of the load is that speed reduces. Gas pressure is raised to reset the speed at the original value, resulting in a new balance.

Three assumptions were made:

1. The ratio of $(\text{Gas Power})_{Out}$ to $(\text{Gas Power})_{In}$ stays constant. This results because at the same speed, the jet-speed ratio (U/C_o) is nearly constant. The ratio is, of course, related to turbine efficiency.
2. The friction and windage are the same because speed is the same.
3. The alternator efficiency is 85 percent.

Based on these assumptions

$$(\text{Gas Power})_{Out} = K\ (\text{Gas Power})_{In}$$

$$(\text{Gas Power})_{In}\ (1 - K) = \text{Dissipated Power} + \text{Gross Power}$$

After the change of conditions because of the load being applied:

$$(1 - K)\ [\Delta\ (\text{Gas Power})_{In}] = \Delta\ \text{Gross Power}$$

or

$$\eta = \frac{\Delta\ \text{Net Power}/0.85}{\Delta\ (\text{Gas Power})_{In}}$$

Gas power can be calculated from observed pressure, temperature, and from flow for which the nozzle has been calibrated.

The results of the tests made are shown in Fig. 23 and 24 and Table 9 . It is evident that turbine efficiency is very comparable to values expected based on data in Ref. 15 and that, at a jet-speed ratio of 0.08, unusually high values are observed. The terry-type turbine was designed to utilize gas recirculation to extract energy from the leaving gas stream in a second pass through the turbine blade. It is possible that at a jet-speed ratio of 0.08, the flow impinged on the housing in a beneficial way, resulting in added energy recovery. This would require added analysis to perfect a conclusion.

To measure power output from the turbine, gas flowrate must be known. Ordinarily, some form of flowmeter would be employed; however, the turbine nozzle was an excellent flowmeter once it was calibrated.

A nozzle calibration was performed. Reference 16 , Appendix , shows the results. This curve was used for all data evaluation.

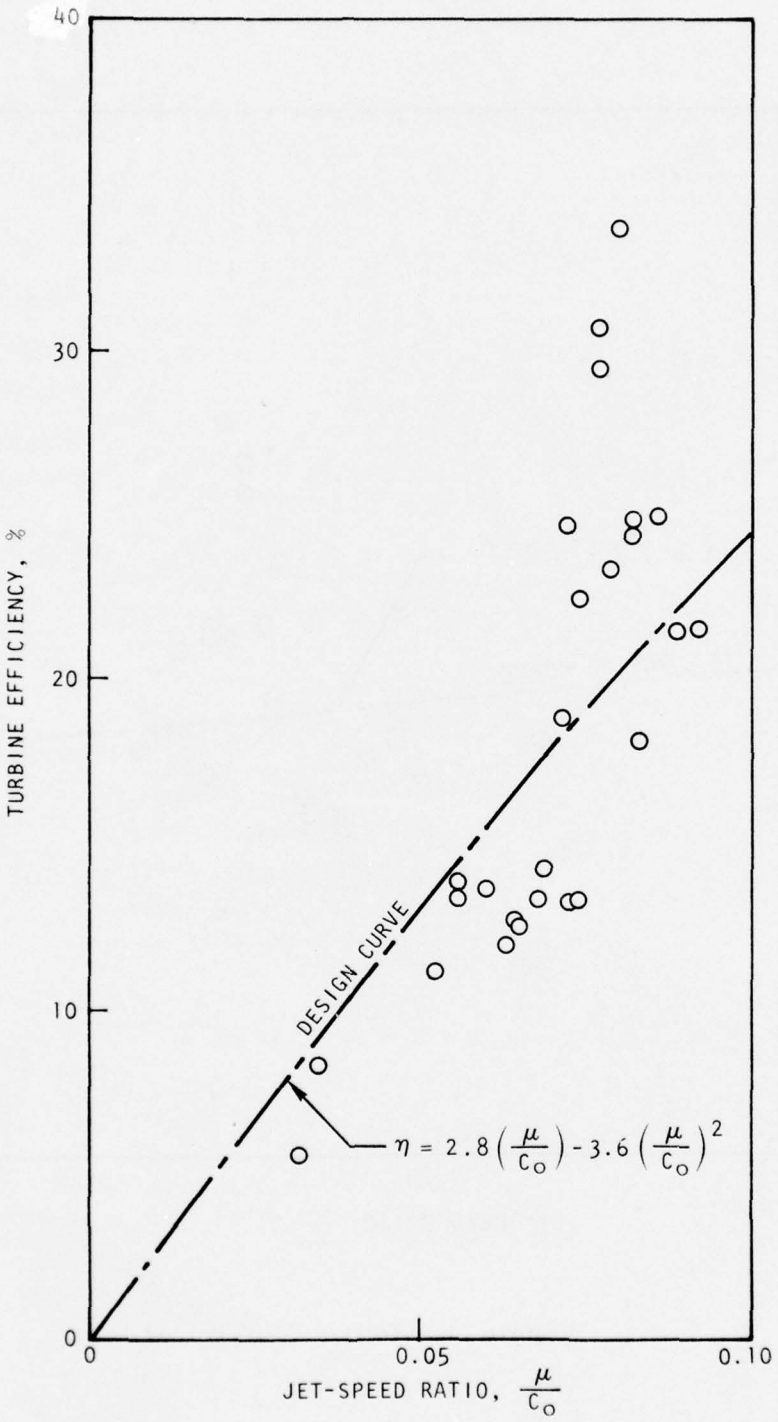

Figure 23. Turbine Efficiency

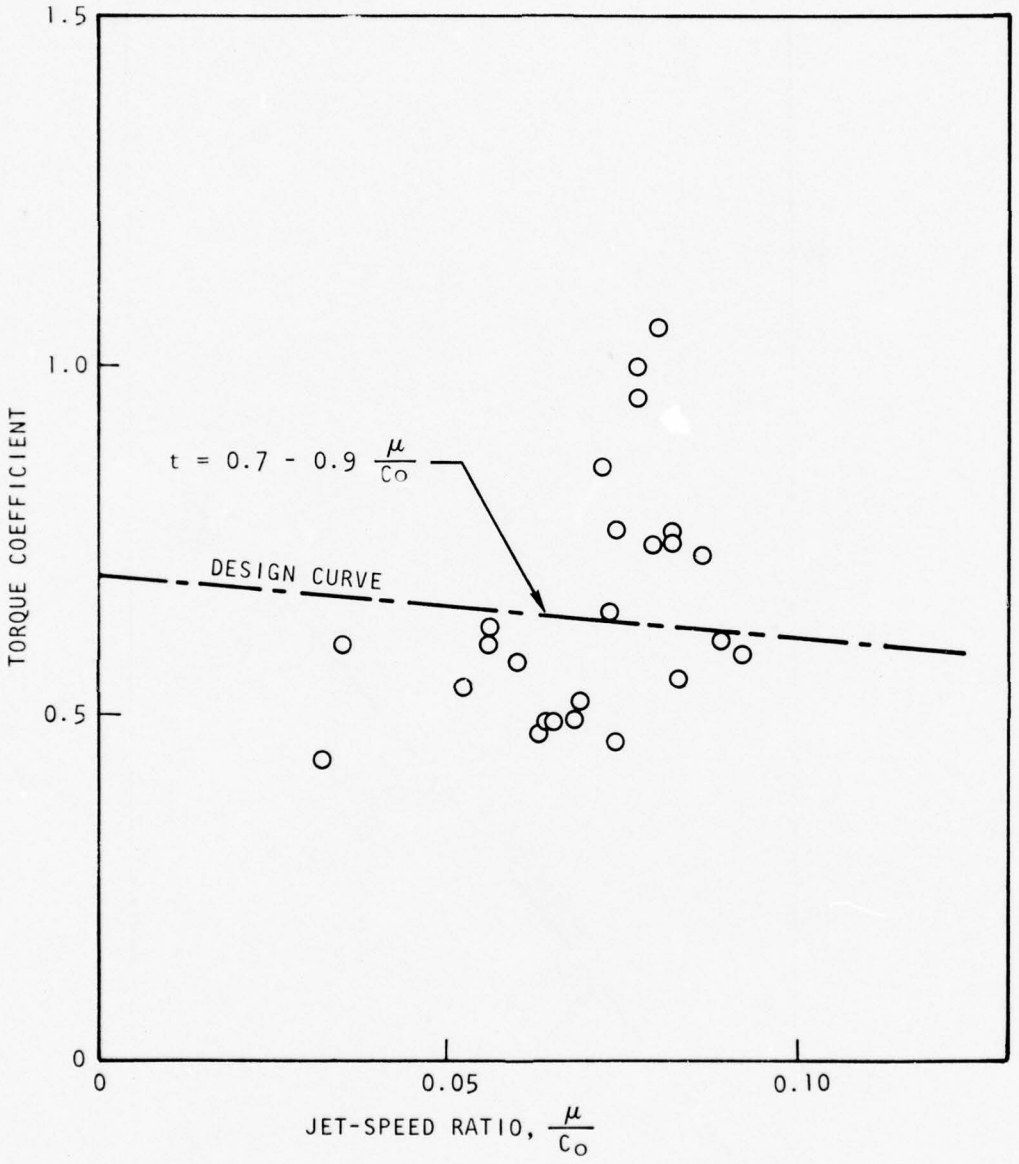

Figure 24. Torque Coefficient

TABLE 9 TEST DATA

Test Date	P_c, psia	T, R	Gas Power, watts	Net Power, watts	Efficiency, percent	Speed, rpm	U/Co	Torque Coefficient	Dissipated Power, watts
1-13-75	302.3	562	22.61	0	--	51,750	0.056		3.03
	344.3	562	26.43	0.435	13.4	52,020	0.056	0.598	
	354.3	562	29.34	0	--	60,990			3.44
	439.3	562	35.25	0	--	60,840	0.065	0.485	
	439.3	562	35.25	0	--	70,770			4.72
	554.3	562	46.20	1.25	13.4	70,590	0.074	0.454	
	554.3	562	46.20	0	--	80,700			8.41
	676.3	562	58.06	1.83	18.2	80,910	0.083	0.547	
	164.3	572	10.70	0	--	28,140			0.60
	184.3	572	12.39	0.080	5.57	28,080	0.032	0.435	
	184.3	572	12.39	0	--	31,110			1.03
	202.3	572	13.93	0.109	8.33	31,260	0.035	0.595	
	264.3	572	19.38	0	--	51,630			2.69
	314.3	570	23.86	0.531	13.9	51,510	0.056	0.623	
	314.3	569	23.84	0	--	60,570			2.96
	396.3	568	31.29	0.798	12.4	60,360	0.064	0.486	
	504.3	576	41.92	0	--	79,320			10.23
	589.3	572	50.05	1.678	24.4	79,260	0.082	0.743	
	414.3	573	33.23	0	--	70.290			4.42
	524.3	573	43.74	1.192	13.3	70,230	0.073	0.457	
	364.3	572	20.52	0	--	64,530			3.82
	454.3	572	36.99	0.962	13.4	64,350	0.068	0.493	
	314.3	573	23.93	0	-	59,490			2.87
	399.3	573	31.81	0.802	12.0	59,520	0.063	0.475	
1-15-75	1004.3	652	97.79	--	--	88,590			24.35
	1094.3	655	107.89	2.14	24.9	88,530	0.082	0.760	
	264.3	690	21.28	0	--	52,320			2.38
	329.3	683	27.61	0.604	11.2	52,500	0.052	0.540	

TABLE 9 . (Concluded)

Date	P_c, psia	T, R	Gas Power, watts	Net Power, watts	Efficiency, percent	Speed, rpm	U/Co	Torque Coefficient	Dissipated Power, watts
1-15-75	329.3	680	27.55	0	--	62,190			3.77
	414.3	674	36.02	0.989	13.7	61,980	0.060	0.572	
	414.3	672	35.96	0	--	71,370			5.14
	526.3	663	47.23	1.371	14.3	71,160	0.069	0.519	
	526.3	662	47.20	0	--	76,950			8.92
	629.3	657	57.77	1.694	18.9	76,830	0.073	0.646	
	629.3	652	57.55	0	--	81,000			17.67
	699.3	650	64.82	1.899	30.7	80,970	0.077	0.998	
	734.3	650	68.54	0	--	84,150			23.17
	804.3	646	75.76	2.073	338	84,120	0.080	1.056	
	804.3	644	75.65	0	--	91,110			18.91
	909.3	638	86.48	2.303	25.0	91,170	0.086	0.727	
	909.3	634	86.21	0	--	93,480			18.54
	1049.3	618	100.02	2.525	21.5	93,450	0.089	0.604	
	1149.3	622	111.07	0	--	96,690			23.99
	1304 3	615	125.81	2.703	21.6	96,600	0.092	0.586	
	564.3	690	52.26	0	--	77,490			12.91
	644.3	681	60.46	1.72	24.7	77,460	0.072	0.857	
	644.3	678	60.33	0	--	80,130			13.57
	734.3	674	69.83	1.82	22.5	79,980	0.075	0.761	
	764.3	671	72.92	0	--	82,980			21.51
	834.3	663	80.58	1.92	29.5	82,890	0.077	0.957	
	864.3	659	83.05	0	--	85,590			19.43
	959.3	655	93.10	2.00	23.4	85,470	0.079	0.741	

Gas Generator Tests

Gas generator testing was performed at the Rockwell International B-1 Division test site. A test gas generator, Fig. 25, was fabricated. Liquid propellant enters through the tube at the upper right, is metered through the narrow hypodermic needle section and enters the gas generator. A dual catalyst pack of iodine pentoxide and Shell 405 is located in the gas generator tube. The large-diameter body at the end of this tube contains the screens to hold the catalyst and the orifice plate which models the turbine nozzle. A pressure tap extends radially from this section to provide pressure data. Thermocouples are tack-welded to the body in various locations.

Tests were made using MHF-5A propellant. The unit operated stably but initiation was very slow. This indicated that the configuration of the catalyst and I_2O_5 bed required changing. However, using neat hydrazine, the gas generator performed very well. Startup was good and operation was stable. It was decided, therefore, to complete further testing with hydrazine.

Hot-Gas Tests

A virtual duplicate of the plastic test rig used for warm-gas testing was fabricated using lava stone. This retains the nonmagnetic feature while providing the capacity for hot-gas operation. Ball bearings were used to support the rotor.

The gas generator was modified by replacing the orifice section with a turbine nozzle. The unit was assembled and run as a complete power package. Speeds in the range of 60,000 rpm were achieved but operation was not good. It developed that a number of leaks occurred in the gas generator where the hypodermic needle sections were welded to the larger tubing. Eventually, the leak was bad enough to cause a minor fire. Operation had to be suspended as a result of this and because of plugging of the gas generator.

At this point some limited successes had been achieved but the unit was far from useable. Therefore, it was decided that bearings must be made available which are reliable and low in power consumption and that a more representative breadboard model must be assembled to provide a demonstration test.

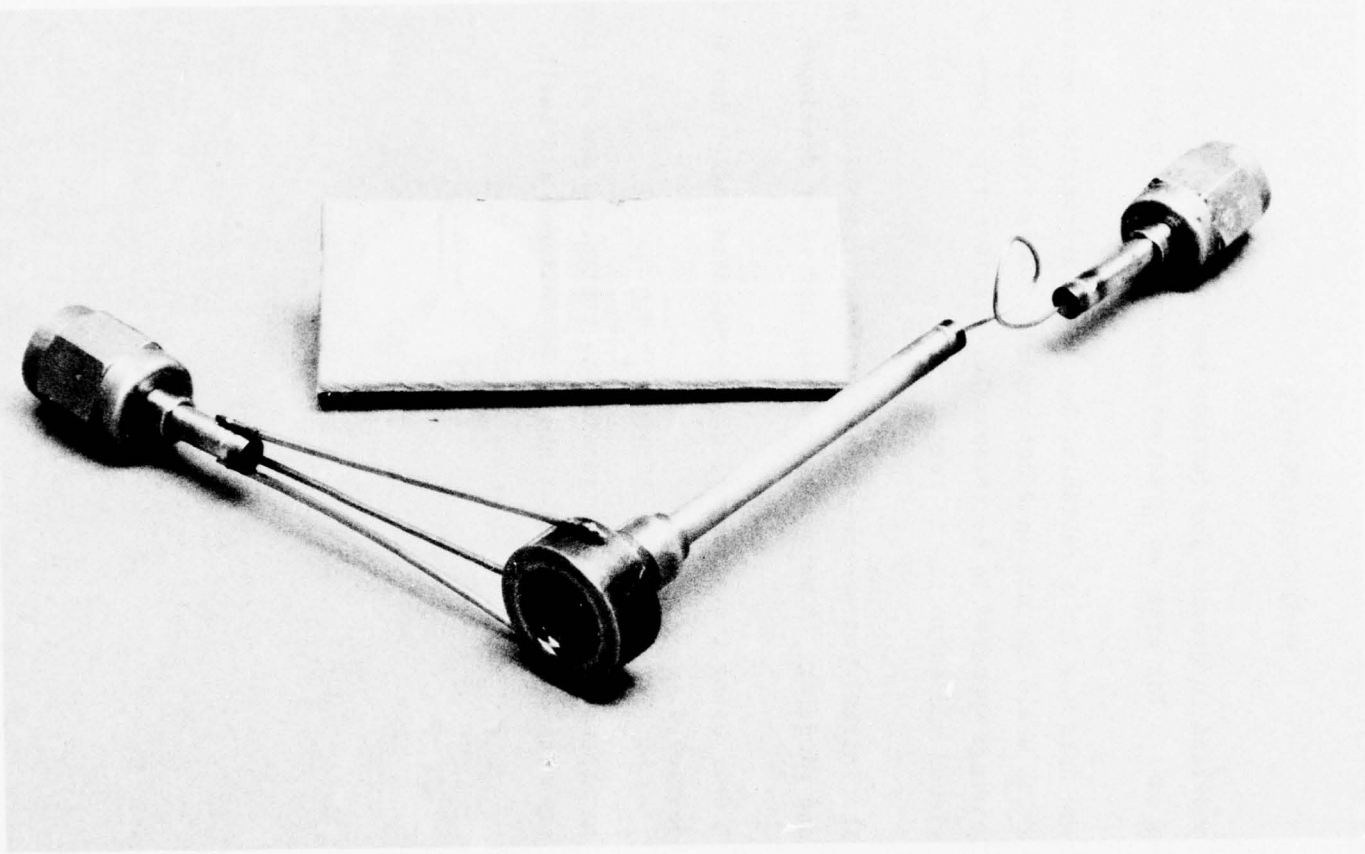

Figure 25. Test Gas Generator

DEMONSTRATION UNIT

The contract was modified to provide for further testing leading to a demonstration test unit. The areas of greatest concern at this point were:

Bearings: The need was for a reliable, low power dissipation bearing which could operate in a hot gas rig. Only fluid film bearings appeared to be reasonable. Various types were reviewed and subjected to test.

Gas Generator: The initial gas generator was too fragile, resulting in leaks and plugging. A more rugged design had to be developed.

Alternator: A unit using the stronger, nonencapsulated magnet had to be developed.

Assembly: An assembly where heat transfer is controlled and all components can operate together had to be designed and built.

BEARINGS

Perhaps the most pervasive problem in the development of the power source was the bearings. It was necessary to identify a type of bearing which would consume reasonable power at very high speed while providing stable operation in an adverse environment.

The first bearing type selected was the plain, hydrodynamic gas journal bearing using gases available in the atmosphere surrounding the bearing. This could be turbine exhaust gases, ambient air, or some of the stored pressurant gas (e.g. helium).

Using the design charts in Ref. 17 showed that no particular stability problems would be encountered under ordinary conditions if adequate rotor balance could be achieved. However, it proved very difficult to start the rotor because of sticking on startup and because it required considerable rotating speed to achieve an adequate load-carrying film. Therefore, early tests were made with ball bearings of the type normally used in dental drills. As expected, these bearings were easy to work with, but absorbed excessive amounts of power. Figure 22 shows the rotor with the ball bearings installed. The power absorption with this configuration, installed in a test rig as shown in Fig. 21 , was about 20 watts at 100,000 rpm. This is obviously much more than can be tolerated for this application. The question naturally arises whether dental drills and other applications also suffer this type of penalty. The answer is, "Yes", but these applications normally do not concern themselves with efficiency, operating with available essentially "free" shop air at low pressure.

Testing was accomplished using these high-loss ball bearings in order to enhance operation and evaluation of components. However, an evaluation of other bearing types was initiated. Two types in particular were determined to be potentially useful: the spiral-groove conical bearing and the three-lobe journal bearing.

Spiral-Groove Conical Bearing

The particular spiral groove bearing utilized for these tests was developed by the Autonetics Division of Rockwell International to provide a minimum drag bearing which nevertheless permits relatively large axial clearance to eliminate difficulties due to thermal expansion. These bearings were successfully used by Autonetics in a gyro application with grease packing as the lubricant (Fig.26). The spiral-groove, conical bearing configuration is shown in Fig. 27 and 28. In principle, grease is pumped by the grooves to the tip end of the bearing. As speed increases, the grease is put under higher and higher pressures in the cavity at the tip end of the bearing, causing a pressurized film between the cones. As speed is increased, the pumping action and friction increase the temperature of the grease, lowering its viscosity. This combined with the large axial and radial clearances, should result in extremely low drag.

The bearing operation was fully described by Muijderman in ASME Paper No. 66-LubS-7. Figures 29 and 30 were reproduced from that source. The equations presented can be combined and simplified to yield

$$\frac{W_t\ C}{M} = \frac{3\ g_1}{g_2}$$

where:

W_t = axial preload
C = radial clearance measured normal to cone
M = frictional torque

To minimize torque, g_1/g_2 must be maximized so that operation in the range

$$0.2 < \delta < 0.4$$

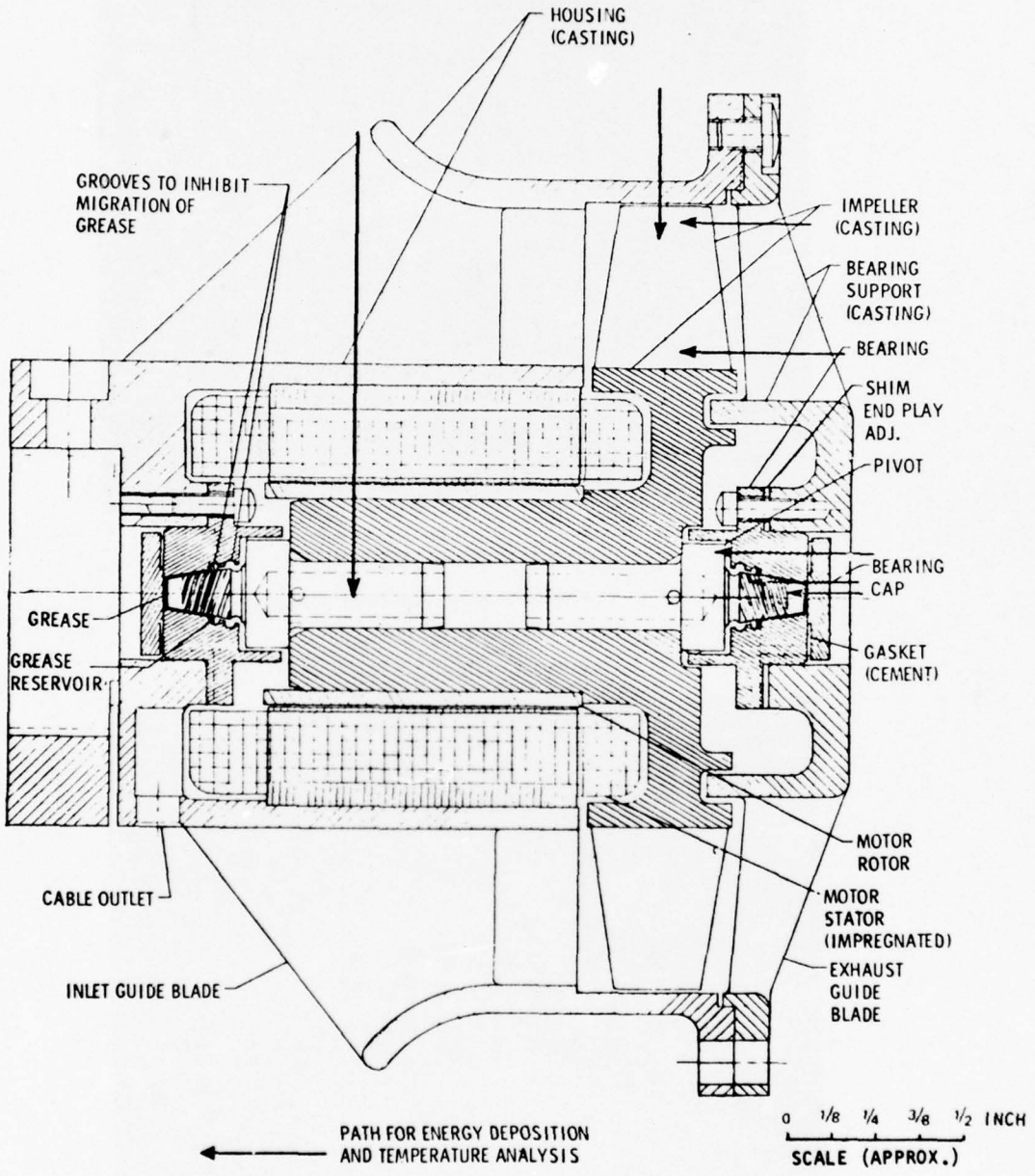

Figure 26. Gyro With Spiral Groove Bearing

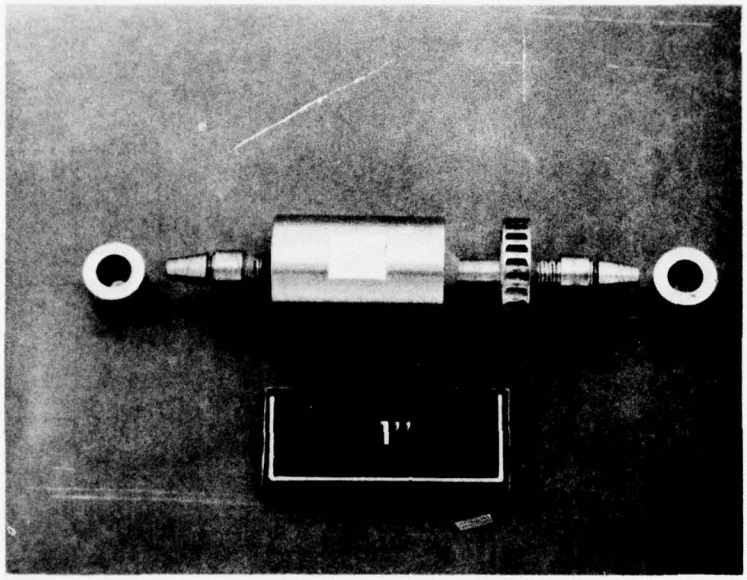

Figure 27. Sprial Groove Conical Bearing Rotor

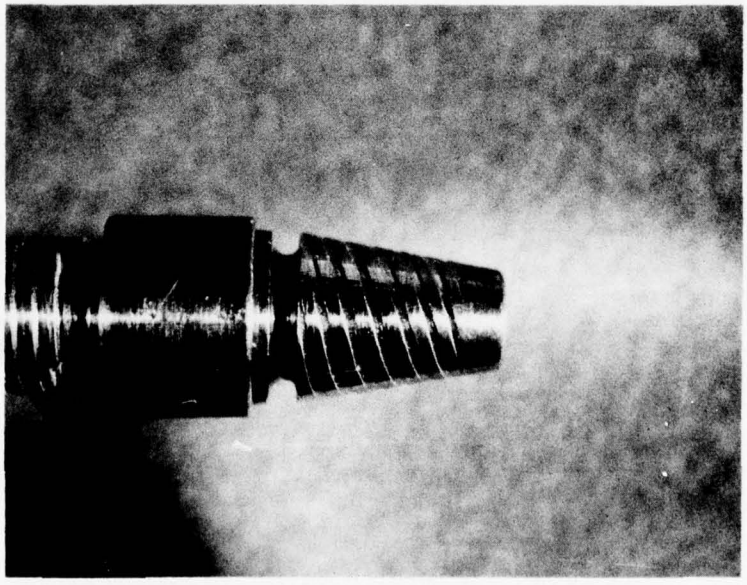

Figure 28. Spiral-Groove Conical Bearing

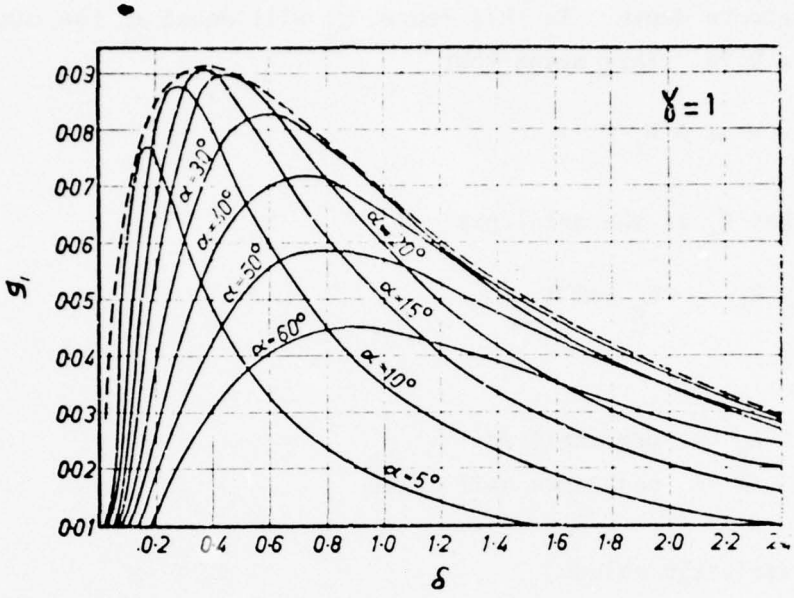

Figure 29. Design Factor g_1 for Spiral Groove Bearing

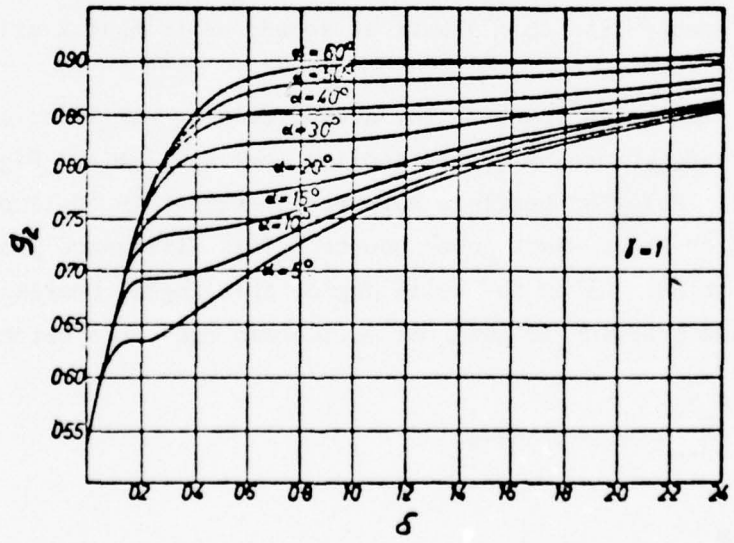

Figure 30. Design Factor g_2 for Spiral Groove Bearing

will be desirable as seen from Fig. 29 and 30. The parameter δ relates clearance to groove depth. In this range, g_1 will equal in the range of 0.008 and g_2 = 0.75. This means that

$$M \approx 3 W_t C$$

Recognizing that W_t is the axial preload,

$$W_t = W_b \tan \beta$$

where:

W_b = bearing load
β = cone apex half angle

so that, for realistic values,

$$M \approx 0.5 W_b C$$

As would be expected, torque varies with clearance and load. Based on the analysis, power absorption for a typical case (W_b = 0.03 lb, C = 0.002 in.) would be considerably less than 1 watt at speeds up to half a million rpm.

The bearing configuration selected for actual testing was identical to that used at Autonetics because parts and tooling were available. Figure 24 shows the application. Here the bearings support approximately 10 times the rotor weight required by the 60-watt power source. This difference proved to be crucial to operation. Given the helix angle, apex angle, bearing radius, groove depth, and grooving length, the Muijderman equations become

$$\frac{W_t C_2}{\eta \omega} = 7.73E\text{-}4g_1$$

$$\frac{M_c}{\eta \omega} = 2.58E\text{-}4g_2$$

Table 10 lists solutions for typical clearances.

TABLE 10. PARAMETRIC DATA FOR AUTONETICS BEARING

Clearance, mils	0.5		1		2		5	
c/h_o	0.4		0.8		1.6		4.0	
g_1	0.091		0.063		0.030		~ 0.01	
g_2	0.78		0.79		0.84		~ 0.87	
$\eta\omega$, lb/in.^{2}	1.78E-4		10.3E-4		86.2E-4		~1620E-4	
η, lb-sec/in.^{2}	E-5	E-6	E-5	E-6	E-5	E-6	E-5	E-6
N, rpm	170	1700	984	9836	8231	82,300	155,000	1,550,000
Power, watts	0.0001	0.0014	0.0024	0.024	0.09	0.90	13.3	

In tests with the 60-watt configuration, these bearings exhibited excessive drag. Looking at the data in Table 10 this turns out to be reasonable. With a reasonable clearance of 2 mils and only ten percent of the weight, operation is correct at very low speed, ten percent of the design value. Therefore, the bearing operates at the wrong helix angle and is inefficient.

The spiral-groove bearing is also dependent on the availability of the proper grease which, in this case, must be able to withstand relatively high temperature, above 600 F for hot operation. Some of the Krytox fluorinated oils were potential candidates but, because of their large variation of viscosity with temperature, any attempt to use them was finally abandoned when it was concluded that the three-lobe bearing offered the best chance for success.

THREE-LOBE BEARING

The use of a three-lobe bearing for this application was first suggested by Mr. Wayne Shank, a consultant who reviewed the 60-watt power source design. He indicated success with this type of bearing for high-speed applications.

Basic theoretical design information for three-lobe bearings can be found in a report in Ref. 6. Quoting from Lund's report, the major advantages of the

three-lobe bearing are that it is relatively simple in construction, it has no moving parts like a tilting pad bearing or a floating sleeve bearing, it can be designed to operate stably at rather high speeds and it is also able to run with a vertical rotor or a rotor in a zero-g field, which is not possible with conventional cylindrical bearings. The limitations of the bearing are its inability to accommodate any appreciable shaft misalignment unless specially mounted, and its relatively high friction power loss. Even though denominated as having high friction power loss, this is relative to more complex bearings, and acceptably low enough for the 60-watt power source.

The geometry of the three-lobe bearing is shown schematically in Fig. 9 . The bearing is composed of three circular arcs whose centers of curvature are removed from the center of the bearing by the distance r. Thus, even when the journal is centered in the bearing, the pads are loaded. In this way, the stability threshold of the bearing is raised and even a vertical rotor, or a rotor operating in a "zero-g field", can run stably, which is not possible with a conventional full circular bearing. However, the improved stability threshold is paid for by an increase in friction power loss and a smaller operating minimum film thickness, which makes the bearing more sensitive to impurities in the lubricant.

To analyze bearing performance, the following parameters are defined (nomenclature in Fig. 9):

Preload : $\delta = \frac{r}{c}$

Length-to-Diameter Ratio : $\frac{L}{D}$

Sommerfeld Number : $S = \frac{\mu NDL}{W}\left(\frac{R}{C}\right)^2$

Reynolds Number : $Re = \frac{2\pi RN\rho C}{\mu}$

where:

L = bearing length

N = rotative speed

μ = dynamic viscosity of lubricant

ρ = lubricant mass density

W = bearing load

C = bearing clearance as defined in Fig. 9

Figures 31 through 38 show the key design charts used in the analysis for two values of L/D. All of these curves use clearance Reynolds number as a design variable. Simple order-of-magnitude analysis shows that the Reynolds number was less than 500 for all conditions contemplated so that its influence will be minor. This includes variations in gas to be used. Viscosity of the most likely gases (air, helium, nitrogen) are relatively the same (at 1 atm and 20 C, air = 1821 x 10^{-7} poise, helium = 1961 x 10^{-7} poise and nitrogen = 1752 x 10^{-7} poise according to Ref. 18). Therefore, only density differences affect Reynolds number.

The bearing stability mass parameter for Fig. 31 and 35 is given by

$$\frac{CM\omega^2}{W} \approx \frac{2C\omega^2}{g}$$

It will exceed 100 at speeds above about 40,000 rpm so that, to all intents and purposes, a limiting value of Summerfeld number results, which is about 0.15 when L/D = 0.5 and 0.058 when L/D = 1.0. Substituting these values into the Summerfeld number results in a parameter ND^4/WC^2 which equals 4.21E8 for L/D = 0.5 and 8.18E7 for L/D = 1.0. Any value less than this will result in a stable bearing.

With the limiting geometry thus defined, the friction and power dissipation can be calculated. This results in a design nomograph for selecting geometry and calculating losses. Figure 39 shows the result. The maximum allowable shaft

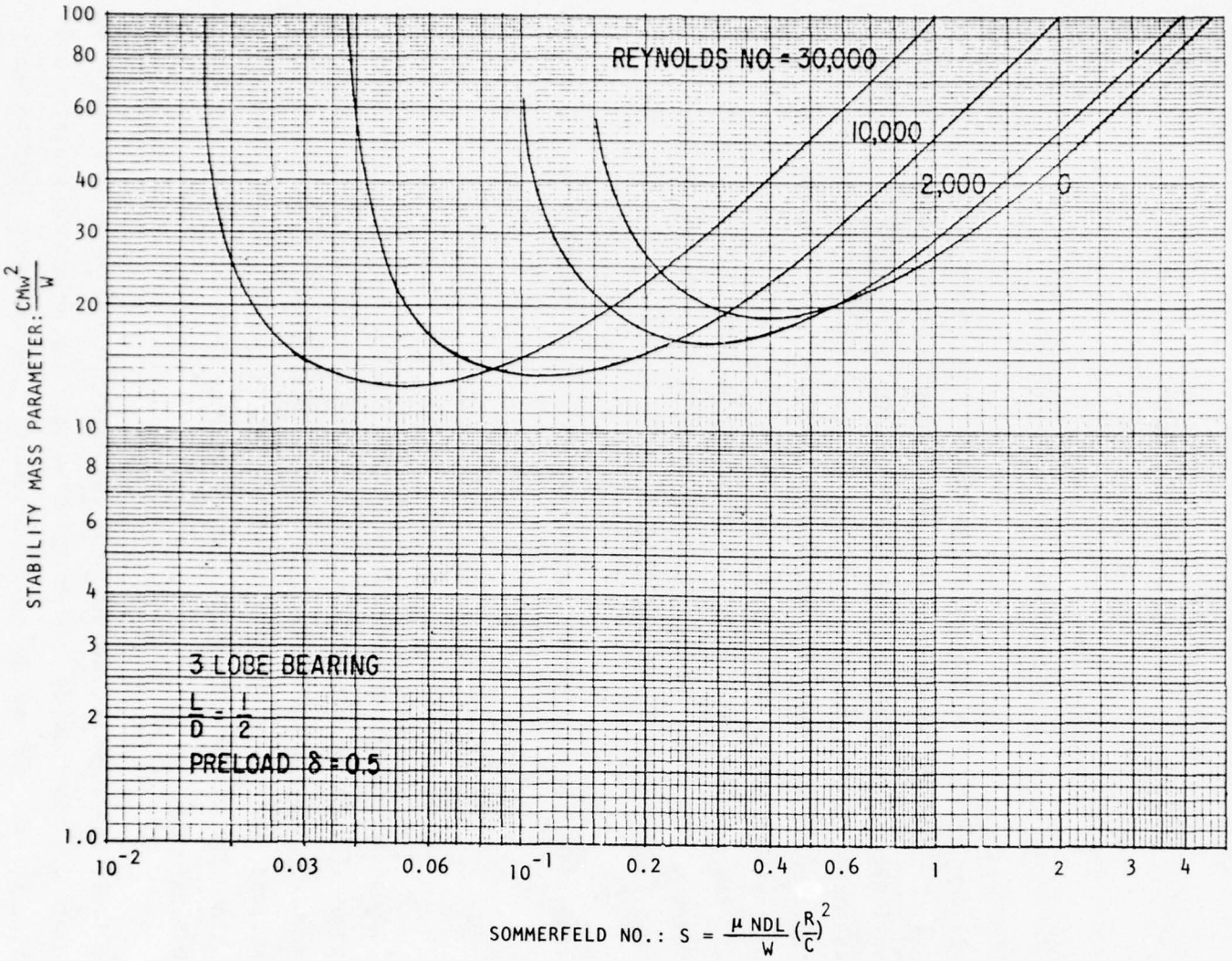

Figure 31. Three-Lobe Bearing, Preload = 0.5, $\frac{L}{D} = \frac{1}{2}$, Stability Map

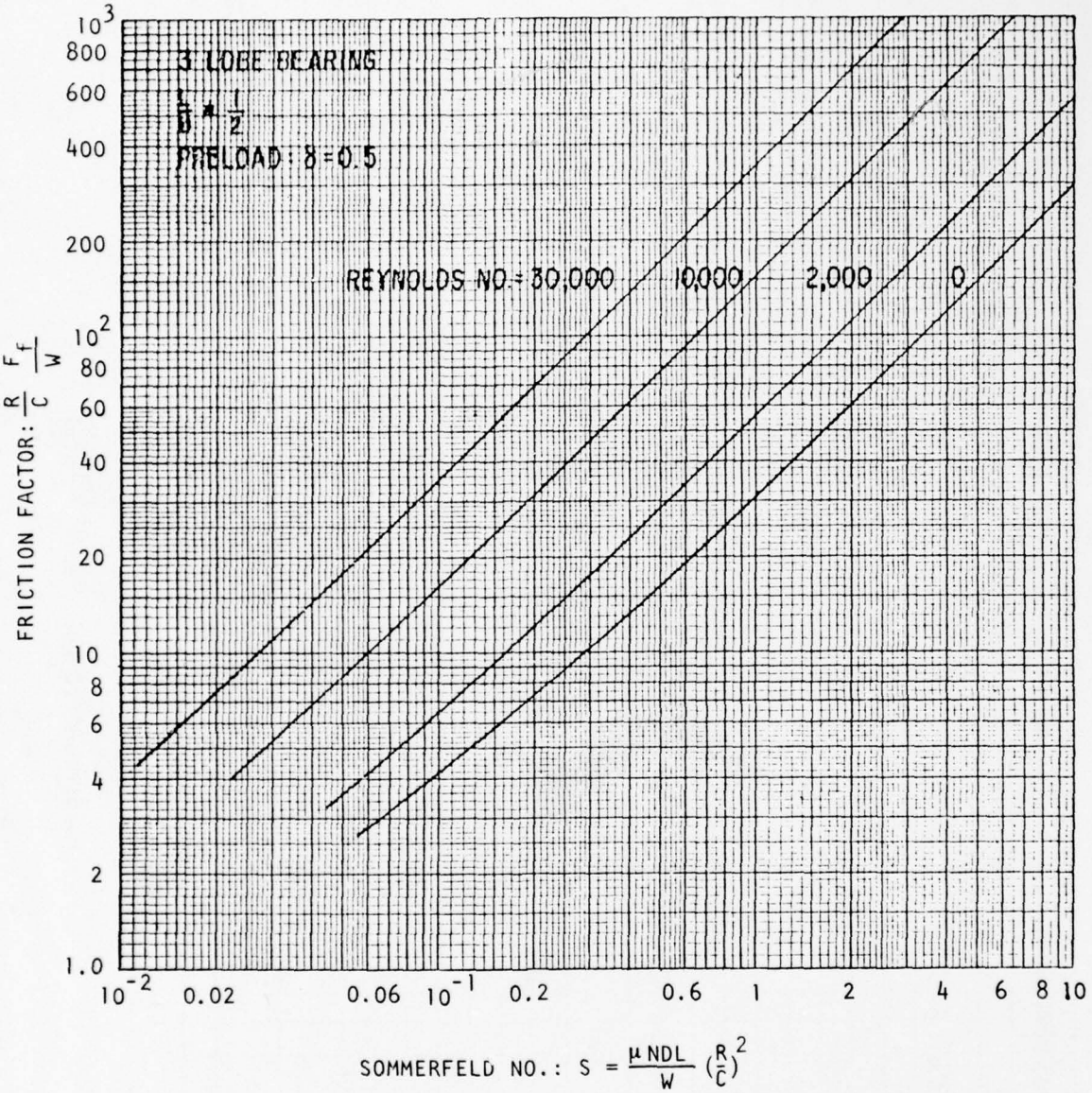

Figure 32. Three-Lobe Bearing, Preload = 0.5, $\frac{L}{D} = \frac{1}{2}$, Friction

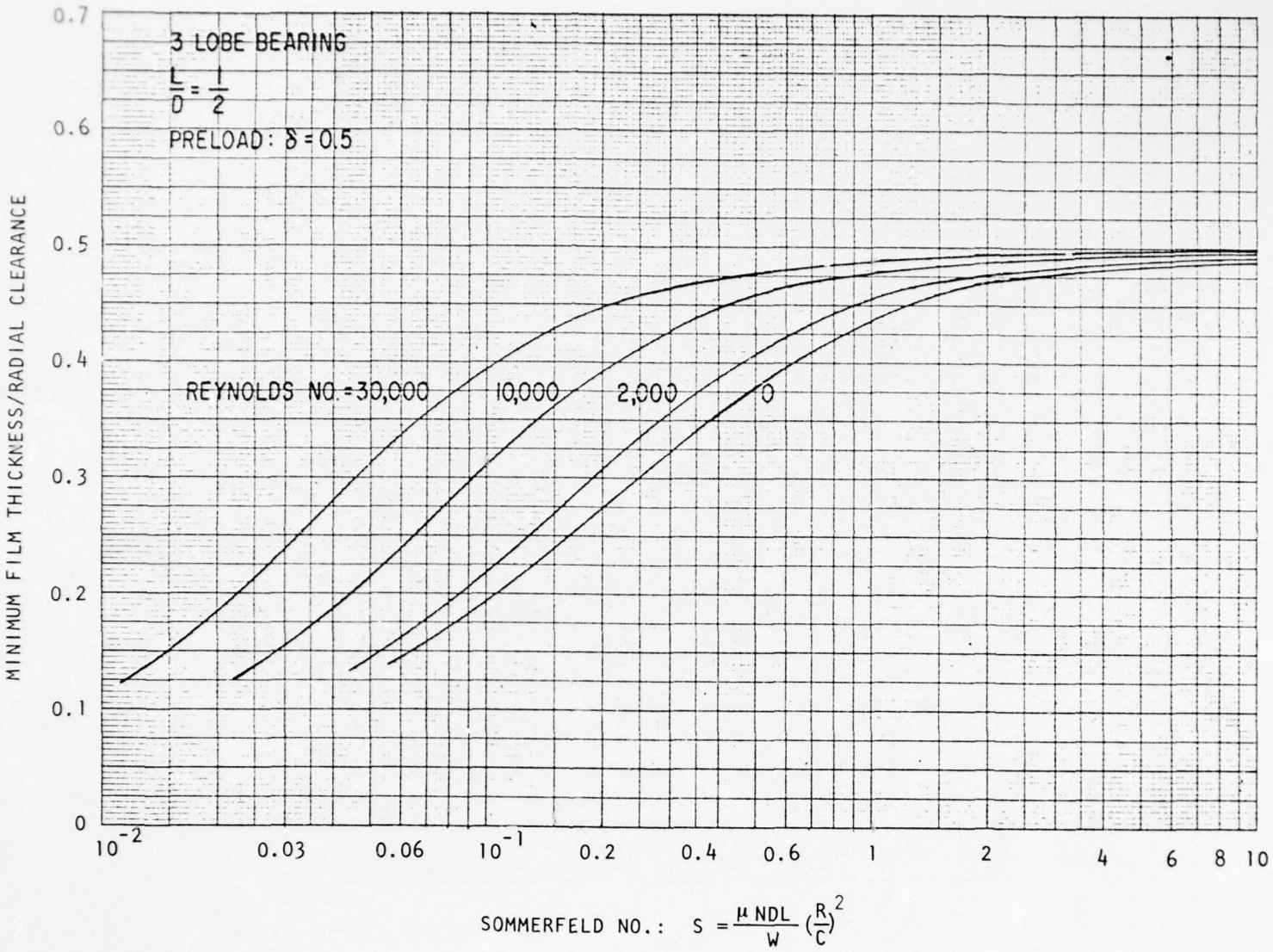

Figure 33. Three-Lobe Bearing, Preload = 0.5, $\frac{L}{D} = \frac{1}{2}$, Minimum Film Thickness

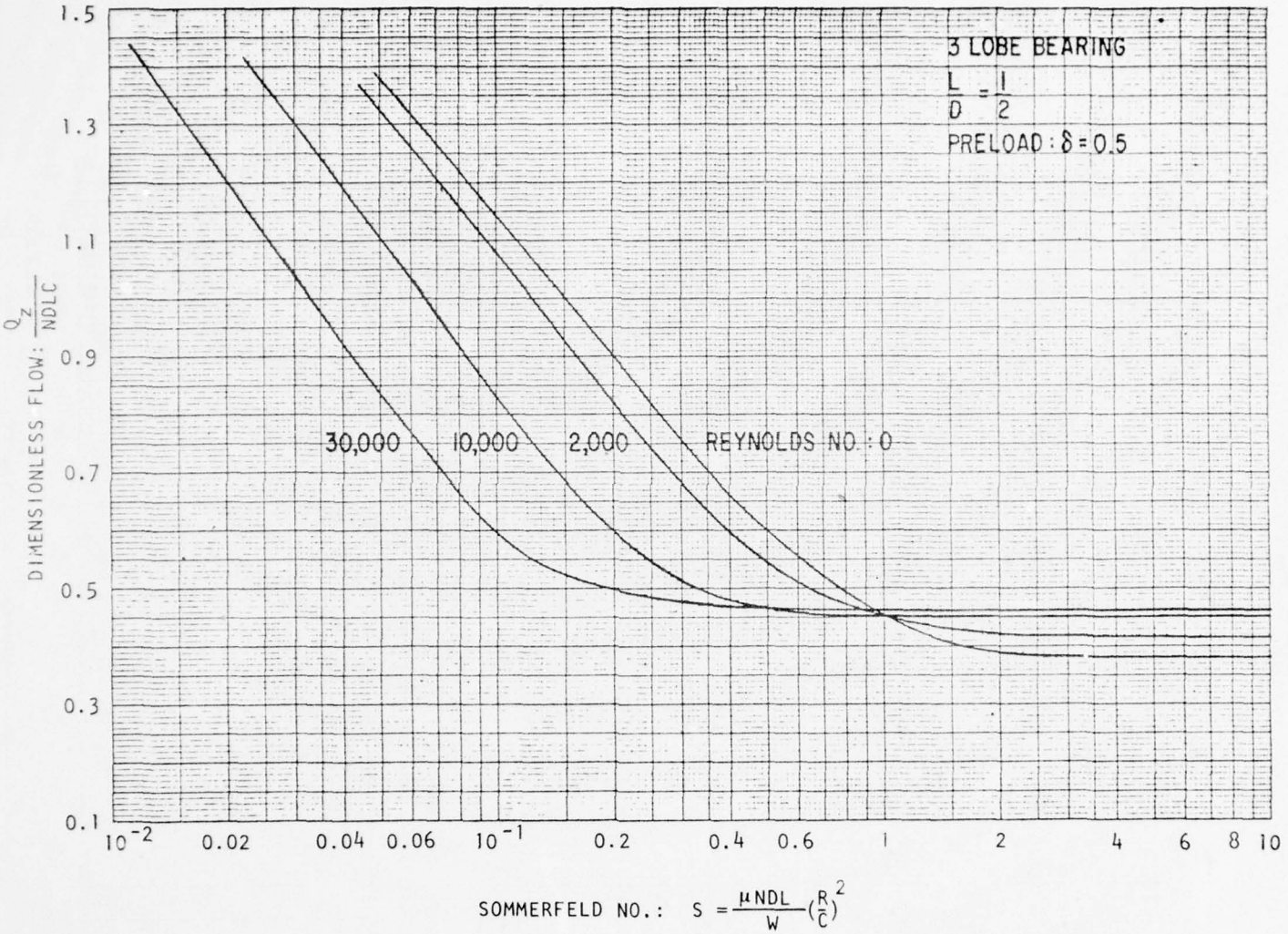

Figure 34. Three-Lobe Bearing, Preload = 0.5, $\frac{L}{D} = \frac{1}{2}$, Flow

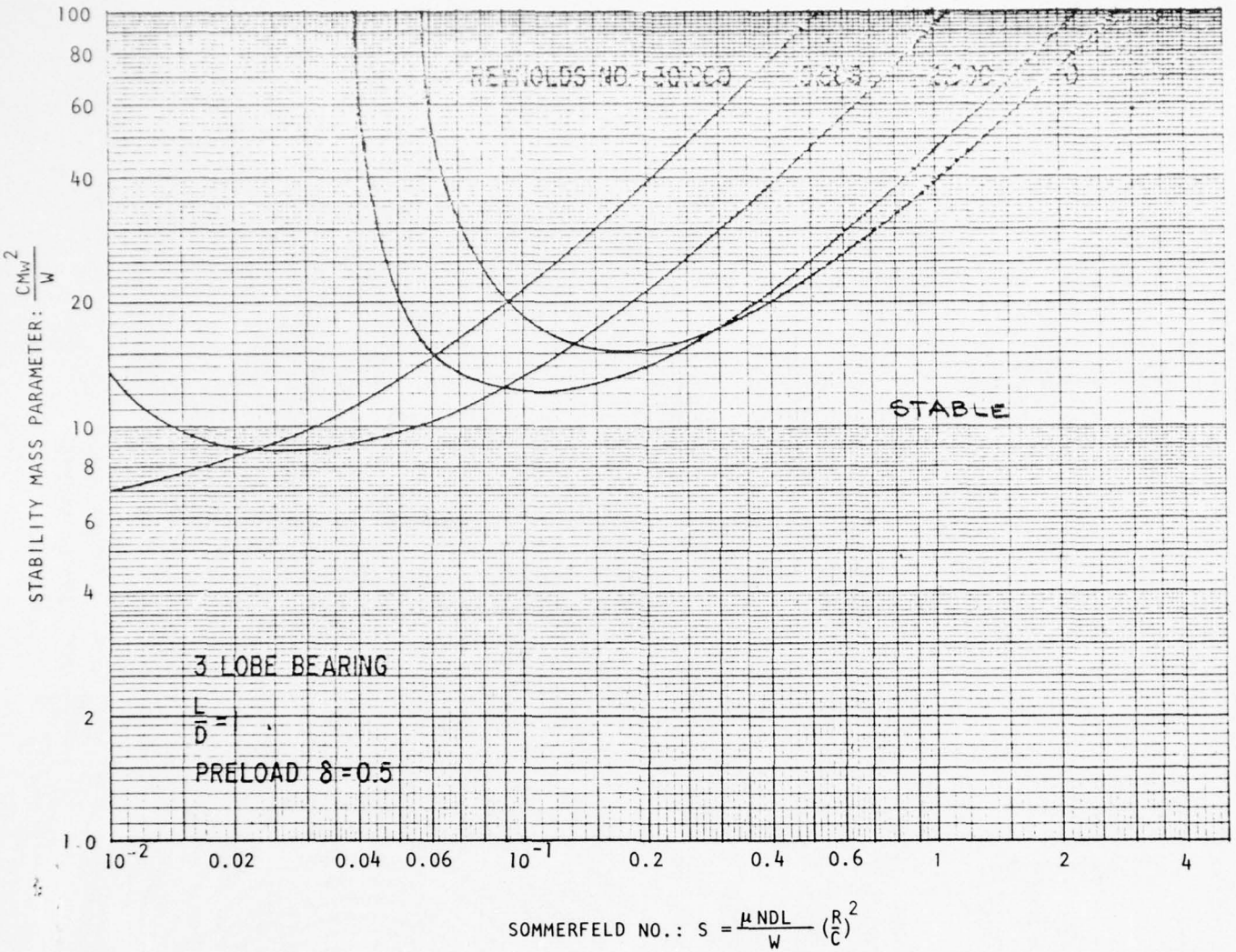

Figure 35. Three-Lobe Bearing, Preload = 0.5, $\frac{L}{D}$ = 1, Stability Map

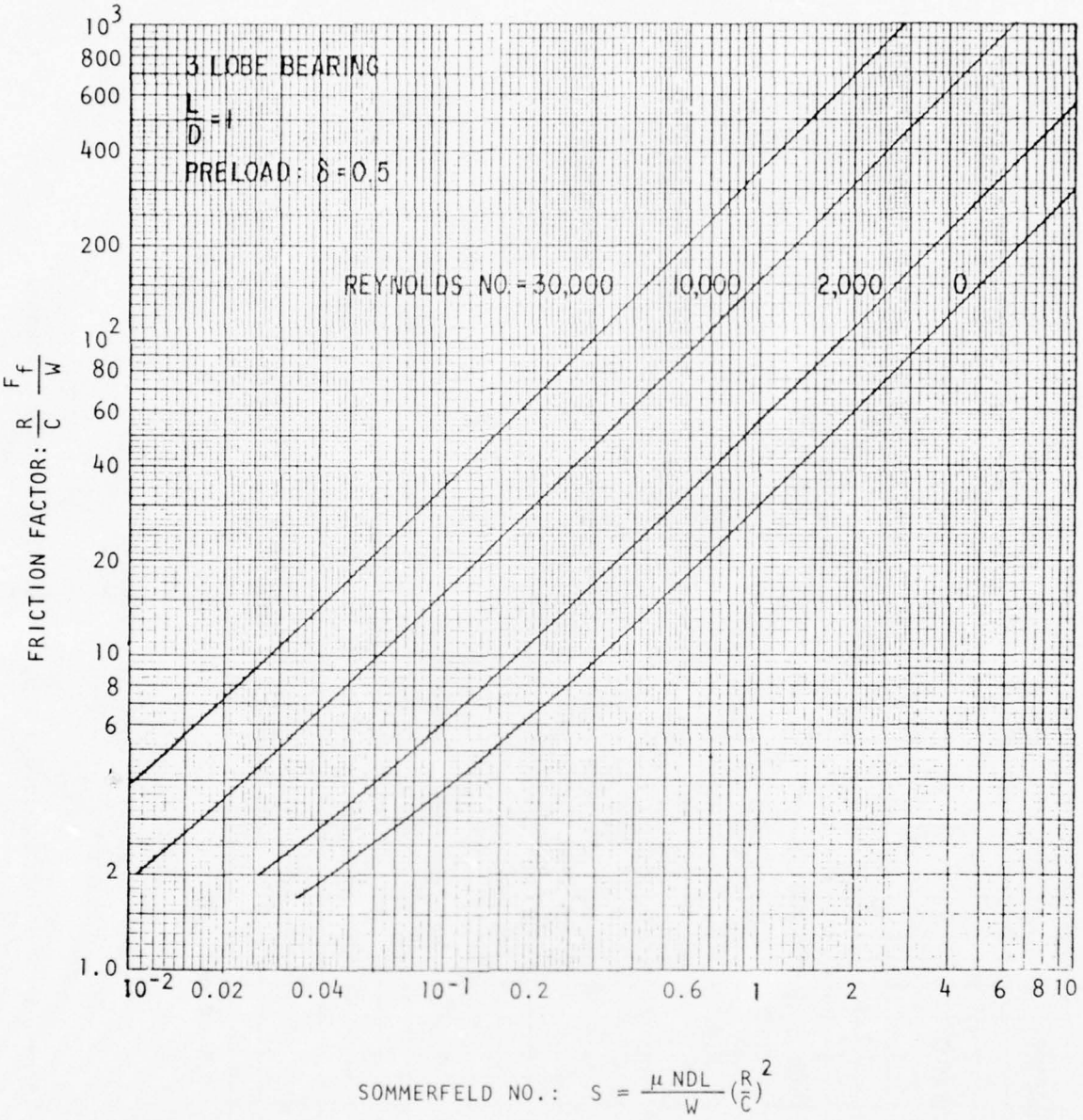

Figure 36. Three-Lobe Bearing, Preload = 0.5, $\frac{L}{D}$ = 1, Friction

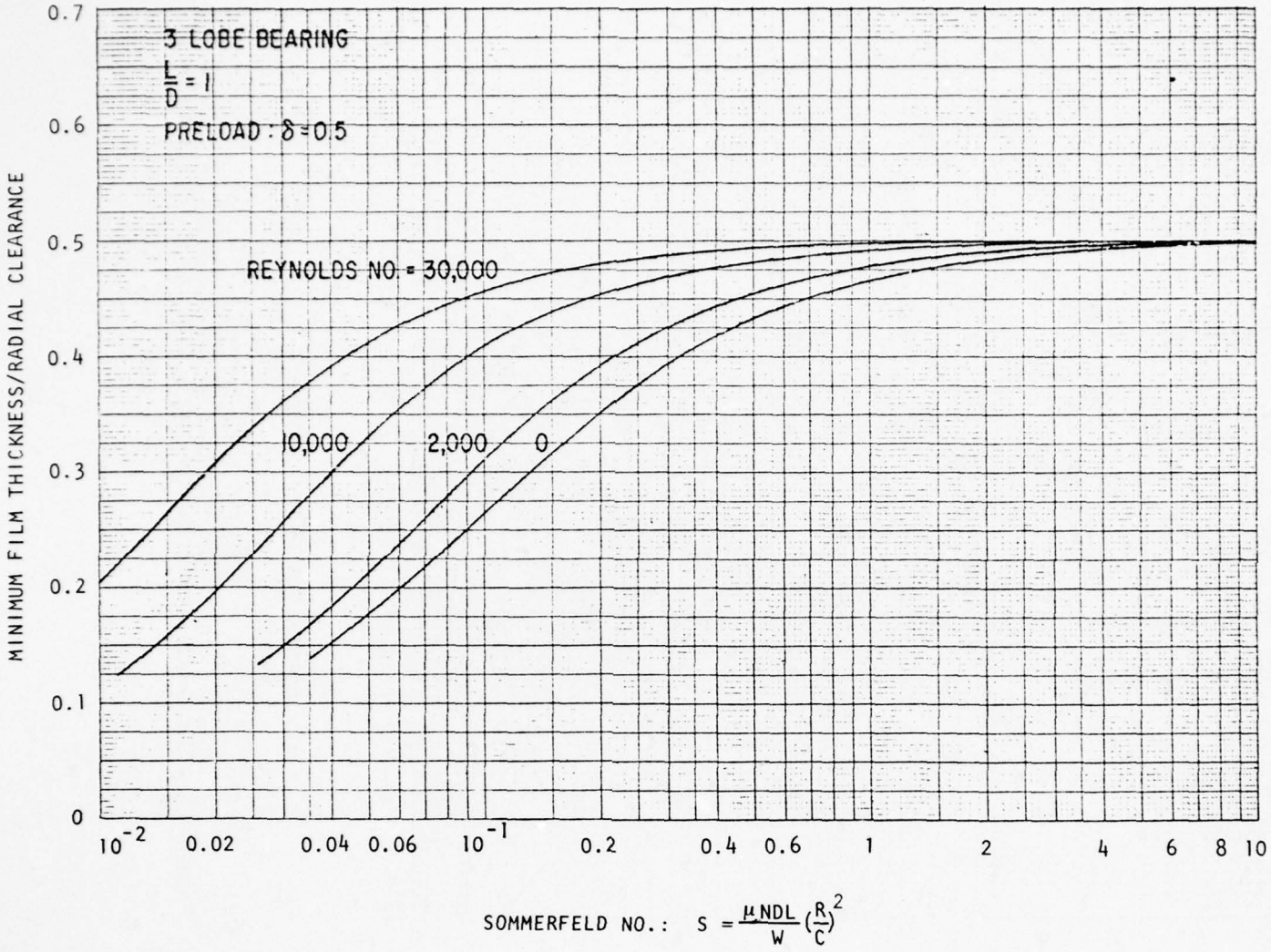

Figure 37. Three-Lobe Bearing, Preload = 0.5, $\frac{L}{D} = \frac{1}{2}$, Minimum Film Thickness

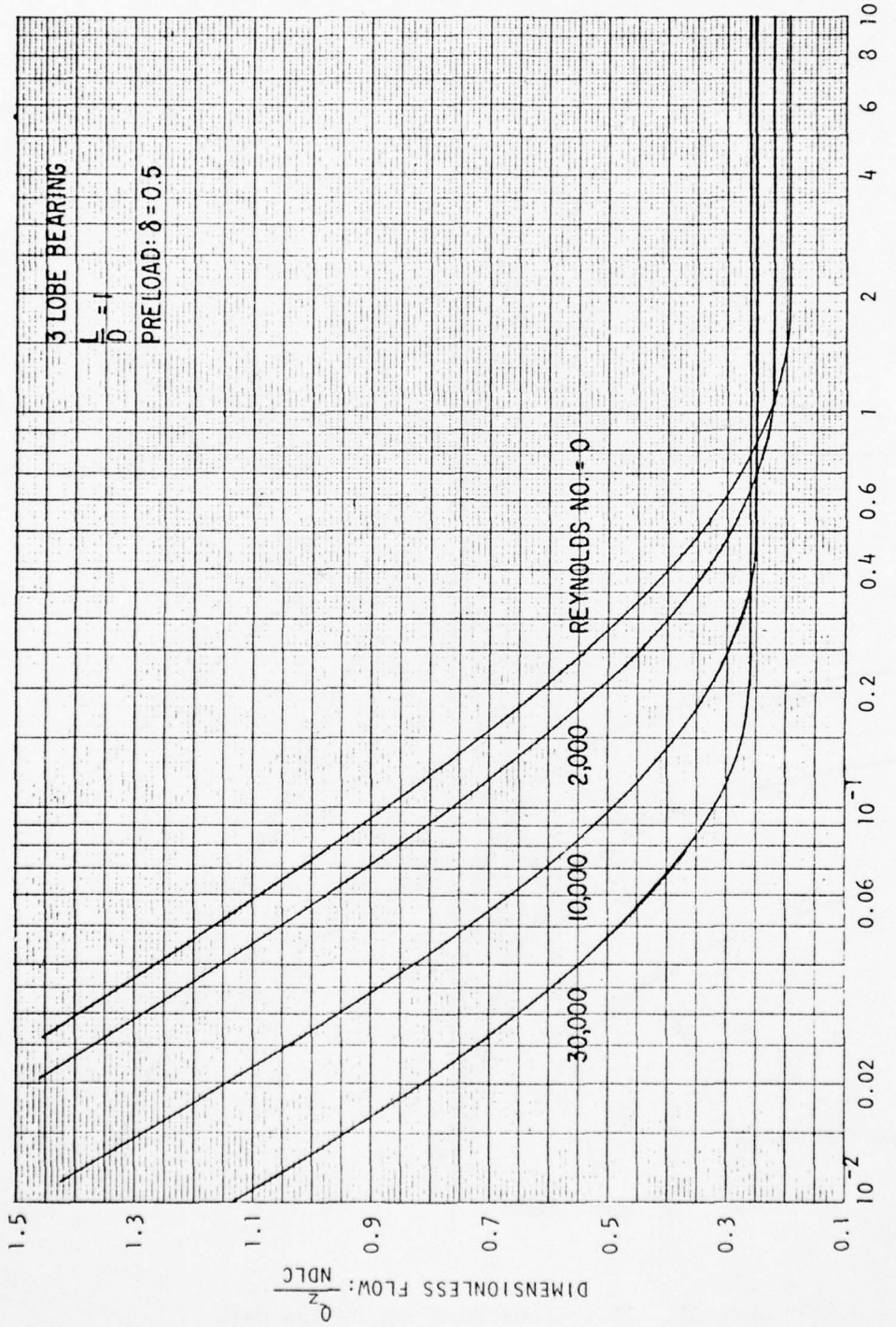

Figure 38. Three-Lobe Bearing, Preload = 0.5, $\frac{L}{D}$ = 1, Flow

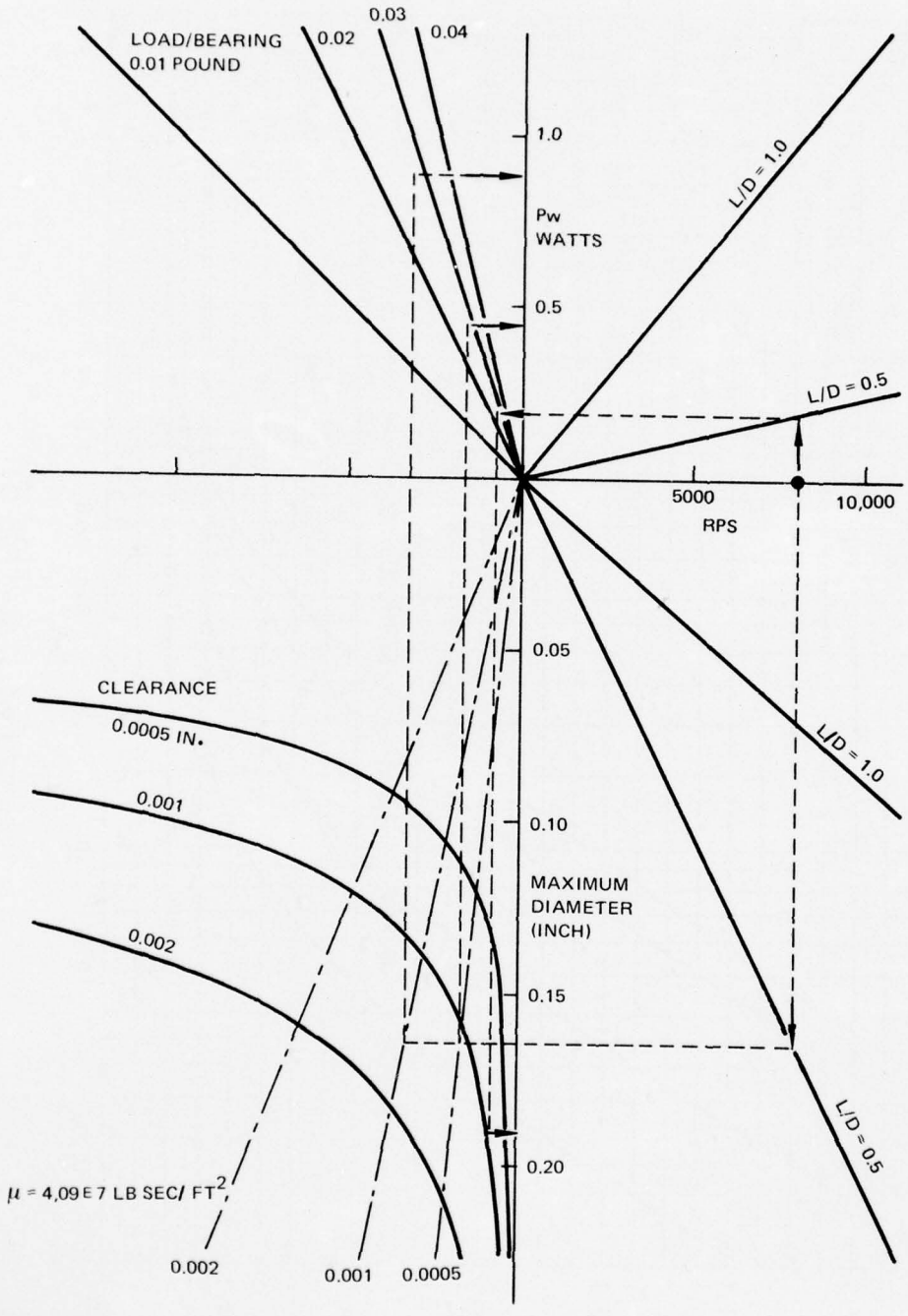

Figure 39. Three-Lobe Bearings Design Data

diameter to maintain stability can be obtained by selecting in turn and reading in a counterclockwise path

speed
L/D
clearance

Power dissipation can be read by a clockwise reading of

speed
L/D
clearance
load per bearing

In the example diagrammed, speed is 8000 rps (480,000 rpm), L/D is 0.5, load per bearing is 0.028 pound, and clearance is 0.0005 inch. The maximum diameter is 0.19 inch, and the power loss 0.45 watt.

Based on the analysis it was concluded that the three-lobe bearing could indeed be usefully installed in the 60-watt power source. Stability margin would be ample, and fabrication would not be too difficult if a broaching technique were employed. It was decided to utilize the spiral-groove rotor by plating and grinding the cylindrical section ahead of the cones (Fig. 27b) to 0.1750/0.1748. Imperfections in the plating process aborted this attempt and a new rotor was made. The bearing for this rotor is shown in Fig. 40 and had a clearance, C, of 0.0030. This assembly was set up in the standard test rig, and operated with cold GN_2. Speeds up to 30,000 rpm were reached. However, operation was both noisy and unsteady, i.e., traces on the oscilloscope showed rapid low-amplitude instabilities. It was felt that the instability might be due to a failure to form an adequate load-carrying film, causing rubbing in the journal. Therefore, the test rig was modified to provide pressurized gas flow to the relief grooves in the three-lobe bearing. By adding the external pressurized gas source, a hybrid hydrodynamic-hydrostatic gas bearing resulted.

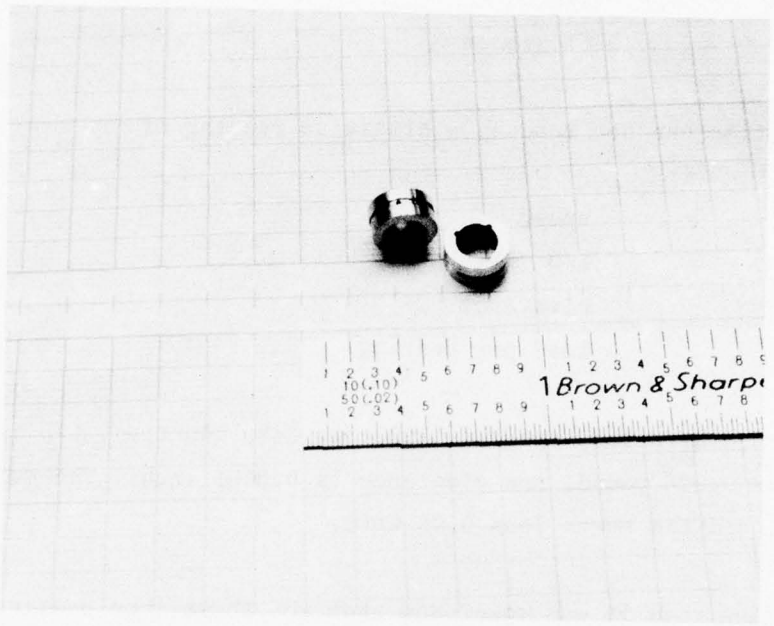

Figure 40. Three-Lobe Bearings

Test results with various gas pressures ranging from 20 psia to 50 psia did not indicate any improvement in operation except that at very low speeds (before a hydrodynamic gas film could be generated) the rotating assembly operated with much less drag. However, once the hydrodynamic gas film was established at speeds of 1000 to 5000 rpm, the addition of external pressurization did not appear to have any significant effect.

It was decided that the clearance was excessive and that it would be desirable to reduce it. Therefore, a new set of bearings with a nominal clearance of 0.0018 inch was fabricated. The rotor was kept the same.

Tests were conducted and the test conditions were duplicated. Speeds up to 60,000 rpm were reached with this arrangement; however, the distinctive bearing noise remained present and indicated that the bearing was not functioning properly. However, even with this handicap, one of the tests consisted of an uninterrupted period of 15 to 20 minutes. It was felt that internal heating of the bearings could not be the cause of the noise because the cold pressurized gas supplied to the bearing maintained the surfaces at a reasonable temperature.

The test rig was disassembled and the bearings inspected. Some indications of rubbing were observed. The bearings were carefully realigned in the radial direction so as to loacte one pad directly below the shaft in the event that gravitational forces had an effect on operation. Bearing supply gas pressures were maintained between 40 and 56 psi, and speeds of 100,000 rpm were reached. Operation appeared to be somewhat better, but the same rubbing noises were still present.

Based on bearing tests conducted on some other film bearings at Rocketdyne, it was theorized that sharp edges in the bearing may be producing the noise due to feathering. Therefore, all edges were rounded off to a minimum radius of 0.005 inch. Retesting of these bearings did not show any improvement; however, examination after test indicated some "machining" on the edge of the bearing, apparently caused by the shoulders of the shaft hitting intermittently. The

shaft was removed and undercut so as to eliminate any possible extraneous contact between the rotating assembly and the bearing. Additional tests with this modified rotating assembly did not show any improvement in operation, however. Rechecking the shaft straightness indicated that the shaft was within 50 microinches straight from bearing to bearing. Bearing alignment was then checked with a gauge shaft, and alignment was also within 50 microinches.

It was then decided to investigate the effect of increasing the clearance in the bearing. A quick test was made by machining the journals from a diameter of 0.17465 in. to a new diameter of 0.17400. The finished dimensions were within 20 microinches. This, in effect, increased the clearance by 0.000325 inch. The only result from this modification was that instabilities occurred at much lower speeds, approximately 10,000 to 15,000 rpm.

One fact relating to the observed instabilities was that the "noise" generated did not appear to be speed dependent once it occurred. A radial instability would be related to rotor unbalance and would exhibit discrete peaks related to critical speeds. It was, therefore, reasoned that an axial instability of some sort must be present. Because the bearings are purely sleeve bearings, this axial instability would have to relate to some other excitation force.

Axial location of the actual power source is by means of the strong magnetic field which causes the magnetic rotor to center itself in the coil. Also, this magnetic centering force has a strong damping effect which prevents any external excitation from becoming objectionable. But with a nonmagnetic rotor, these beneficial forces are not present. Centering is achieved by the forces put on the shaft by the impinging gas jet. It has often been demonstrated that the rotor easily follows axial movement of the nozzle, maintaining a definite position between turbine bucket and jet centerline. With no damping in this setup, it was felt that it might be possible for an axial instability to develop in the turbine and this could be responsible for the observed noise. Tests with conical spiral-groove bearings would not have exhibited this behavior because the cones position the shaft.

Axial control could be achieved by placing stops in the axial direction. With the configuration under test, only one stop could be placed conveniently; that is, without a rework. Therefore, the test rig was mounted at a slight incline toward the stop, in the hope that the the gravitational component would prevent axial motion. This proved to be partly successful but did not eliminate the noise.

Because the instability was apparently unavoidable, being turbine related, and because the only plausible solution was to introduce damping into the system, it was decided to put some oil into the bearing. One drop of turbine oil was introduced into each bearing. This proved to be almost miraculous. The bearing almost immediately ran stably at 150,000 rpm and, when the rig was reworked by providing a second axial stop, up to 235,000 rpm. At these speeds, operation continued satisfactorily but driving gas pressure limits were reached. It was also evident that the bearing was not operating on an oil film because drag was much too low to account for shearing of an oil film.

The following arguments are put forth to explain these results. Even though the bearing is brass and the shaft is steel, this material combination is slightly incopatible, resulting in some galling. When axial instability is encountered, the shaft and bearing tend to touch momentarily. If galling is present, this produces the noise heard. The galling is momentary and recurring. With the oil in place, the surfaces are coated and contact produces no galling, even though bearing operation remains on an air film between the two oil films. In analyzing this result it became obvious why prior tests with air bearings had not encountered a similar result. On all prior runs, molybdenum disulfide had been worked into the metal surfaces. Because of the irregular shape of the three-lobe bearing, this was not possible and was not done. The moly disulfide, of course, acted to avoid galling.

With the rotor running smoothly at high speeds, it became possible to observe the axial instability that had previously been masked by the materials-related problems. Close observation with stroboscopic illumination showed that the axial instability appeared to be caused by the gas forces from the nozzle tending to push the turbine in one direction, overshooting a stable position of operation

and then returning beyond its original point of operation. Because this test rig used a simulated rotor which was nonmagnetic, there were no magnetic damping forces to stabilize this axial motion and hence it acted in a totally undamped fashion.

Having apparently isolated the cause of the problem which had impeded progress for some time, the test rig was modified to incorporate two Teflon stops, one at each end of the two bearings, so that the axial motion of the shaft could be completely controlled. With this arrangement, tests were conducted up to speeds of 235,000 rpm. Operation was smooth and completely satisfactory. The speed limitation was due to the fact that cold GN_2 was being used and the spouting velocity was limiting the operation. At this speed, U/C_o equals approximately 0.25, which is near the peak of the efficiency curves for Terry-type turbines. Therefore, increases in pressure, while increasing available energy, do not increase energy output because efficiency decreases.

Once it was shown that the oil made it possible to operate the bearing stably at high speed, the basic bearing problem which had plagued the program to this point appeared solved. Bearing friction appeared to be reasonable, and a series of tests to determine its magnitude were scheduled to be performed together with the alternator tests.

GAS GENERATOR

A series of tests were initiated to develop a reliable micro gas generator using hydrazine for the 60-watt power system. Previous development had resulted in a gas generator that had a somewhat complex configuration and was not totally reliable, although when it functioned, its performance was well within specifications. Based on the experience gained in the earlier development, a new gas generator design was evolved. The primary difficulties with the previous gas generator centered around mechanical features, e.g., structural failure of the hypodermic injection tube, and failure of the catalytic bed support screen. During tests, this gas generator had a marked tendency to plug either at the injection tube or at the exit nozzle.

The new gas generator design is shown in Fig. 41. This unit consists of a 1.65-inch-long catalytic bed contained in a 1/8-inch-O.D. stainless-steel tube. The bed is filled with Shell 405, 20- to 30-mesh catalyst. To eliminate a small injection orifice, a 1-1/2 inch-long by 0.01-inch-I.D. hypodermic tube is welded to the injector and provides the required injection pressure drop. The catalytic bed is supported by two 60-mesh Monel screens welded to the end of the 1/8-inch tube. The nozzle assembly is welded to the catalytic bed tube and contains an adaptor which is filled with 0.025-inch-diameter, stainless-steel balls contained by a 35-mesh Monel screen directly in front of the nozzle, which is welded to the adaptor.

One of the two major features of this design is the injector plate. The difficulties of structural failure of the hypodermic injection needle was eliminated by providing a completely radiused entrance on the upstream side of the injector plate and locating the weld of the hypodermic needle to the injector plate on the downstream side of the plate. In this fashion any flexing of the hypodermic tube during installation would not result in kinking or abraiding of the hypodermic since the radius provides a suitable bend angle. No further failures of the hypodermic tube weld has been encountered since this design was implemented.

AD-A032 076 ROCKWELL INTERNATIONAL CANOGA PARK CALIF ROCKETDYNE DIV F/G 10/2
60-WATT POWER SOURCE.(U)
APR 76 J A SPEEDS, R SPIES F33615-73-C-4071
UNCLASSIFIED R-9651 AFAPL-TR-76-44 NL

2 OF 2
ADA032076

END
DATE FILMED
1 -77

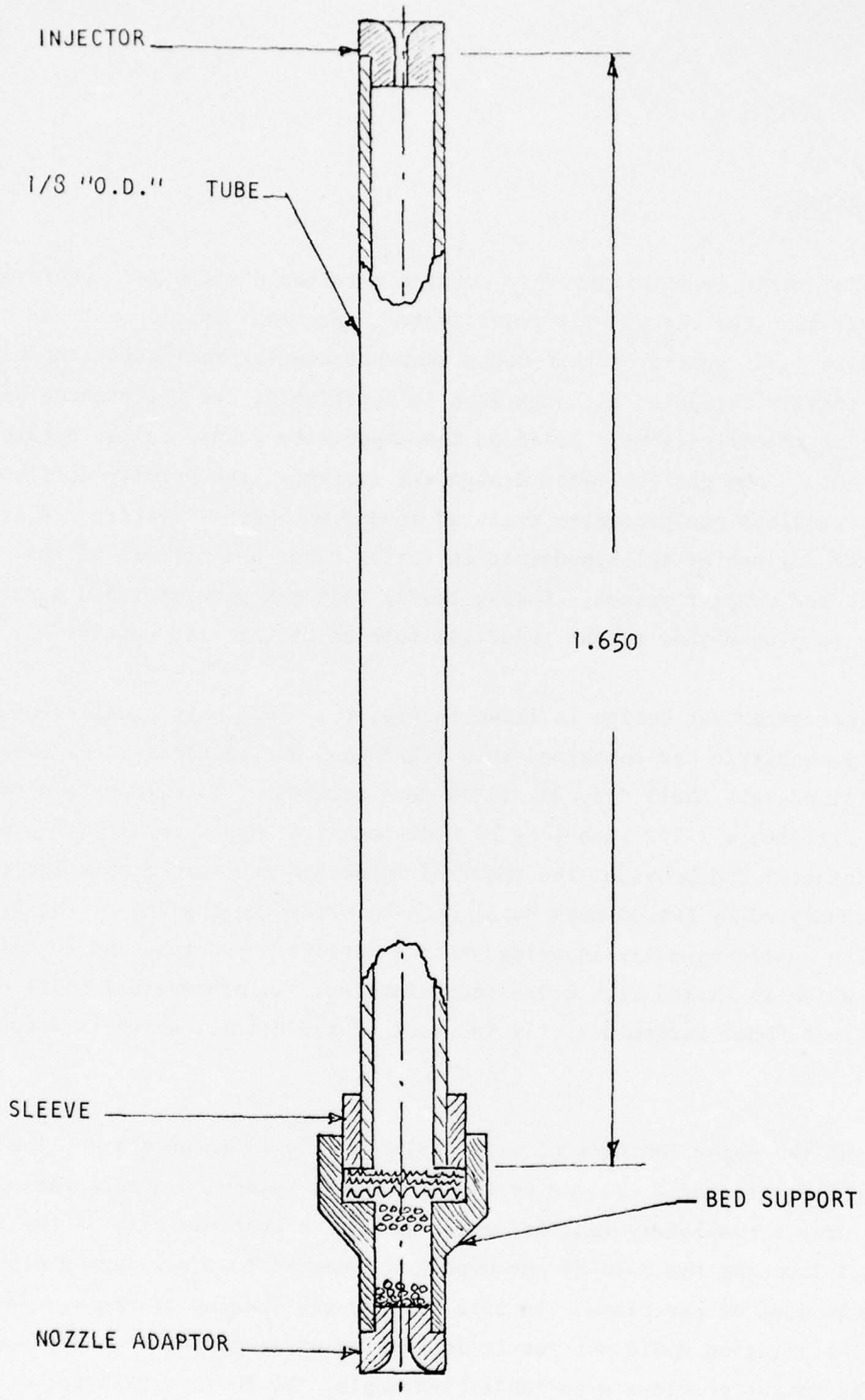

Figure 41. Gas Generator Assembly

The second feature of this design was devised to eliminate the problem that was observed with the previous gas generator; namely, after each disassembly it was found that the two fine-mesh screens retaining the catalytic pack had a small hole "burned" through the center of the screens. Because the gas temperatures are not high enough to melt Monel, it was assumed that Monel was sufficiently weakened at 2000 F to be eroded by the gas stream. To eliminate this problem, the bed support adaptor was designed to provide two major remedies. Rather than allow the gases to converge to the nozzle orifice at the fine-screen location, the ball-packed adaptor permitted the gases to continue over the entire diameter of the screens and not converge until they reached the ball pack, which was immune to this type of failure. The screen which contained the ball pack was of sufficient size to prevent erosion. The other feature was complete support of the fine screens by the ball pack so that structural integrity of these fine screens could be maintained. The partially assembled test gas generator is shown by the photograph in Fig. 42 . It should be noted that the nozzle was an orifice plate to simulate the actual nozzle and was used only for gas generator test purposes. The fine screens retaining the catalytic pack had already been welded to the end of the tube when this photograph was taken, and only the heavy screen supporting the ball pack is shown.

The planned development test series ended with a successful test. The test gas generator was installed at the B-1 facility of Rockwell International in the small hydrazine test cell. Tests were initiated by opening the main valve, and the gas generator immediately came up to pressure, and temperature followed instantly. The tank pressure was then raised to various levels until the chamber pressure reached 700 psig. At this point, the gas generator was operated for 300 seconds and the tank pressure was reduced; further operation of the gas generator was conducted at 500-psig chamber pressure until the hydrazine tank was empty. Segments of the temperature and pressure traces are shown in Fig. 43.

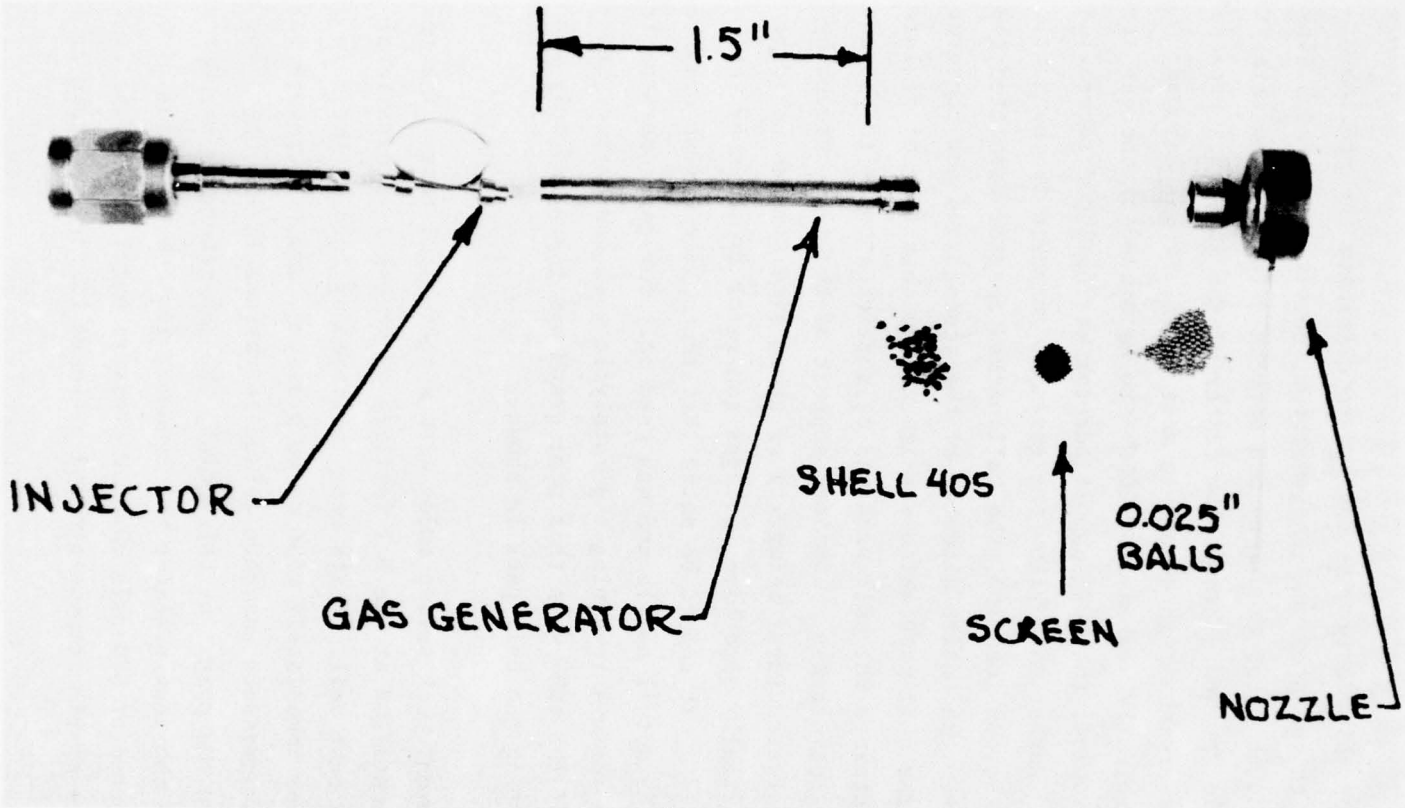

Figure 42. Gas Generator Components

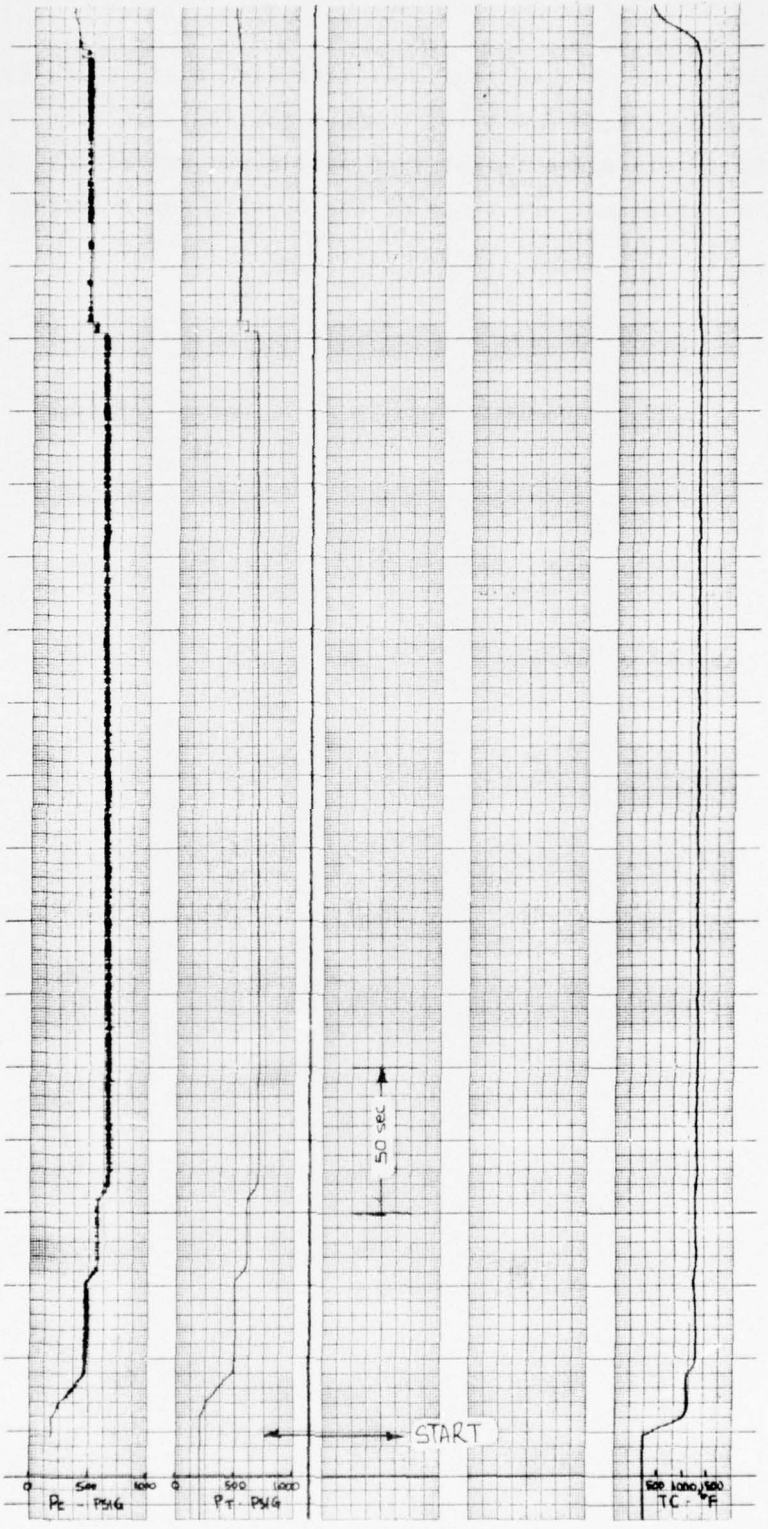

Figure 43. Gas Generator Test

Posttest examination of the gas generator indicated that it was in excellent condition and could be used again for further testing. In fact, the test nozzle was machined off and a flight-type nozzle was welded on. The assembly was used for the subsequent hot tests of the 60-watt power system brassboard unit.

ALTERNATOR AND ASSEMBLY

Alternator tests were performed as a final cold-gas check prior to complete systems testing. To produce useful power with the present setup an overall efficiency in the mid-thirties could be expected. Therefore, nearly 200 watts of gas power would be needed. Using the nozzle designed to operate with the turbine, the gas power available can be expressed as:

$$\text{watts} = (6.53\text{E-}3)\sqrt{T}\ p\left[1 - \left(\frac{14.3}{p}\right)^{.286}\right]$$

Therefore, using room-temperature gas, about 1800 psi would be required. Conversely, at reasonable pressure (using supply bottles), temperatures in the range of 1500 F would be required. Prior attempts at heating the gas had proved to be very difficult. It was found that at the very low flowrates required, the system was very slow to heat up and the turbine lost too much heat to control the temperature as flow varied. Therefore, a different tack was attempted for the alternator tests. By increasing nozzle size, flow was increased, increasing available power without the need for heat. Turbine efficiency will be adversely affected because the gas stream is wider than desired and because the spouting velocity will be lower than design. However, turbine efficiency was not of prime consideration for these tests, which were being conducted to show that the alternator design operated properly at high speed and to permit data to be obtained on bearing and windage losses with the alternator acting as dynamometer. A nozzle with a throat diameter of 13.5 mils was fabricated. This increased the flow by a factor of 2.9 so that pressures of 700 psi sufficed with room-temperature gas. Figure 44 shows this new nozzle which was constructed with integral pressure taps. Prior nozzles using hypodermic tubing had proved very fragile for test purposes and so a sturdy configuration, capable of easy handling was selected. Of course, flight-type hardware would again use hypodermic tubing.

The rotating assembly used for the alternator tests is shown in Fig. 45. . Prior testing, as detailed above, had used a samarium cobalt magnet encapsulated in a steel sleeve. This steel sleeve served to contain the very brittle

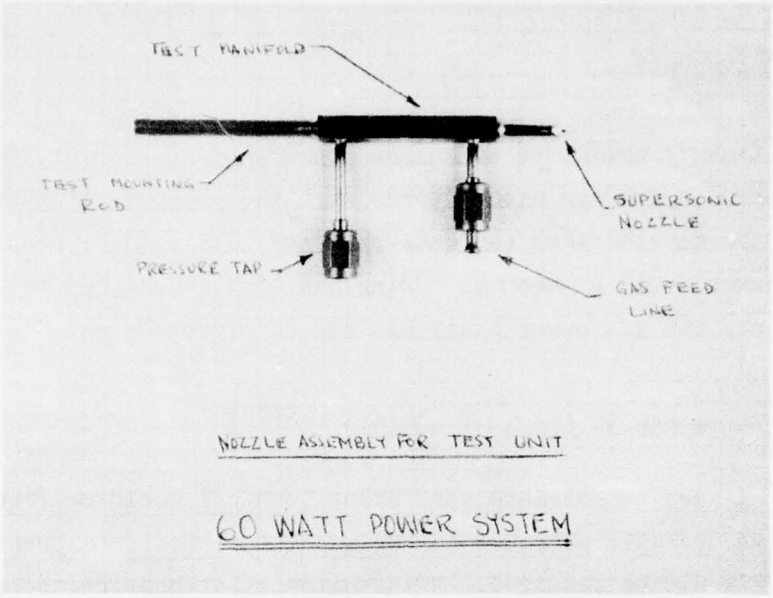

Figure 44. Nozzle Assembly for Test Unit

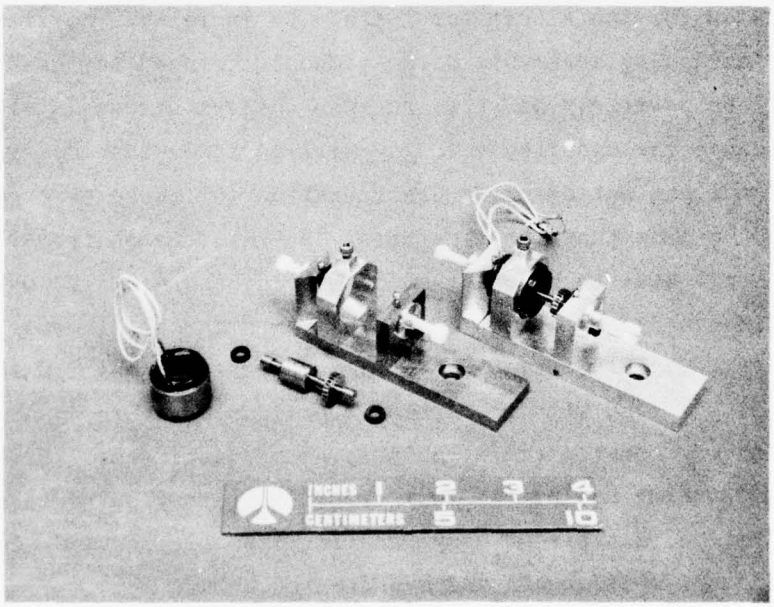

Figure 45. Test Rigs

magnet, and a speed of 335,000 rpm was achieved with this configuration without damage to the rotor. However, in this design the turbine is closely coupled to the magnet thermally so that a hot test would result in overheating of the magnet with consistent loss of strength. A design to prevent this had to be evolved.

Discussion with Hamilton Technology, Inc., revealed that use of a platinum cobalt magnet would be beneficial. This material has greater thermal latitude and greater structural strength, and calculations revealed that it could be used without the need for encapsulation. This meant that the rotor diameter could be decreased to 0.4 inch and the magnet could be mounted on a shaft by placing the shaft through a central bore. With this type of configuration, thermal resistance can be built into the shaft to reduce conductive heat transfer.

The first design evolved contemplated the use of a spirally wound, flexible wire shaft using a double helix. From a heat transfer point of view, this shaft concept is particularly attractive because heat conduction is limited through many points of contact with high contact resistance and along a very thin wire path. To determine actual resistance to heat flow, a simple experiment was conducted.

A short piece of 0.098-inch-diameter flexible shafting was set up with two thermocouples, 1 inch apart. An oxyacetylene flame was used to heat the shaft approximately 0.25 inch from the first thermocouple (Fig. 46). The first thermocouple reached a maximum temperature of 1300 F after 12 minutes. During this interval, the second thermocouple increased slowly to 210 F. As can be seen in Fig. 46, the temperature at the point of flame application reached the melting point of the steel wire (2550 F). Therefore, this type of shafting is an excellent barrier to heat flow.

A rotor using this type of shaft was constructed (Fig. 47). Ball bearings were used because they had been successful before, and these tests were made before the journal bearing problems were solved. A dummy steel mass was used instead of the magnet for the initial tests.

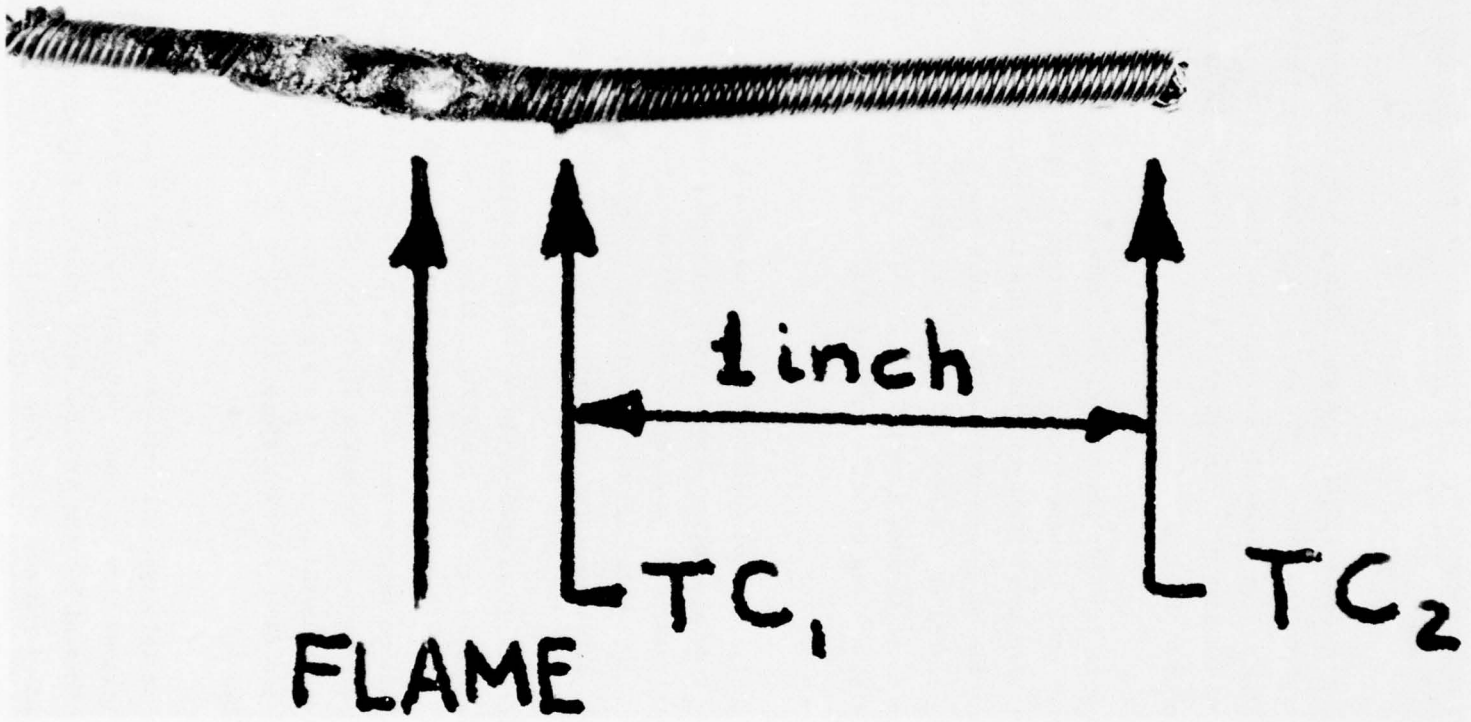

Figure 46. Flexible Shaft Used for Heat Barrier Test

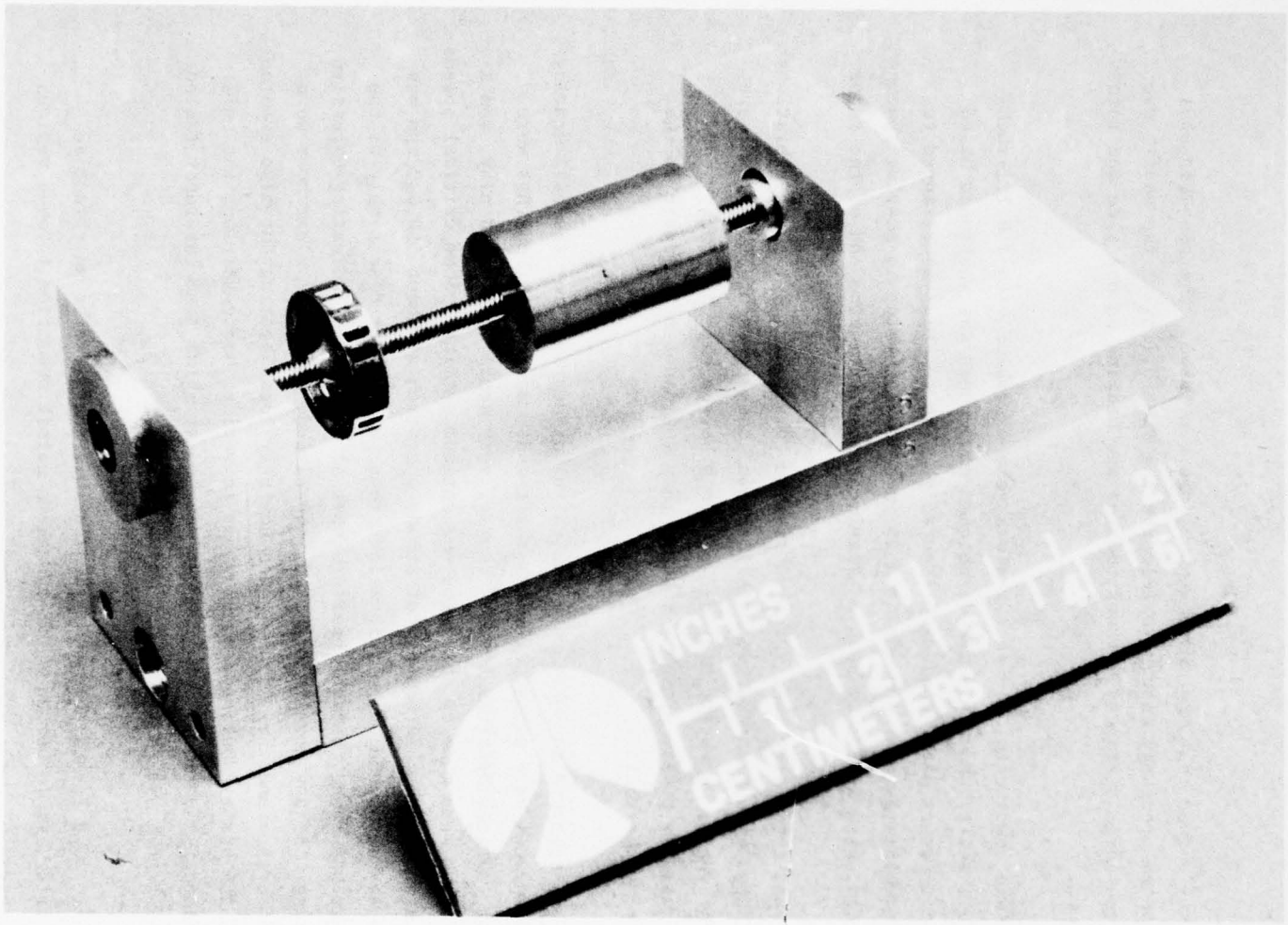

Figure 47. Rotor with Flexible Shaft

Initial tests showed that rotordynamics would be a problem. The assembly could not be balanced precisely enough to tolerate the flexibility of the shaft, due mainly to the large distances between turbine and bearing on one side and rotor on the other.

Using the same components, the test rig was next assembled with a 0.122-inch-O.D. flexible shaft, and the distance between components was shortened based on the heat transfer data found experimentally. The new rig was arranged to provide a turbine-to-rotor spacing of 0.25 inch and a turbine-to-bearing spacing of 0.125 inch, with a closely coupled bearing at the antidrive end of the rotor.

At 14,000 rpm, this rotor configuration started to vibrate, but these vibrations were eliminated with minor radial stabilization, and speeds of 35,000 rpm were readily achievable. However, the ball bearings became extremely noisy, and consumed excessive power, probably because they could not accommodate to the flexibility of the shaft.

The rotor was reworked to substitute conical pivot bearings for the ball bearings. Conical end pieces were placed over the shaft ends, and mating bearings were fabricated. Conical bearings are, of course, very sensitive to end play, and a series of tests were made to determine the optimum setting. Some critical speeds were encountered with this setup, but steady operation at about 150,000 rpm was achieved. At that speed, minor vibrations recurred. After disassembly of the test rig, it was found that the bearings were straw-colored indicating excessive local heating. As any heating occurred, the already low axial clearances were diminished further and they might induce not only local heating but also eventual flexing of the shaft. During a second test to verify this condition, the unit ran satisfactorily until 141,000 rpm was reached, at which time the rotor failed. Photographs in Fig. 48 show the test setup.

The conclusion was inescapable that the flexible shaft, while an effective thermal barrier, would not be stiff enough to permit operation through various critical speeds.

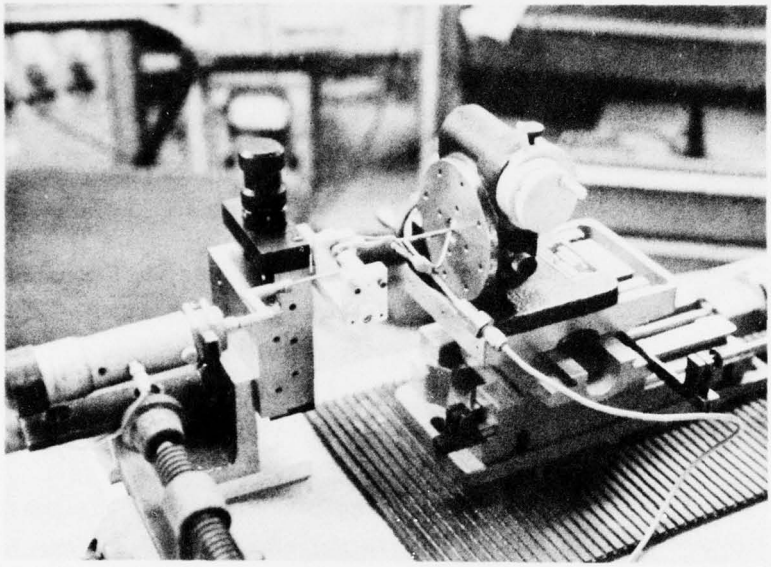

Figure 48. Rotordynamics Test Setup

Another means of reducing thermal conduction to the magnet while increasing shaft stiffness had to be found. It was suggested that a solid shaft which has threads cut onto it in the area where it passes through the magnet might be acceptable. While conduction down the shaft would not be reduced, the flow to the magnet would be minimized by the fact that only live contact existed between the magnet bore and the thread tips.

Two rotors using this concept and the platium cobalt magnets were constructed. Each was balanced; one to 15 micro-inches and the other to about 50 micro-inches. It was not obvious why the second rotor could not achieve better balance, but the magnet may have been just slightly looser on the shaft permitting it to shift under radial growth due to centrifugal force.

At this juncture the three-lobe bearing had been developed making it possible to use this configuration. Two test rigs were therefore assembled, one for the cold gas tests and one for the hot-gas brassboard demonstration. Both of these rigs were identical except that the test rig for cold flow was fabricated with aluminum while the brassboard demonstration model was made out of stainless steel. The photograph in Fig. 45 shows one assembled and one disassembled test rig. For purposes of the cold flow alternator tests, a set of precision machine shop XYZ adjustable tables were used to position the nozzle with respect to the turbine, this setup is shown by the photograph in Fig. 49 . The details of the nozzle location with respect to the turbine are shown by the photograph in Fig. 50.

Three new stator coils were wound for this test series. The coils originally made at the Rockwell International Autonetics Division had proved to have too low a voltage output. Now with the use of new magnets, with a smaller diameter and greater strength, new coils which would have the proper output were designed. Two coils were wound and found acceptable but marginal because of a length limitation which caused the end turns to be sharp. Therefore, a third coil with an added length of 0.1 inch was made and found to be excellent in all respects. Tests were made with all three coils.

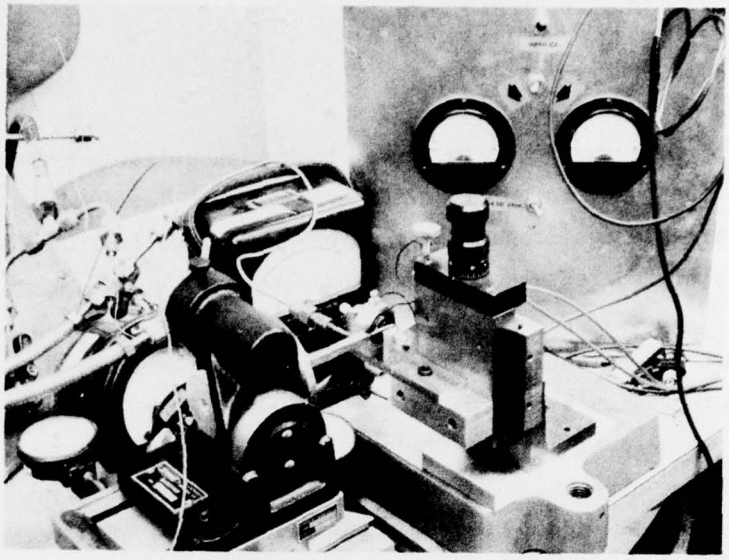

Figure 49. Test Setup

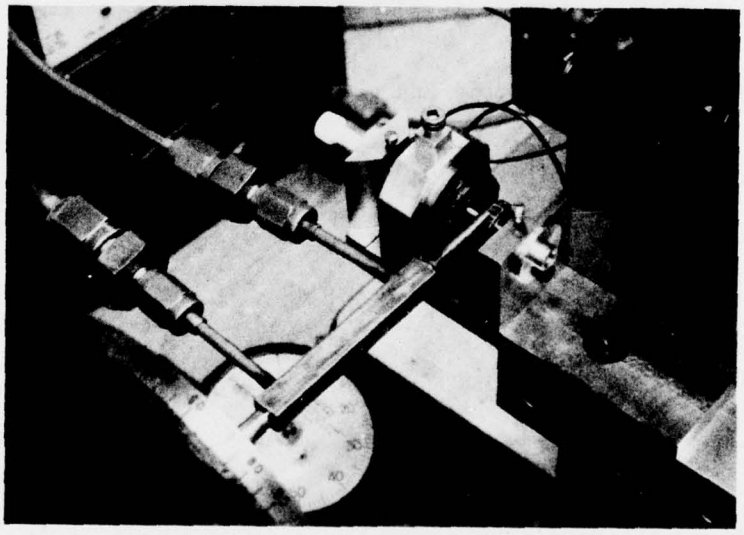

Figure 50. Nozzle Location

The output of the coils was fed into a load bank with suitable meters provided to measure the power output from the alternator. The load bank consisted of a variable resistance and a three-phase rectifier bridge as well as the necessary current and voltage indicators.

Various measurement techniques exist for measuring high-frequency a-c power; however, complexity in instrumentation and availability of this type of equipment dictated the use of a rectification circuit in order to measure power with standard laboratory d-c equipment. Initially, both voltage and current were measured on the d-c side of the bridge. However, even with the use of precision transistors in the bridge, the voltage drop across the transistors was a significant portion of the measured value and, therefore, it was decided to measure voltage on the a-c side of the bridge and current on the d-c side. For the type of bridge used, a well-established relationship exists for relating d-c current to a-c current. Combining the two measurements, power is expressed as follows:

$$\text{Power} = \left[\left(\sqrt{3}\right)\left(\text{Volts a-c}\right)\right]\left[\left(0.85\right)\left(\text{Current d-c}\right)\right]$$

The technique proved very acceptable and gave consistent results.

SYSTEM TESTS

At this point, the various components were operating satisfactorily and tests were initiated to operate the breadboard system. Cold-gas tests were planned to check out all aspects of operation, and hot-gas tests completed this test phase.

Cold-Gas Tests

A series of cold-gas tests were performed using nitrogen gas, the three-lobe bearings, the threaded rotor with the platium cobalt magnet, and the new stator coils. In addition to attempting stable high-speed running, these tests were intended to measure bearing and windage losses by the method previously described. Basically the unit is operated without external load at a steady speed. The gas flow and energy are calculated. With a load applied, the rotor decreases in speed. By increasing gas flow, the speed is restored. The added gas power is compared to the power output yielding an efficiency and an indication of losses. These steps are repeated at various speeds to map the regime.

Table 11 shows the results of one test series together with calculated values. Even though a top speed of 175,000 rpm was achieved during this whole series, the operation was not nearly as smooth as the bearing tests indicated when using the one-piece rotor of same configuration. Upon checking, it was found that two adverse conditions had developed. First the power output of the three phases on the coil were not balanced. One phase consistently produced 1.6 times as much voltage as the other two, which were nearly the same. The cause of this unbalance is not known and would require disassembly of the coils to determine. However, it is evident that it places an unbalanced force field on the rotor, similar to a rotor unbalance, and the bearing tests had shown that this condition is a potential trouble source for bearings. Also, the magnetic rotor had loosened on the shaft and could turn on the shaft.

TABLE 11. TEST RESULTS

Nozzle Pressure, psig	Speed, rpm	Voltage, vac	Current, adc
70	75,000	9.7	0
70	15,900	1.9	0.085
345	76,200	8.9	0.95
345	174,000	-	0
165	108,000	14.5	0
250	128,000	15.5	0
300	68,600	8.1	0.86
300	128,000	16.5	0
200	110,500	13.5	1.45
500	152,000	19.0	0

This probably is the result of repeated radial centrifugal growth which loosens the rotor and permits some slippage, wearing away the tips of the heat barrier threads. It must be remembered that the interference fit between these threads and the rotor was maintained minimal to ensure minimum heat flowpath area. The net effect of permitting the rotor to turn on the shaft is a potential change in the balancing. In fact, it proved to be remarkable that the unit operated with known unbalance once the rotor turned. In fact relatively good, though noisy, operation was possible.

To check these two effects, the unit was operated without the stator coil, the unbalanced electrical field and, without a coil to retard the magnet, relatively smooth operation was re-established.

At this point in the program, it was too late to rework the whole rotor assembly, and rebalance and check out everything. It was decided, therefore, to use epoxy cement in an attempt to fix the magnet to the shaft in the hope that, for the relatively short duration required for hot testing, this would be adequate. Tests showed that it was and hot testing could be accomplished.

Hot-gas Tests

The primary aim of the program had been to operate all components in a brassboard configuration using decomposition products of hydrazine-based fuel. While the original goals were not fully achieved, a power unit was operated for ~3 minutes using hot decomposition products and generating electrical energy. Each

component of the system functioned properly, and the system demonstrated it would be able to operate if some additional rework, by now identified and understood, were accomplished. However, at this point in the development stage, the bearing losses were still greater than could be tolerated by the design goal of 2 W/hr/in.^{3} Considerable development effort would be required to refine the bearing design commensurate with the required power density. It would also require the addition of at least three re-entry passages for the turbine gases similar to the one developed during this program.

The brassboard was assembled with the components that were successfully operated under the component development phase of this program. The assembled unit is shown by the photograph in Fig. 45. Stainless-steel shields have been removed to show the nozzle and turbine. During operation, these shields were mounted to surround the nozzle and turbine and to prevent hot gases from impinging directly on either the bearing or the alternator.

The basic assembly consisted of the hot-test, stainless-steel brassboard into which are mounted the stator, the rotating assembly, using the platinum cobalt magnet, bronze three-lobe hydrodynamic gas bearings, brass axial-play limiters, and a gas generator. For this brassboard, the test gas generator was modified by removing the test orifice plate and welding the same gas generator onto one of the two test nozzles. The only refurbishment to the previously used gas generator consisted of repacking the ball pack below the catalytic bed and supporting them with a new Monel screen. This was necessary because the ball pack could not be saved during the refurbishment operation. The detailed description of all these components has been covered in the section dealing with the component development phase of this program.

The hot-test facility for this program is located at the Rockwell International B-1 Division. A small test pad had been equipped with the necessary hydrazine and ancillary supplies during the previous part of this program and was backed up with a comprehensive control room. The hydrazine system consisted of a use tank (which is a high-pressure sight gage), a pressurization source for the use tank,

and a three-way valve to provide either hydrazine flow to the hardware or a nitrogen purge flow. Other minor components were provided for proper and safe operation.

The demonstration model was assembled at the cold-flow facility, and complete checkout tests were performed with GN_2. Cold gas was introduced into the nozzle through the pressure tap on the nozzle assembly. Tests were performed to ensure proper operation of the rotating assembly as well as optimum location of the nozzle. Once the highest speed under constant supply pressure was reached, the nozzle clamping device was tightened, thus locking the nozzle position with reference to the turbine for the hot tests. The nozzle location was maximized for axial clearance between turbine and nozzle face while maintaining optimum speed to prevent possible rubbing between nozzle and turbine due to thermal expansion. At completion of the mechanical checkout tests, the assembled unit was taken to the B-1 facility and installed on the small hydrazine pad.

The small hydrazine pad had been maintained in standby condition to provide the necessary facility for this series of tests. Installation was accomplished by connecting the gas generator to the use tank. The volume of the use tank ultimately limited run duration to approximately 3 minutes. Instrumentation of the brassboard unit was accomplished by connecting thermocouples to the nozzle and gas generator as well as to the standard pressure transducers to show chamber pressure and tank pressure. Electrical instrumentation was provided by the special load bank. Speed was either recorded or observed on the frequency converter, which measured the frequency output from the alternator.

The first test was conducted with the stator, the 0.0135-inch-diameter nozzle, bronze three-lobe bearings, the stainless-steel test rig, the gas generator with new nozzle, and the rotor, which had a significant amount of residual imbalance (i.e., the rotor which had no epoxy applied to it). There remained the fear that the epoxy could cause problems. To prevent direct impingement of the hot gases onto the stator, rotor, or bearings, a stainless-steel shield was installed around the nozzle and turbine.

Test initiation was excellent. As soon as the valve was opened, temperatures came up very quickly, and tank pressure could be increased to the required level of chamber pressure. Once tank pressure had been brought up to about 1000 psig, the turbine speed reached approximately 30,000 to 40,000 rpm, and it was evident that some instability was causing this speed limitation. It was assumed that the instability was due to the excessive imbalance remaining in the rotor assembly. The test was continued until all hydrazine had been used up, approximately 3 minutes, as anticipated. It should be noted that the power output from the alternator was correct magnitude for the speed attained. Because it was impossible to run a meaningful test that would yield relevant data with this rotor assembly, it was decided to use the better-balanced rotor and run a second test.

This decision was based, in part, on the fact that posttest inspection showed the rig to be in excellent condition without any indication of overheating of any of the components. Therefore, replacement of the rotor should result in a very satisfactory test because the epoxy would not overheat.

As discussed before, the magnetic portion of the rotor was loose enough to permit it to turn. Rework of the rotor required locking the permanent magnet onto the shaft in its correct location. Various approaches were considered, including staking, deforming the shaft, EB spot welding, and the addition of split collars to lock the rotor. None of these approaches appeared to be suitable with the materials of the rotor, and the addition of locking collars presented a balancing problem. It had been decided, therefore, to use a high-strength epoxy bonding technique.

The brassboard unit with a new rotor was again installed at the cold-flow facility, and final checkout tests were conducted to locate the nozzle properly and ensure correct operation of the hardware. After completing checkout tests, the unit was taken to the B-1 facility and installed in the hydrazine test facility.

As soon as the main valve was opened, the unit came up to speed, and tank pressure was increased as the test progressed (Fig. 51). A speed of 200,000 rpm was reached under open-circuit conditions and, during the tests, various electrical loads were imposed on the unit. Naturally, as loads were increased, unit speed was reduced. Typically, 15 watts of electrical power were generated at 72,000 rpm. When this is extrapolated to full speed (300,000 rpm), it results in 60 watts of electrical power, which is the design point. This test was conducted until all hydrazine in the tank was used up. Posttest inspection of the rig indicated that it was still in good condition, and the gas generator, operating for the third time without modification, appeared to be in reuseable condition. There was no indication of damage due to heating, nor was there any indication during the test that the rotor had gotten excessively hot, since this would have been indicated by a decay of the voltage and power.

Data obtained during this final test are listed in Table 12.

TABLE 12. TEST DATA

Voltage, vac	Current, adc	Power, watts	Speed, rpm
11	0.45	7.3	
9	0.80	10.6	
8.5	1.00	12.5	~ 72,000
6.5	1.55	14.8	
4.0	2.00	11.8	

While failure to achieve all goals is always a disappointment, some positive conclusions did emerge from these tests. Much of the design work had centered around a design for which heat transfer to the rotor and to the bearings would be minimized to ensure 12 minutes of operation. The hot-gas tests showed that, after 3

minutes of continuous operation, no adverse heat transfer had taken place. All hardware was in excellent condition. There had been some fear that the need to secure the rotor to the shaft with epoxy might cause problems if the epoxy melted. It did not melt and appeared to be in excellent shape at the end of the test.

The alternator, while unbalanced in its output, is cable of sustained high-speed operation and can easily put out the required power. The bearings operate well even in a hot environment.

Based on the performance of this unit, feasibility of achieving a 2W-hr/in.^{3} power density is primarily a function of reducing the parasitic losses, particularly the bearing friction, below that which was attained during this program. With a 60-watt power system, a significant development effort would be required to reduce bearing friction to an acceptable level. Based on the results from this program, it appears that a 200- to 400-watt power system would be a much better application for this technology.

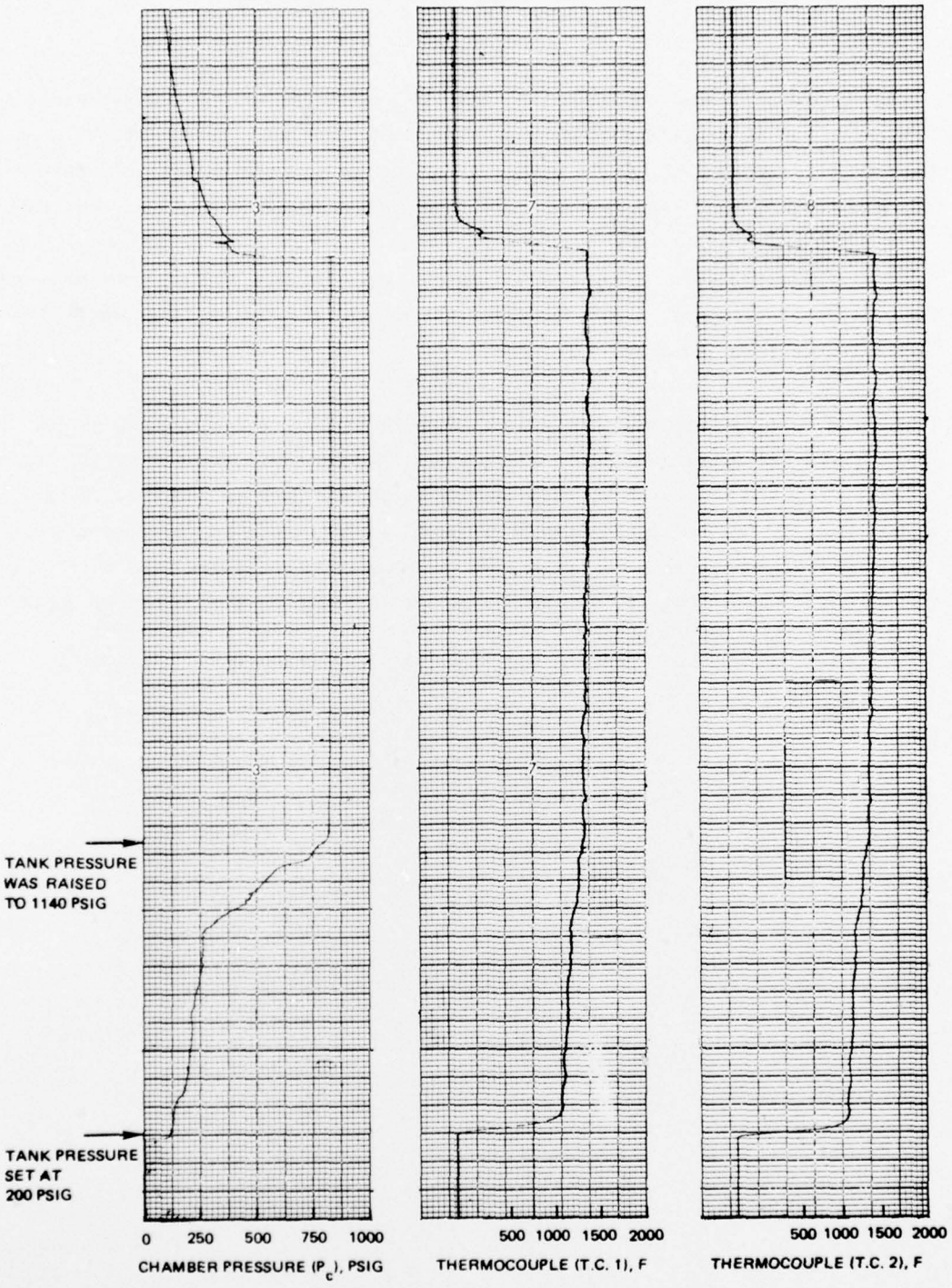

Figure 51. Test Record, Hot Firing

APPENDIX

REFERENCES

1. Advanced Development of a 60-Watt Dynamic Power Source, Rocketdyne Report R-9114P, 11 December 1972.

2. Barber, H. E.: Pressure Regulator for 60-Watt Power Source, Rocketdyne Internal Report ASR F3-199, n.d.

3. Etheridge, F. G.: An Experimental Evaluation of Representative Metals and Elastomers Utilized in Hydrazine Expulsion/Positioning Systems, Space Div. Report SD 73-SA-0047, 28 September 1973.

4. Wrubel, J. A.: Monpropellant Gas Generator for 60-Watt Power Source, Rocketdyne Internal Letter Report C&P 73-19, 29 May 1973.

5. Spies, R. and M. Dubey: Design of Low-Speed Turbines for Long-Duration Missile Secondary Power Units, Sundstrand Turbo Report, S/TD No. 1769, December 1959.

6. Lund, J.: Rotor-Bearing Dynamics Design Technology, Part VII: The Three Lobe Bearing and Floating Ring Bearing, AFAPL-TR-65-45, Part VII, February 1968.

7. Ellis, J. N.: 60-Watt Alternator, Rocketdyne Internal Report ASR73-220, 19 June 1973.

8. Carriker, R. C.: Miniature Generators and Alternators Using Rare Earth-Cobalt Permanent Magnets, Hamilton Technology, Inc., Report (no number, no date).

9. Carriker, R. C. and G. H. Ludewig: "Production of $SmCo_5$ Magnets Using Single Phase Sintering Aid," AIP Conference Proceedings Number 5, Magnetism and Magnetic Materials, 1971, American Institute of Physics, 1972.

10. Carriker, R. C.: "The Use of Sm_3Co in Sintering $SmCo_5$ Magnets," Appl. Phys. Lett., Vol. 20, No. 7, pp. 250, 1 April 1972.

11. Carriker, R. C.: "Intrinsic Coercive Force in (Pr, Sm)Co_5 as a Function of Samarium Content," Appl. Phys. Lett., Vol. 22, No. 4, pp. 160, 15 Feb. 1973.

12. Vanevenhover, D. E.: Transient Temperatures at Critical Locations in the 60-Watt Power Source Assembly, Rocketdyne Internal Report ASR F4-8F, 14 March 1974.

13. Spies, R.: Test Plan for 60-Watt Dynamic Power System, Rocketdyne Report R-9365, n-d.

14. Burowick, E. A.: Force Transducer Calibration, Rocketdyne Internal Report EDL #73-61, 31 October 1973.

15. Balje, O. E.: Notes on Turbomachinery, Lecture Notes for UCLA Course, 1971.

16. Spies, R.: Nozzle Calibration - 60 Watt Power Source, Rocketdyne Internal Report ASR74-346, 13 November 1974.

17. Lund, J. W. ed: Rotor-Bearing Dynamics Design Technology, Part III: Design Handbook for Fluid Film Type Bearings, AFAPL-TR-65-45, Part III, May 1965

18. Kestin, J. and W. Leidenfrost: The Effect of Moderate Pressures on the Viscosity of Five Gases, Brown University, AD233173, 1959